Influence of Swimming Marine Organisms on Turbulence in the Ocean from In-Situ Measurements

By

Shani Rousseau
B.Sc., Université du Québec à Rimouski, 2006

A Thesis Submitted in Partial Fullfillment of the
Requirements of the Degree of

MASTER OF SCIENCE

in the Department of Earth and Ocean Sciences

Influence of Swimming Marine Organisms on Turbulence
in the Ocean from In-Situ Measurements

By

Shani Rousseau
B.Sc., Université du Québec à Rimouski, 2006

SUPERVISORY COMMITTEE

Dr. Eric Kunze (Department of Earth and Ocean Sciences)
Supervisor

Dr. John Dower (Department of Biology)
Co-Supervisor

Dr. Richard Dewey (Department of Earth and Ocean Sciences)
Departmental Member

SUPERVISORY COMMITTEE

Dr. Eric Kunze (Department of Earth and Ocean Sciences)
Supervisor

Dr. John Dower (Department of Biology)
Co-Supervisor

Dr. Richard Dewey (Department of Earth and Ocean Sciences)
Departmental Member

ABSTRACT

Microstructure and acoustic data were collected in Saanich Inlet, British Columbia, and at Ocean Station P in the eastern subarctic North Pacific Ocean with the objective of observing krill-generated turbulence. At Ocean Station P, although a number of species composing the zooplankton community are large enough to generate turbulent flow ($Re > 10^3$), no turbulence events could be correlated with presence of swimming marine organisms and measurements indicated turbulence generated by internal wave shear. Zooplankton densities were likely too low to produce turbulence at the scale of an aggregation and the $O(10^{-2}$ m) scattered turbulent signals generated by individuals are difficult to detect in the natural environment.

In Saanich Inlet, higher dissipation rates were observed in regions of high acoustic backscattering, suggesting that zooplankton-generated turbulence was occurring. Although presence of zooplankton was often correlated with high dissipation rates, high dissipation rates were frequently observed in the absence of zooplankton, suggesting multiple sources of turbulence. High dissipation rates were observed in the presence of

non-migrating zooplankton as much as in the migrating layer. These turbulence events occurred at a scale of more than 1 m as they were positively detected by our dissipation rate estimation technique. This suggests that marine organisms can act together to generate turbulence at scales that can produce diapycnal mixing. Over all time-series collected, dissipation rates in the presence of zooplankton averaged 1.4×10^{-8} W kg^{-1} whereas the average in the absence of zooplankton was 0.7×10^{-8} W kg^{-1}.

Table of Content

List of tables

List of figures

Acknowledgements

I would like to thank my supervisor, Dr. Eric Kunze for his help and ideas for my research. I would also like to acknowledge my co-supervisors, Dr. John Dower for his help with the biology part of this work, and Dr. Richard Dewey for his numerous explanations on spectral analysis and for providing the dissipation rate estimates. I would also like to thank our lab technician, Kevin Bartlett, for his help with everything that is related to matlab and computers, Jody Klymak for his suggestions for the analysis, and Moira Galbraith for analyzing the zooplankton samples.

I shared my office with some amazing people who helped me keep a high spirit during hard times and were of great assistance when needed: Wendy Callendar, Reyna Jenkins, Jeannette Bedard and Ian Beveridge. Also, I would like to thank my family and friends for their support and enthusiasm in regard to my studies.

Field work would not have been possible without the help of many people, and I would like to thank Chris Mackay, as well as the Captains and Crews of *MSV John Strickland* and *CCGS John P. Tully* for their professional assistance. More specifically, I would like to thank Captain Ken Brown and his crew for their willingness to work long night shifts so that we could catch zooplankton migrations at dawn and dusk. Doug Yelland is also acknowledged for getting the acoustics to work on the Tully before the cruise.

Funding was provided through *NSERC Discovery Grant* funds to Dr. Eric Kunze, as well as NSERC CFI fund, Dr. Kunze's Canada Research Chair and ONR grant N000014-08-1-0700. Additional funding was also provided by the School of Earth and Ocean Sciences (*University of Victoria Graduate Award*).

Chapter 1
Introduction

1.1 Motivation

Swimming marine organisms have long been known to generate turbulence (Wiese and Ebina, 1995, Muller et al., 1997; Yen et al., 2003), but the importance of this energy input and its potential impacts on oceanic processes have yet to be examined. Studies on the role that physical processes play in regulating biogeochemistry in the oceans abound (Denman and Gargett, 1995; Gargett et al., 2003; Whitney et al., 2005), but the idea that biological processes could impact physical processes such as turbulence and mixing is not well understood, although a rapidly increasing literature is now available on the subject (Huntley and Zhou, 2004; Dewar et al., 2006; Kunze et al., 2006; Gregg and Horne, 2009). Turbulence generated by zooplankton (Kunze et al., 2006) and fish (Gregg and Horne, 2009) have been observed in-situ. However, how general this process can be and to what extent the observed turbulence is responsible for diapycnal mixing is not yet understood.

We examined zooplankton-generated turbulence through in-situ measurements of dissipation rate of turbulent kinetic energy with concurrent acoustic tracking of swimming zooplankton. Our goal was to discover a correlation between zooplankton vertical migrations and the occurrence of turbulence, and understand to what extent this turbulence is translated into diapycnal mixing. In-situ measurements were made at Ocean Station P and in Saanich Inlet, British Columbia, two locations differing greatly in terms of physical and biogeochemical properties.

It is interesting to consider zooplankton because their biomass in the world's oceans is extremely high, as they are the secondary producers of the marine environment, just above phytoplankton. Dewar et al. (2006) estimate a total zooplankton biomass of 30 Gt for all open ocean regions of the world. An unknown fraction of this biomass exhibits

diel vertical migration, swimming periodically between the ocean's surface and the deeper waters. According to the same authors, ocean mixing by swimming of marine organisms could contribute to 1 TW of the energy budget of the abyssal ocean (defined as below 200 m), a value comparable to deep ocean tidal dissipation and the energy delivered by winds to the stratified ocean interior (Munk and Wunsch, 1998).

By injecting kinetic energy of mechanical source into the oceans' energy budget through swimming, marine organisms could contribute to diapycnal mixing in certain regions of the ocean. This process could be particularly important in coastal surface waters, where biomass is high, and where mixing by processes such as winds and tides is low, such as Saanich Inlet. The swimming of zooplankton through the pycnocline could have an impact on mechanisms that require mixing near the surface. For instance, the occurrence of turbulence in the pycnocline due to zooplankton migration might influence ocean-atmosphere gas exchange where zooplankton abundance is high. Zooplankton species feeding on phytoplankton spend a significant amount of time in the euphotic zone and in the surface mixed layer, near the air-sea interface. Air-sea gas exchange is highly dependent upon turbulent mixing processes, and mixing processes in the euphotic zone are not well-understood (Hamme and Emerson, 2006).

1.2 Background

Ocean turbulence is the energetic, rotational and eddying state of motion of a fluid. When turbulence occurs in the oceans, large eddies break into smaller eddies until the eddy scale is small enough that it is dominated by molecular viscosity, following the so-called energy cascade. It generates large velocity gradients at small scales (typically 1 mm to 1 cm), leading to increased transfers of kinetic energy to heat through viscous dissipation (Thorpe, 2005). As a consequence, turbulence in the oceans constitute a very efficient mean of transfer of momentum, solutes and heat, far more efficient than molecular processes alone (Thorpe 2005).

Turbulence in the oceans plays a key role in many oceanic processes. Turbulent mixing drives biogeochemical processes by redistributing passive tracers such as nutrients, carbon and oxygen. Mixing of active tracers such as salinity brings changes to the buoyancy of water particles, driving the global overturning circulation (Munk and Wunsch, 1998). The density of seawater plays an important part in determining the nature and onset of turbulence in the ocean. Variations in density of seawater lead to pressure gradients that, if unopposed, drive motion to re-establish a gravitationally stable environment (Thorpe, 2005).

From a biological point of view, diapycnal mixing is required to move nutrients from deeper, nutrient-rich waters into the near-surface euphotic zone of the stratified ocean, where phytoplankton are found. Without mixing, the upper ocean would become rapidly nutrient depleted, resulting in low primary productivity and subsequent weakening of the entire food web (Thurman and Trujillo, 2004). Winds and tides are well known to generate upwelling events and deepening of the surface mixed-layer, contributing to bring nutrients into the euphotic zone, and are known as the two main sources of turbulent mixing in the world's oceans (Munk and Wunsch, 1998).

Swimming marine organisms as a source of ocean turbulence has been examined in recent papers (Huntley and Zhou, 2004; Dewar et al., 2006), and their significance in ocean mixing is currently under debate (Kunze et al., 2006; Visser, 2007; Gregg and Horne, 2009). Hydrodynamic analysis of swimming has focused mostly on energetic consequences for the animal rather than on energetic consequences for the fluid medium, but recent experimental studies give great insight on turbulence generated by zooplankton at the scale of the individual (Yen, 2000; Yen et al., 2003; Catton et al., 2008). For instance, studies found that individual *Euphausia pacifica* generate jet-like flow fields extending to up to twice the individual's body length (Yen et al., 2003; Catton et al., 2008). Aggregating zooplankton are able to use these jets to detect their neighbours (Yen et al., 2003). These jet flows also contribute to the spreading of chemical cues and can be used by hovering males to track a female by following its wake (Yen, 2000).

The mechanisms for turbulence generation differ greatly between swimming organisms and shear-driven turbulence. Shear-driven turbulence occurs at large scales and the kinetic energy is dissipated through the energy cascade down to scales where viscosity overcomes inertia (Thorpe, 2005). In swimming organisms such as zooplankton, turbulence is caused by velocity fluctuations arising from animal motion and can occur at relatively small scales. In addition, zooplankton-generated turbulence at the scale of the individual is not isotropic but forms an inclined jet-like flow in a structured, cooordinated fluid motion (Catton et al., 2008).

Munk (1966) was the first to assess the role of biologically-generated mixing in the ocean's energy budget, and identified approximately 1 TW of energy available from turbulent production by swimming marine organisms. In 2004, Huntley and Zhou published a study addressing biologically-generated turbulence by analyzing the mechanical energetics of eleven marine species of schooling organisms of sizes ranging from few centimeters (euphausiids) to tens of meters (blue whale). They estimated the mechanical energy required by marine organisms for locomotion and related it to the production of turbulent energy. They quantified the rate of energy production of individual animals and estimated turbulent kinetic energy production rates at the scale of social aggregations. They derived an equation describing the total energy production (W kg^{-1}) of a group of organisms:

$$E_p = e_t N / \rho V \qquad (1.1)$$

where N is the total number of organisms, and ρ and V the density and volume of water, respectively. e_t is the total rate of energy utilization by an individual animal and depends on two parameters: the propulsive efficiency, which accounts for the fact that swimming animals are not 100% efficient in their use of energy for propulsion, and the rate of energy expenditure by an individual animal (in Watts), which depends upon swimming speed and the work required to overcome drag. They found that, regardless of the

organism's size, turbulent dissipation rates generated by aggregating marine species were of order 10^{-5} W kg^{-1}, a value comparable to that found in the ocean during storms.

Kunze et al. (2006) published the first study using in-situ data to suggest the importance of biologically generated turbulence in coastal waters. They found very high dissipation rates (~ 10^{-6} W kg^{-1}) correlated with the upward migration of zooplankton aggregations, suggesting that vertically migrating zooplankton could generate enough turbulent mixing to increase the daily-averaged mixing in a coastal inlet by a factor of 100. Visser (2007) argued that, although high dissipation rates might be observed, the mixing efficiency associated with zooplankton turbulence had to be low due to the organism's small scale which is close to the Kolmogorov scale $(\nu^3/\varepsilon)^{1/4}$, suggesting that swimming marine organisms cannot generate overturning events larger than their size, resulting in insignificant mixing. Results from Gregg and Horne (2009), finding a mixing efficiency 100 times smaller within a fish school in comparison to outside, tend to support Visser's argument. They used

$$\Gamma = \kappa_T C N^2/\varepsilon \tag{1.2}$$

to determine the mixing efficiency, where κ_T is the molecular thermal diffusivity coefficient (1.4 x 10^{-7} m^2 s^{-1}) and C is the Cox number

$$C = 3\frac{\langle \partial T'/\partial z \rangle^2}{(\partial \langle T \rangle/\partial z)^2} \quad . \tag{1.3}$$

Although they observed dissipation rates reaching 10^{-5} W kg^{-1} in the presence of fish aggregations, Gregg and Horne's mixing efficiencies (0.0022 and 0.23 inside and outside the aggregation, respectively) resulted in a similar diapycnal diffusivities

$$K_\rho = \Gamma \frac{\epsilon}{N^2} \tag{1.4}$$

inside and outside the aggregation. As well as reduced temperature-gradient spectra, they reported that the spectra for both shear and temperature gradient had lower than expected variance at lower wavenumbers as compared to shear-driven turbulence. Kunze et al. (2007) argued that the shear spectra in Saanich Inlet were well resolved at length scales of 0.01 to 1 m and resembled those of shear-driven turbulence, suggesting that mixing was occurring at scales larger than an individual zooplankton, although the mechanism by which this would occur remains to be understood.

Increasing evidence suggests that an individual zooplankton cannot generate turbulence on a scale larger than one or two times its body length (Yen et al., 2003; Catton et al., 2008). This implies that, although swimming zooplankton can generate turbulence, at the level of an individual, it occurs only at the scale of 10^{-2} m, and the energy cascade characteristic of mixing does not occur because of viscous damping. Catton et al. (2008) find, during an experiment in a water tank using 4 freely swimming *Euphausia superba*, that water particles were moved from the top to the bottom of the group of swimming euphausiids. They suggest that the thickness of an aggregation would be a more appropriate length scale for the Ozmidov length scale than the size of an individual, as aggregating species would act as whole to move water particles.

For vertical mixing to occur in a turbulent flow, the largest eddies must be at the Ozmidov scale

$$L_o = \varepsilon^{1/2} N^{-3/2} \tag{1.5}$$

where ε is the dissipation rate and N the buoyancy frequency. The Ozmidov scale is a measure of the largest scale that can overturn stratification. Usually, the Ozmidov scale is much larger than the typical size of an euphausiid (~ 1-2 cm), but much smaller than the size of an euphausiid aggregation (~20-40 m). This suggests that zooplankton aggregations, acting together, could generate significant mixing.

Chapter 2
Observations

2.1 Sampling sites

In-situ microstructure and acoustic measurements were collected at Ocean Station P (OSP) in the eastern subarctic North Pacific (figure 2.1) during June 2007, and in Saanich Inlet (figure 2.2) during June 2006, May 2007 and May 2008 (tables A2.1.1, A2.2.1). Data were collected at dusk and dawn during zooplankton migration periods, and extended before and after the migration period. Each of the four field measurement seasons (OSP, SI06, SI07, SI08) are termed datasets and the measurement periods within them (dawn, dusk), time-series.

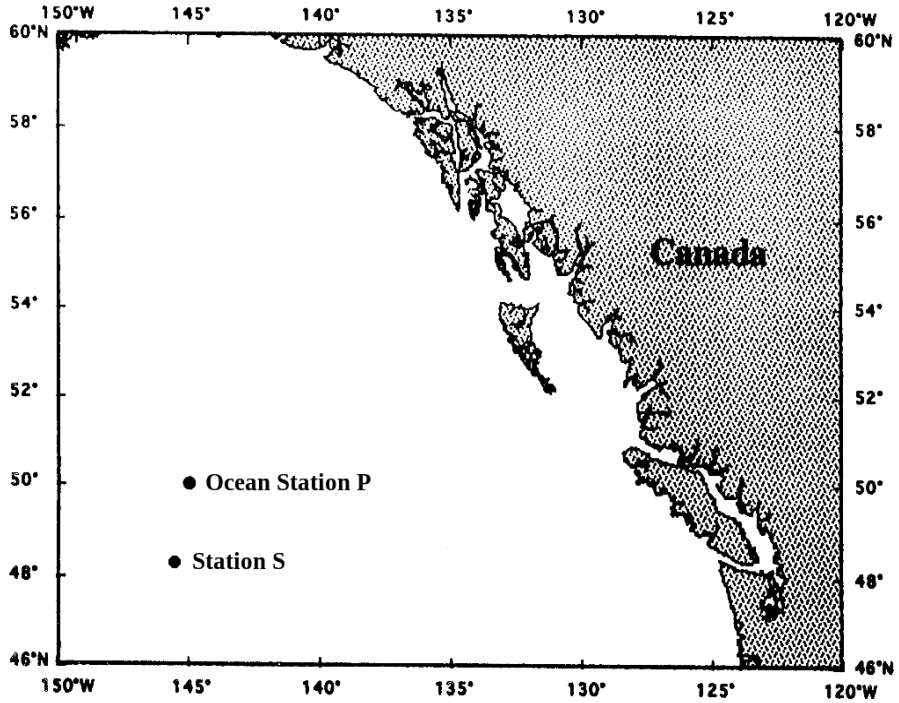

Figure 2.1. Ocean Station P off the coast of British Columbia, Canada. The two last time-series (*SSJun10Dusk*, *SSJun11Dawn*) were collected 180 km south of Ocean Station P (here named Station S) due to bad weather.

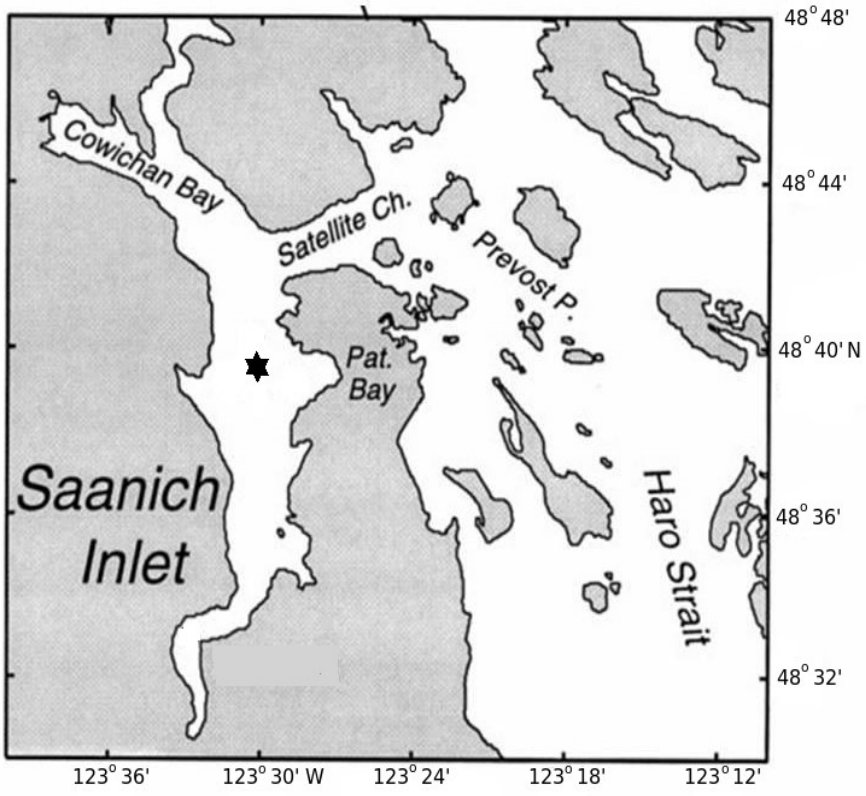

Figure 2.2. Saanich Inlet, British Columbia, Canada. The black star indicates the sampling location.

Ocean Station P is a well-studied open-ocean area in terms of water characteristics, zooplankton communities and biogeochemical properties. Measurements were collected on June 6-9 and June 10-11, 2007 with 3 dusk and 3 dawn sampling periods (table 2.1). The two last time-series collected in this region (one dawn and one dusk) were sampled 180 km south of Ocean Station P due to a storm. This new sampling station is named Station S. At Ocean Station P and Station S, a cast took on average 20 minutes, and the average fall speed of the Vertical Microstructure Profiler (VMP) was 0.6 m/s. Both sites had a similar buoyancy period $2\pi/N$ of approximately 5 minutes within the seasonal and permanent pycnoclines and 20 minutes within the rest of the water column.

Saanich Inlet measurements were made in June 09-11 2006, May 08-10 2007 and May 07-09 2008 (table 2.1). Saanich Inlet was chosen for its incredibly productive yet low turbulence waters. It is characterized by a highly productive environment, including an extremely high biomass (up to 10 000 m^{-3}) of *Euphausia pacifica* (Mackie and Mills, 1983), a daily migrating zooplankton species. A VMP cast took on average 6-10 minutes, with a VMP fall speed averaging 0.6 m/s. The buoyancy period is approximately 11 minutes below the surface pycnocline and outside the halocline found around 60 m. Within the surface pycnocline, the buoyancy period is 6 minutes. Data from 2006 and 2008 were collected during slack tide. One time-series of the 2007 dataset was collected during this period as well, whereas two time-series were collected during flood (figure A2.2.1).

Dataset	Date	# dawn time-series	# dusk time-series	# profiles
OSP	June 06-09 2007	2	2	40
SS	June 10-11 2007	1	1	22
SI06	June 09-11 2006	2	2	111
SI07	May 08-10 2007	1	2	60
SI08	May 07-09 2008	2	2	161

Table 2.1. Summary of the number of microstructure profiles collected at each station.

2.2 Instrumentation

Table 2.2 summarizes the instruments used during each dataset collected at Ocean Station P, Station S and in Saanich Inlet. 394 profiles of microscale shear was measured using a tethered, free-falling Rockland Scientific Vertical Microstructure Profiler (VMP) (figure 2.3). Use of a freefall instrument greatly reduces vibration noise. Two air-foil shear probes mounted on the instrument measure the horizontal velocity (u) of the water

column at a rate of 512 Hz. The shear probes are located at the lower extremity of the instrument, so are surrounded by undisturbed waters as the instrument falls through the water column. The VMP fall speed is 0.6 m/s on average and allows resolution of horizontal velocities to scales of 1 cm.

Also mounted on the VMP are conductivity and temperature microstructure sensors, as well as SeaBird CTD fine-scale temperature and conductivity sensors. Accelerometers with axes along *x*-, *y*-, and *z*-directions differentiate real from body-induced velocity fluctuations. During all sampling sessions, the instrument was deployed, recovered and redeployed without interruption for the entire migration period in order to detect zooplankton-generated turbulence.

Acoustic backscattering data were collected to track zooplankton migrations. The echosounders used differed between the sampling stations. In Saanich Inlet, a single-beam 200 kHz ASL Environmental Sciences Water Column Profiler with an 8^{o} beam angle was used. Single frequency echo-sounders are most useful when analyzing homogeneous zooplankton communities that have been well identified using tow nets prior to the acoustic data collection. They do not distinguish properly between zooplankton and co-located scattering from turbulent microstructure (Stanton et al., 1994).

Dataset	**Date**	**EK60**	**ASL**	**ADCP**		**VMP**	**Nets**	**Nitrate**
		38-120-200 kHz	200 kHz	38 kHz	300 kHz		250-0 m	
OSP, SS	June 07-11 2007	X		X		X	X	X
SI06	June 10-11 2006		X			X		
SI07	May 08-10 2007		X			X		X
SI08	May 07-09 2008		X		X	X		

Table 2.2. Summary of data collected at Ocean Station P (OSP) and Saanich Inlet (SI). EK60 echosounder also recorded at 72 and 400 kHz but these frequencies were not used in the analyis. See text for details.

Figure 2.3. The Vertical Microstructure Profiler on the deck prior to profiling. The CTD unit is visible on the right side. The temperature and shear microstructure sensors are visible at the bottom of the image.

The echosounder sampled at a frequency of one hertz (Hz) and the pulse duration of each ping was 300 μs. The vertical resolution of the instrument is 8 bins per meter. This echosounder uses an 8-bit (28) A/D converter, resulting in a digital resolution of 256 counts ranging from 0 to 255 (Beveridge, 2007). Counts were converted into volume backscattering strength for the analysis.

At Ocean Station P and Station S, a hull-mounted split-beam, multi-frequency Simrad EK60 echosounder was used to track zooplankton migrations. Multi-frequency echo-sounders are useful for distinguishing between sizes and species of zooplankton because scattering behaviour is strongly size- and frequency-dependent. The transducers were located at 4.5 m depth. Frequencies of 38, 72, 120, 200 and 420 kHz were available but only the 38, 120 and 200 kHz frequencies were used for this analysis. The sampling frequency used is 0.25 Hz and the pulse length is 512 μs at frequencies 38 and 120 kHz, and 128 μs at 200 kHz. Calibration parameters are summarized in appendix 1.

The ADCP used at Ocean Station P and Station S was a hull-mounted, downward-looking RDI instrument and measured the three dimensional velocity of the water column. The ADCP operated at 38-kHz frequency and 16-m vertical resolution.The ADCP used in Saanich Inlet was also an RDI instrument. It operated at a frequency of 300 kHz and had a vertical resolution of 1 m.

One vertical net tow was collected at Station P using an open net for zooplankton communities. The net was 0.56 m in diameter with a 236 um mesh. The vertical tow was collected on June 07, at 02:06 PDT and covered a range of 250 m to the surface. The samples were either preserved in a formalin solution or in frozen alcohol for further analysis. They were analyzed at IOS by Moira Galbraith for zooplankton species, growth stage, length, mass and abundance. No net tows were collected in Saanich Inlet.

At Ocean Station P, Station S and in Saanich Inlet in 2007, surface nitrate concentrations were measured before and after each migration of the zooplankton layer for signs of nutrient mixing, but these measurements did not lead to any significant conclusion. Nitrate concentrations in the surface waters vary according to a number of factors, such as phytoplankton consumption, zooplankton excretion and deepening of the mixed layer at night. It was not possible to control or measure all of these factors and the results cannot be interpreted in a useful way. These results are thus not considered in the present study.

2.3 Data processing

All the microstructure (VMP) and acoustic data (ASL, EK60 and ADCP) were analyzed using Matlab. Modified Matlab routines from Rick Towler (EK60) from the Alaska Fisheries Science Center and from Richard Dewey (ASL, ADCP) and Kevin Bartlett (VMP) from University of Victoria were used for processing the raw acoustic and microstructure data.

2.3.1 Bioacoustic data

The backscattering intensity is expressed in terms of the volume backscattering strength (S_v) for overlapping targets. The SONAR equation (appendix 1) is used to convert the voltage or counts output of the echosounder to volume backscattering strength. The calculation of S_v corrects for propagation losses due to beam spreading and absorption.

External noise was found in the data due to interference with the ADCP when used. All time-series collected concurrently to ADCP data were despiked by eliminating all values that exceeded one standard deviation of a 15-second sample (Emery and Thomson, 2001). Gaps were filled by linear interpolation. Acoustic data was averaged over one meter and one minute for correlations with the other variables.

Although five frequencies were recorded with the EK60 to track zooplankton migrations, only frequencies 38, 120 and 200 kHz were used in this work because these frequencies cover detection of organisms of sizes ranging from fish to copepods. These frequencies correspond to a wavelength of 4, 1 and 0.8 cm, respectively. The 120 kHz frequency was used for comparisons with other measurements. This frequency has proven to be the most useful for our data analysis as it is sensitive to both the surface mixed layer and the migration layer observed at Ocean Station P and Station S. Trevorrow (2005) also mentions that this frequency is sensitive to both zooplankton and fish aggregations in

addition to being a good compromise between the long range 38 kHz and the very short range 200 kHz.

2.3.2 Acoustic Doppler Current Profiler

Noise was also present in the ADCP data due to interference with the bioacoustic echosounders. Using the method described in section 2.3.1, ADCP data were despiked and gaps were filled by linear interpolation.

During the 2008 fieldwork in Saanich Inlet, there was a malfunction of the ADCP and it was not possible to retrieve ship location from the GPS. However, we can still obtain accurate shear data as the relative difference in horizontal velocity with depth.

Total shear from *x* and *y* directions were estimated as:

$$S = \sqrt{((du/dz)^2 + (dv/dz)^2)} \qquad (2.1)$$

where *u* is the northward velocity and *v* the eastward velocity. The ADCP shear data was further cleaned by averaging over five minutes. At Ocean Station P and Station S, the 16-m vertical resolution of the echosounder allows detection of velocity features larger than 32 m (Nyquist wavelength = 1/32 m^{-1}). In Saanich Inlet, the resolution is 1 m, resulting in a Nyquist wavelength of 0.5 m^{-1}, allowing resolution of features larger than 2 m.

2.3.3 Determination of the dissipation rate

In the present study, we used microscale velocity gradients to quantify the turbulence. Turbulence is measured in terms of the rate of loss of the kinetic energy of turbulent motion per unit mass through viscosity to heat (Thorpe, 2005) and is denoted ε. At high Reynolds number, turbulent flow is assumed isotropic and the dissipation rate ε is customarily approximated as

$$\varepsilon = \nu \frac{15}{2} \left(\frac{\partial u}{\partial z} \right)^2 \tag{2.2}$$

where ν is the molecular kinematic viscosity (~ 1 x 10^{-6} m^2 s^{-1}) and $\left(\frac{\partial u}{\partial z} \right)^2$ the vertical shear variance of the horizontal velocity.

Microstructure shear data were despiked by comparing the instantaneous signal to the signal's local variance. Spikes in the microstructure data can originate from instrument vibration, collision with particles, or if the tethered cable of the instrument becomes taut during freefall.

To estimate the dissipation rate, observed shear variance spectra were generated from 4-m segments of each shear profile using a 2-m overlap. Observed spectra are not well resolved at larger and smaller spatial scales and were therefore fitted to the Nasmyth theoretical spectrum to estimate the dissipation rate. The shear probes' size do not allow resolution of scales as small as the Kolmogorov length scale

$$l_k = (\nu^3 / \epsilon)^{\frac{1}{4}} \tag{2.3}$$

which is the scale of turbulent motion at which viscous dissipation becomes significant (Thorpe, 2005). This scale ranges from 0.01 to 0.001 m in our data ($10^{-10} \leq \varepsilon \leq 10^{-6}$ W kg^{-1}). The 4-m interval on which the spectra are generated results in a large scale resolution of the shear-variance spectra of approximately 1-m (see figures 3.9 and 4.3).

Observed and theoretical curves were fitted by iteration, cutting the highest and lowest wavenumbers until the best fit was found. Integration under the curve leads to a dissipation rate estimate. The average error is related to the portion under the spectral curve excluded in the best-fit estimate and is about 50 %.

Dissipation rate profiles were further cleaned up by comparing values obtained by the two shear probes. A dissipation rate estimate was eliminated if the logarithms of the two values differed by more than 1.5.

2.4 Physical and ecological settings

2.4.1 Ocean Station P

Ocean Station P is located at 49º59'N and 145º00'W in the eastern subarctic North Pacific Ocean. It has been the site of oceanographic research for over 50 years (Tabata and Weichselbaumer, 1992), and this has given rise to a very rich literature on the water characteristics and ecosystem dynamics of this part of the ocean. Other than the time-series data collected by Canadian weatherships from 1956 to 1982, a number of major research projects [World Ocean Circulation Experiment (WOCE), Subarctic Pacific Ecosystem Program (SUPER), VERTical Exchange program (VERTEX), Institute of Ocean Sciences Line P program] have allowed for an increased understanding of the region in terms of the water column physics and the biogeochemistry and foodweb dynamics characterizing this region (Boyd et al., 1999).

The water column in the subarctic Pacific is characterized by a permanent pycnocline at 100-150 m controlled by salinity and a seasonal pycnocline regulated by temperature near 50-m depth. In regions not affected by coastal runoff such as Ocean Station P, salinity stratification is weak above the permanent pycnocline throughout the year and stratification will therefore depend on temperature in the upper part of the water column. Winds increase in fall (Freeland et al., 1997) and are high throughout winter, mixing the upper 150 m until mid- to late spring after which seasonal increase in insolation and weaker winds allow the formation of a seasonal thermocline (Mackas et al., 1993).

Ocean Station P is located in one of the three High Nitrate Low Chlorophyll (HNLC) regions in the world oceans (Boyd et al., 1999). Primary production rates are lower (140 gC m^{-2} yr^{-1}) than those observed in BC coastal waters where annual primary production ranges from 250 to 500 gC m^{-2} yr^{-1}. Higher primary production in coastal waters is due to enhanced upwelling of deep, nutrient-rich waters and estuarine outflow (Whitney et al., 2005). Due to the low primary production, zooplankton biomass in the open ocean near Ocean Station P is generally lower by several orders of magnitude than in BC coastal waters.

Zooplankton biomass in the subarctic Pacific is dominated by four regionally endemic species of calanoid copepods: *Neocalanus plumchrus, Neocalanus flemingeri, Neocalanus cristatus* (figure 2.4) and *Eucalanus bungii* which feed on phytoplankton and the herbivorous microzooplankton community in the upper part of the water column (Goldblatt et al., 1999). *N. cristatus* may also feed on sinking detrital particles (Mackas and Tsuda, 1999). All exhibit ontogenetic migration, which means that their vertical distribution depends on their life cycle. In spring, the season during which our samples were collected, the three species of *Neocalanus* are found in the upper ocean as actively feeding fourth and fifth copepodites (Miller, 1984). *Neocalanus sp*. descent to depths between 400 and 2000 m (Mackas and Tsuda, 1999) around June for their over-winter diapause stage, which is a dormancy response that minimizes autumn and winter exposure to predation risks and poor feeding conditions (Mackas and Tsuda, 1999). Some *N. cristatus* have been found in the upper water column as late as August (Mackas et al., 1993). *Neocalanus sp*. mate and spawn at depth in autumn and early winter using metabolic reserves accumulated during spring-early summer active feeding stage (Mackas and Tsuda, 1999). The life cycle of *E. bungii* is more complex and involves both biennial and annual patterns (Miller et al., 1984). The adults are known to migrate back to the upper layer in spring in order to feed prior to spawning (Mackas et al., 1993). There is no evidence that any of the four species exhibit diel vertical migration (Mackas et al., 1993). Mackas et al. (1993) found that *N. plumchrus* and *N. flemingeri* aggregate in areas

of high turbulence in the lower part of the surface mixed layer, whereas *N. cristatus* and *E. bungii* stay within the thermocline, where turbulence is usually low.

The most abundant macrozooplankton species found at OSP are the chaetognaths S*agitta elegans* (figure 2.4c) and *Eukrohnia hamata*. Although they constitute a smaller percentage of the total biomass in the water column, they are important to consider in this study because they exhibit diel vertical migration (Goldblatt et al., 1999). In spring, *E. hamata* is present throughout the upper 250 m while S. *elegans* is found strictly above the seasonal thermocline at 50 m. These two chaetognath species are important predators of the copepod community (Goldblatt et al., 1999).

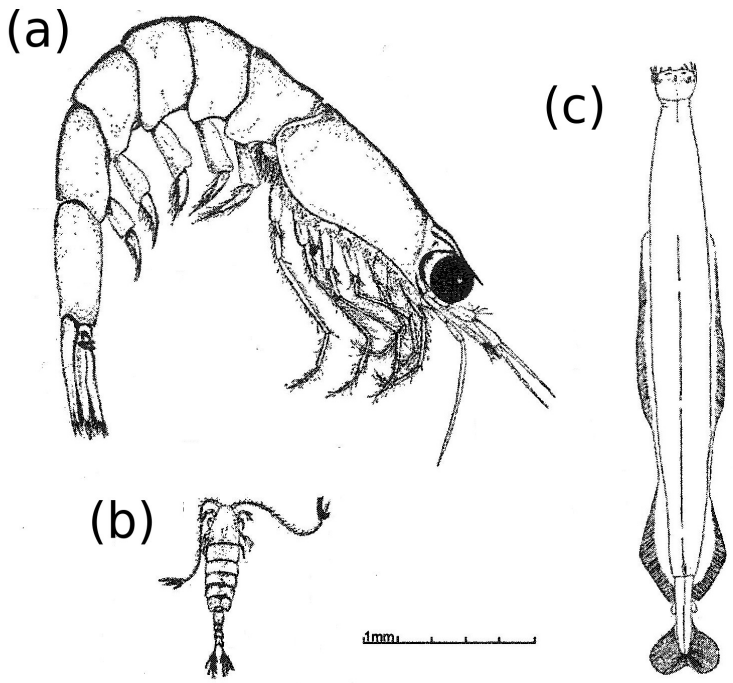

Figure 2.4. A few of the zooplankton species found at Ocean Station P: (a) euphausiid T*hysanoessa sp*.; (b) copepod *Calanus sp*.; (c) chaetognath *Sagitta sp*. Taken from Parsons and Takahashi (1973).

In terms of acoustic backscatter, copepods are likely to be important due to their dominant number. Trevorrow (2005) found that euphausiids, pteropods and myctophid fish (15, 1.5, and 28 mm, respectively) dominate the backscatter at OSP in the upper 30 m. He found an abundance of 1.7 m^{-3} for euphausiids in the upper 15 m and 3.6 m^{-3} at 15-30 m, and an abundance of 1.8 m^{-3} for pteropods at 15-30 m depth as well. He also identified myctophid fish of length 20-60 mm which he suggested were *Stenobrachius leucopsarus*. Goldblatt et al. (1999) found a vertically integrated (over 250 m) abundance of 200-1600 m^{-2} for euphausiids (mostly *Thysanoessa inspinata* and *Euphausia pacifica*) in the summer of 1996 and 1997 (figure 2.4).

2.4.2 Saanich Inlet

Saanich Inlet is a fjord with a maximum depth of 240 m. The inlet is characterized by very high primary productivity throughout the year, and a high abundance of the diel migrator *Euphausia pacifica* which can reach concentrations of up to 10 000 individuals m^{-3} (Mackie and Mills, 1983). At the mouth of the inlet, a 75-80 m sill restricts circulation of the deep basin waters (Gargett et al., 2003). The inlet is also characterized by a seasonally anoxic environment below 100 m (Jaffe et al., 1999). This condition is caused by the very high primary productivity and the low deep-water renewal rate due to the weak circulation within the inlet. Bacterial decomposition of organic material might also be responsible for the anoxic conditions found at the bottom of the deep basin (Hobson, 1983; Juniper, 1986). Saanich Inlet is an inverse estuary, with dominant freshwater inputs outside the inlet: in winter from the nearby Cowichan River, in summer from the massive freshet of the Fraser River (Gargett, et al., 2003).

Saanich Inlet is characterized by very weak wind and tidal forcing, hence very low turbulence. Observations suggest that the mixing required to bring nutrients into the euphotic zone arises from strong tidal mixing just outside the inlet (Gargett et al., 2003). Parsons et al. (1983) argue that a frontal zone forms at the mouth of the inlet where the strongly mixed water (during spring tides) outside the inlet comes into contact with the

stratified water inside the inlet. Other studies, such as the one by Takahashi et al. (1977) which show a fortnightly variability in primary productivity, tend to support this hypothesis. Tidal excursion into the inlet can only account for the increase in nitrate concentration and primary production at its mouth because the maximum frontal excursion cannot exceed the maximum tidal excursion of O(3km) in the vicinity of the mouth (Gargett et al., 2003). The pressure gradient mechanism originating from mixing at the mouth is likely responsible for mixing at the head. A recent dye experiment undertaken in Saanich Inlet indicates a low-frequency cyclonic circulation around the inlet strong enough to carry water from the sill to the inlet head in less than a week (J. Klymak, University of Victoria, personal communication, 2009).

Saanich Inlet is home to a high biomass zooplankton community. *Euphausia pacifica* is the dominant macrozooplankton species (figure 2.5), with abundances one or two orders of magnitude greater than typical open ocean concentrations (Greenlaw, 1979). Beveridge (2007) found that zooplankton density was higher near the mouth of the inlet in spring and summer. Also present in Saanich Inlet are a number of copepods species (*Calanus spp*.), chaetognaths (*Sagitta elegans*) and amphipods (*Parathemisto pacifica*), as well as medusae (*Aglantha digitale*), ctenophora (P*leurobrachia sp.*) and appendicularia (O*ikopleura sp.*) (Mackie and Mills, 1983), plus a number of fish species including hake, dogfish, herring and salmon (Greenlaw, 1979).

During the day, euphausiids form a deep acoustic backscattering layer in Saanich Inlet just above the oxycline (Mackie and Mills, 1983; Beveridge, 2007), along with amphipods, chaetognaths (*Sagitta elegans*) and some migrating copepods (Greenlaw, 1979). At sunset, they migrate upward into the surface mixed layer to feed. Juveniles of many fish species are sometimes found within the zooplankton layer during the day and always at night (Greenlaw, 1979). In Saanich Inlet, body length of *E. pacifica* averages around 12-22 mm (DeRobertis et al., 2003). The comparatively large size of *E. pacifica* makes it a significant prey item for marine planktivores (Jaffe et al., 1999).

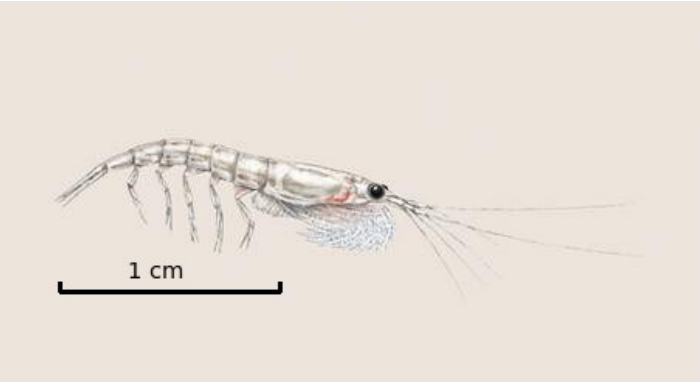

Figure 2.5. *Euphausia pacifica*, the main vertically migrating species in Saanich Inlet.

Given its relatively large size and very high abundance, *Euphausia pacifica* dominates the acoustic backscattering signal in Saanich Inlet (Greenlaw, 1979; Mackie and Mills, 1983; DeRobertis, 2002). It is also the principal daily migrator in the inlet, although *Sagitta elegans*, *Pleurobrachia sp*. and *Aglanta digitale* also display diel vertical migratory behaviour (Mackie and Mills, 1983). However, none of these species are very abundant in comparison to *E. pacifica* (Mackie and Mills, 1983). Given their gelatinous composition, their acoustic signals are negligible (Trevorrow, 2005). A study by Jaffe et al. (1999) finds target strength values ranging from -78 to -71 dB re 1 m for 15-20 mm long *E. pacifica*. Swimming speeds for *E. pacifica* range from 4-19 cm/s (Torres, 1984; Miyashita et al., 1996; Torres and Childress, 1983; De Robertis et al., 2003). Swimming speeds are greatly reduced (close to 0 cm/s) during daytime (Jaffe et al., 1999; De Robertis et al., 2003). Such a decrease in swimming activity has been suggested to confer advantages in reducing encounter rates and lowering metabolic costs (DeRobertis et al., 2003).

Chapter 3
Results and Analysis: Ocean Station P and Station S

Profile time-series of dissipation rate ε, acoustic backscatter and ADCP shear were collected during two dawns and two dusks at Ocean Station P plus one dawn and one dusk at Station S during June 2007 and are analyzed using a statistical approach. It is the first time, to our knowledge, that measurements of biologically-generated turbulence were attempted in the deep ocean.

3.1 Acoustic characterization of the aggregations and species identification

One net tow sample of the upper 250 m at Ocean Station P is used to characterize zooplankton species and abundances. The single net tow is not used for statistical purposes but only to indicate the nature of the zooplankton community which is further investigated using bioacoustic data. Copepods (*E. bungii, N. cristatus, N. plumchrus* and *N. flemingeri*) constituted 61.2% of the total biomass (table 3.1). Chaetognaths were also present in high abundance (19.6% of total biomass), particularly *E. hamata* (16.6% of total biomass). Very few euphausiids were found (~ 2%) and it is likely that the diameter of the net used (0.56 m) was too small to accurately sample this species (J. Dower, University of Victoria, personal communication, 2009). Euphausiids are typically abundant in the summer at Ocean Station P (Goldblatt et al., 1999) and are also present in the spring (Trevorrow, 2005). Many studies have suggested that euphausiids exhibit strong net avoidance behaviour (Lawson et al., 2008, Zhou et al., 1994). The use of coloured, slow-moving or small-mouth-area net tows often results in undersampling the largest, most agile crustaceans such as euphausiids and amphipods (Mackas and Tsuda, 1999).

Acoustic backscattering reveals a 10-25 m thick near-surface layer just above 50-m depth (figure 3.1), coinciding with both the seasonal thermocline and a high-shear (6×10^{-5} s^{-1}) region (figure 3.7). A diel migrating zooplankton layer is observed between 300 m and the depth of the non-migrating near-surface layer.

Species	Life stage	Average length (mm)	Average mass (mg)	Abundance m^{-2} (0-250 m)	Percentage of total biomass
Copepods					
N. plumchrus	C4, C5	**2.6, 3.8**	0.2, 0.6	7508	**20.0**
N. flemingeri	C5	**3.1**	0.4	2860	**7.0**
N. cristatus	C4, C5	**4.1, 6.4**	0.7, 1.6	3125	**28.1**
E. bungii	C6F	**6.2**	0.7	973	**6.1**
Chaetognaths					
E. hamata	S2, S3	**7.5, 18.0**	0.2, 1.4	2860	**16.6**
P. scrippsae	S3	**30.0**	6.5	45	**1.8**
S. elegans	S3	**20.0**	1.1	180	**1.2**
Euphausiids					
T. inspinata	S1, S2, adult	**4.5, 7.5, 17.1**	8.7, 0.2, 0.8	203	**2.0**
E. pacifica	nauplii	0.4	0.0	358	0.0
Gastropods					
L. helicina	S0 (veliger)	1.0	0.1	180	0.1
C. limacina	S1	4.0	0.5	358	1.1
Cnidarian					
Solmissus sp	S3	20.0	21.0	8	1.1
Foraminifera					
Globigerininae sp	S1	0.4	0.1	16538	6.6

Table 3.1. Dominant zooplankton species between 0-250 m at Ocean Station P, from a single net tow collected on June 07, 2007 at 2:06 PDT. Life stages: Copepods: C4, C5: copepodite stages; C6F: adult female. Other species: S1: < 5 mm; S2: ≥ 5 mm < 10 mm; S3: ≥ 10 mm. Numbers in bold highlight species with high biomass or length.

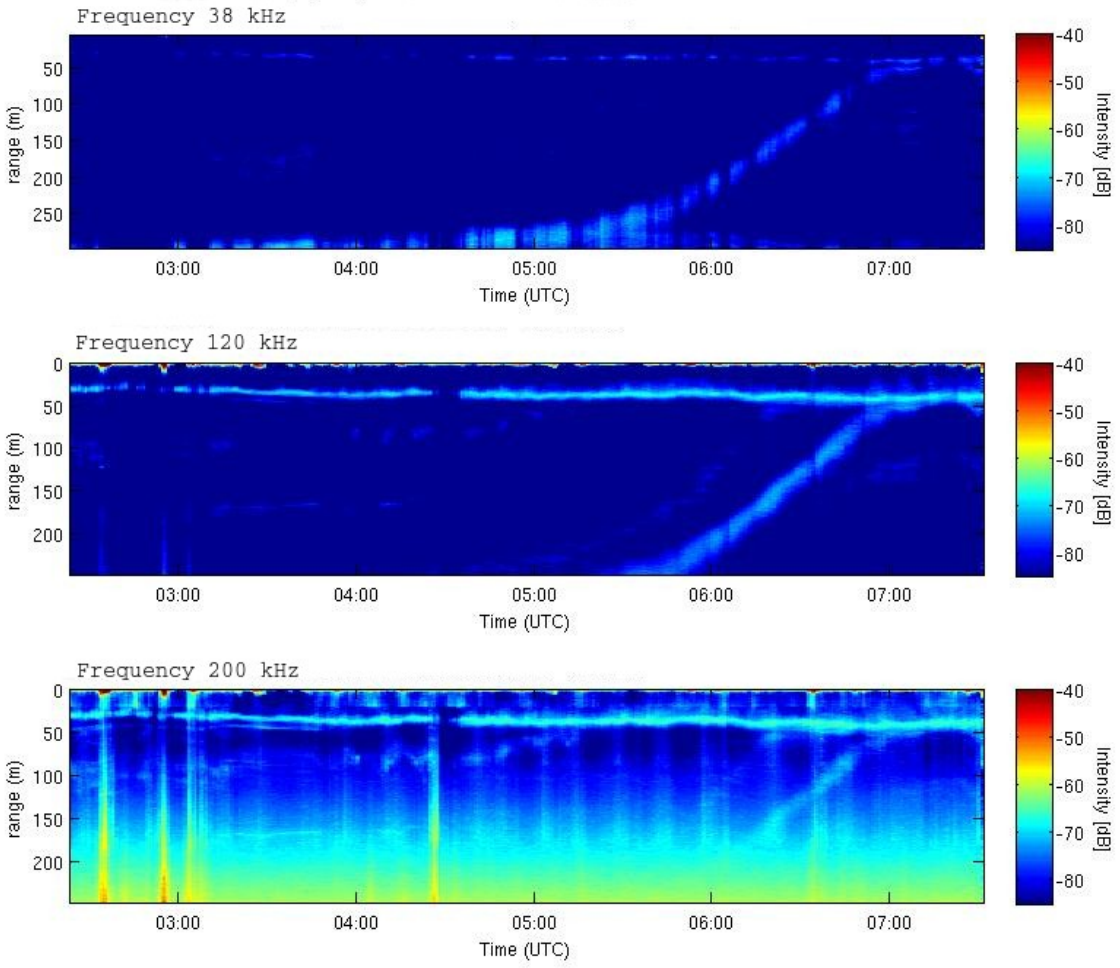

Figure 3.1. Acoustic backscattering at frequencies 38, 120 and 200 kHz during dusk upward migration at Ocean Station P, June 06 2007. Scattering strength is shown as volume-backscattering (dB). The scattering strength of the surface layer increases with frequency. A less pronounced increase is observed in the migrating layer.

3.1.1 Non-migrating surface layer

The acoustic signal of the near-surface backscattering layer increased with increasing echosounder frequency (figure 3.2) as is typical of copepods and euphausiids (figure 3.3). The strongest volume-backscattering strength at 200 kHz was -66 dB decreasing to -68 and -82 dB at 120 and 38 kHz, respectively. This layer was likely dominated by 2-6 mm copepods (Mackas et al., 1993; Mackas et al., 2005; Miller, 1984). Our net tows support this interpretation since the bulk of the biomass above 250 m is composed of the four copepod species *Neocalanus plumchrus, Neocalanus flemingeri, Neocalanus cristatus* and *Eucalanus bungii.* Our bioacoustic data show that this biomass must be concentrated either above 50-m depth, or within the migrating layer. Since none of these copepod species display strong vertical migratory behaviour (Goldblatt et al., 1999), they likely constitute the near-surface backscattering layer.

It is possible to estimate the abundance of zooplankton in a homogeneous aggregation by knowing the volume-backscattering strength (S_v) of the aggregation and the typical target strength (TS) value for the species (appendix 1):

$$S_v = TS + 10\log_{10}(N) \qquad (3.1)$$

where N is the number of individuals per m^3. Using an average target strength for copepods of -95 dB (Trevorrow, 2005) and assuming that copepods dominate the backscattering layer, the inferred density is ~ 800 copepods per m^3. Multiplying by the average thickness (17.5 m) of the surface backscattering layer, we obtain an integrated abundance of 14 000 m^{-2}, in agreement with our net tow results (integrated abundance for copepods is 14 365 m^{-2}). This value is also in agreement with results from Goldblatt et al. (1999) (also integrated over 0-250 m) for May 1996 (14 100 m^{-2}) whereas their abundance estimate for June 1997, the month where our net tows were collected, was 1 840 m^{-2}, much smaller.

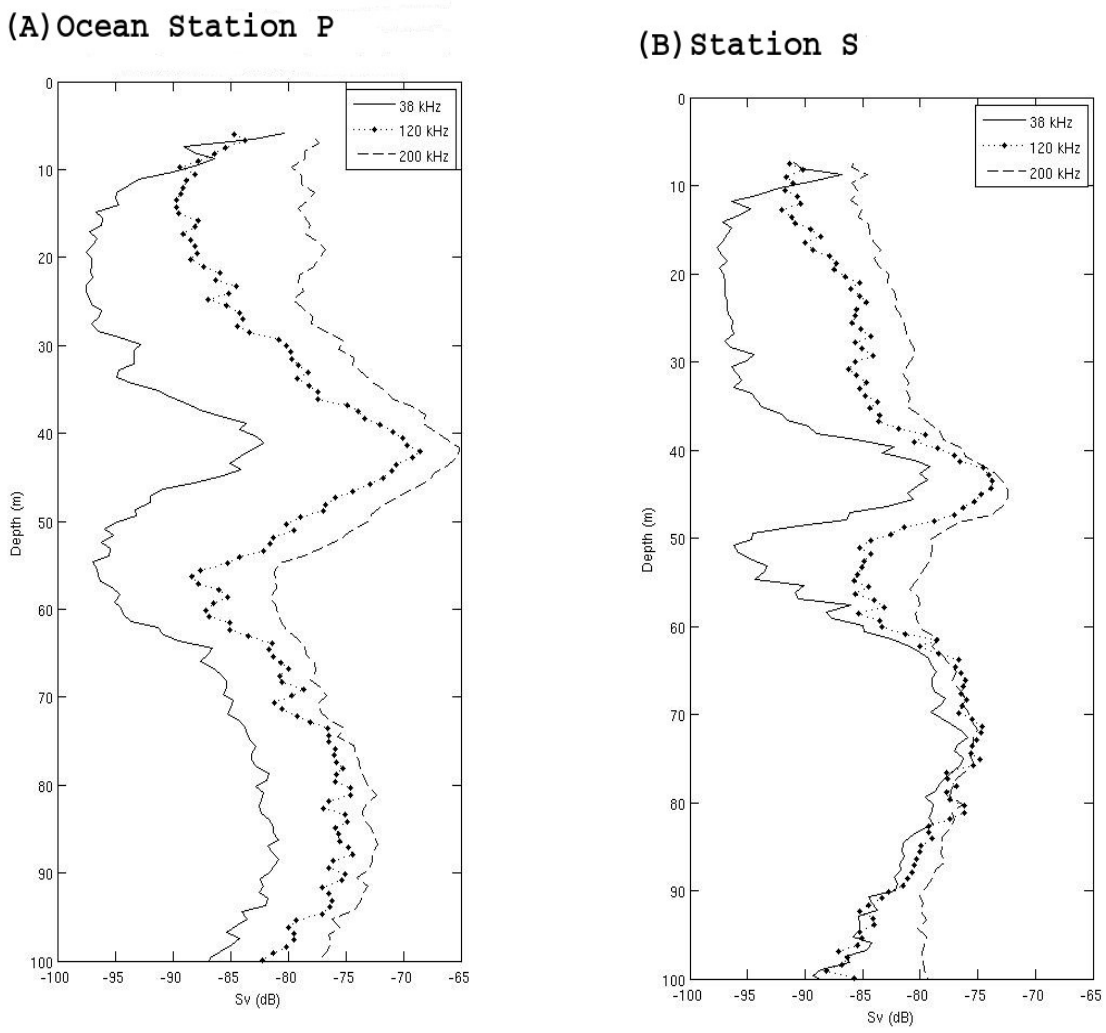

Figure 3.2. Profiles of volume-backscattering strength from 6 to 100 m, showing near-surface and migrating zooplankton layers. Profiles in (A) are from Ocean Station P, June 06 2007 at 0645 UTC during dusk ascent, and profiles in (B) are from Station S, June 10, 2007 at 0635 UTC during dusk ascent. A surface zooplankton layer occupies the 30-50 m depth interval. The migration layer is observed between 70 and 100 m in (A) and between 60 and 90 m in (B). Volume scattering strength increases with frequency in both (A) and (B) profiles in the surface zooplankton layer. In the migrating layer, there is an increase of Sv with frequency at Ocean Station P (A), but not at Station S (B).

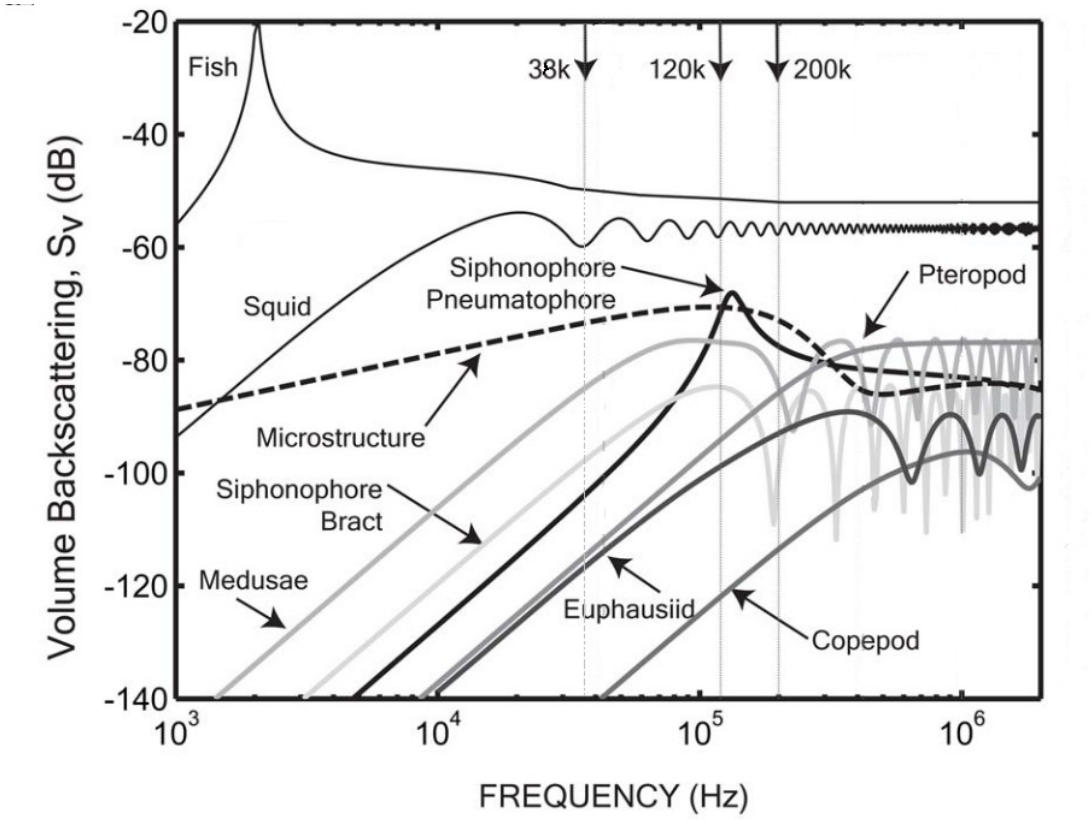

Figure 3.3. Scattering model of volume backscattering as a function of frequency for different biological scatterers, assuming a numerical abundance of 1 organism/m^3. Mean lengths used for the organisms of interest are: copepod = 1.53 mm, euphausiid = 9.79 mm, fish = 1 cm diam swim-bladder, squid = 90 mm, medusae = 16.53 mm. Modified from Lavery et al. (2007).

3.1.2 Migratory layer

The thickness of the migratory layer varied between 25 and 90 m. An increase in volume-backscattering strength with acoustic frequency was observed (figure 3.2), consistent with the acoustic signature of euphausiids (figure 3.3), but was neither as pronounced nor as consistent as the near-surface backscattering layer. The maximum volume-backscattering was approximately -73 dB and -74 dB at 200 kHz and 120 kHz, respectively, decreasing to approximately -81 dB at 38 kHz. Volume-backscattering values at 200 and 120 kHz were frequently overlapping (especially at Station S, figure 3.2b), suggesting that species other than euphausiids and copepods were present and sometimes dominated the acoustic signal. Previous studies have found a number of other species in the water column at OSP that are also present in the migratory layer along with euphausiids. For instance, the pteropod *Limacina helicina* is known to be a strong acoustic scatterer (Trevorrow, 2005) but its biomass was very low in our net tows (0.1 % of total biomass). Chaetognaths (E*ukhronia hamata, Sagitta elegans, Parasagitta scrippsae*) constituted 19.6 % of total biomass in our net tow and are known to exhibit daily vertical migration between 250 to 150 m and the surface (Goldblatt et al., 1999; Mackas et al., 2005), but are unlikely to contribute significantly to the scattering signal due to their gelatinous bodies (Trevorrow, 2005).

Myctophid fish are more likely to contribute to the backscattering signal in the migratory layer. Myctophids have been observed at Ocean Station P in the migratory layer along with zooplankton upon which they feed (Moku et al., 2000). They are known to migrate daily as well (Yatsu et al., 2005). A mixed migrating layer including both euphausiids and myctophids would explain why the acoustic signal does not consistently increase with frequency, as is more typical of fish backscattering (figure 3.3). However, it is unlikely that myctophids alone constitute the migratory layer. Trevorrow (2005) estimates a target strength ranging from -65.9 to -56.3 dB for myctophids which, using (3.1), would lead to an abundance of 0.2 to 0.02 individuals m^{-3} if the acoustic layer was composed only of myctophids. In this case, the backscattering layer would be granular as we would be able

to distinguish individual targets, which is not the case in our acoustic data at Ocean Station P and Station S where the acoustic signal is very smooth, characteristic of overlapping targets. Trevorrow (2005) analyzed acoustic data at OSP and concluded that the -72.7 dB (at 200 kHz) volume-backscattering strength that they observed between the 15-30 m depth was caused by both euphausiids and myctophids. They obtained an abundance of 0.03 m^{-3} for myctophids and 3.5 m^{-3} for euphausiids in this layer. Marlowe and Miller (1975) also found euphausiids abundances of 1-10 m^{-3} in their net tows during night surface sampling (0-100 m) using 70-cm opening-closing nets. However, it is likely that their net size (0.7-m diameter) undersampled euphausiids.

At Station S, the zooplankton community composition differed from that at Ocean Station P. Two migratory layers were observed in time-series *OSPJun11Dawn* (figure 3.4) with their descents starting approximately 40 minutes apart. The first descending aggregation (Z1) was much thicker than the second, exceeding 100 m at times. This aggregation started descending at approximately 1220 UTC to depths exceeding 250 m. The second backscattering layer (Z2) was 25-30 m thick and descended at a slower rate than the Z1 layer. It started descending at approximately 1300 UTC, settling at 180-m depth. This difference in migration timing between the two aggregations could be explained by a difference in the size of the individuals composing the two layers. Larger individuals are more visible to visual predators and their migration behaviour might differ from smaller individuals. Presence of predators within one of the aggregations could also contribute to modifying the migration behaviour.

In terms of migration timing, depth of migration and acoustic behaviour, layer Z1 shares the same characteristics as the migrating layer observed at Ocean Station P. It showed no increase in volume-backscattering intensity with increasing frequency (figure 3.5a), suggesting that the acoustic signal here is not dominated solely by euphausiids and that myctophids might be present as well. The acoustic signal of the Z2 layer increased with increasing frequency (figure 3.5b), suggesting that it could be dominated by euphausiids or other types of zooplankton such as copepods or pteropods. Using our observed

volume-backscattering value at 200 kHz (-68 dB) and a target strength of -79.8 dB for euphausiids (Trevorrow, 2005), we obtain an abundance in the Z2 migrating layer of 12.6 m^{-3}, in good agreement with Marlowe and Miller (1975) (1-10 m^{-3}).

3.2 Swimming speed and turbulence

Migration rates were estimated from the acoustic backscattering data. A minimum threshold was applied to exclude all data outside the migratory layer (figure 3.6). A best linear fit to the migration curve was determined and used to estimate the migration rate. At OSP, the average upward migration speed was 4.4 cm/s.

The Reynolds number, Re, represents the ratio of viscous to inertial forces and is used to indicate the ability of a medium (or an organism in the present case) to be the source of turbulent mixing. It is defined as:

$$Re = \frac{uL}{\nu} \tag{3.2}$$

where u is velocity, L a representative length-scale and $\nu = 1.0 \times 10^{-6}$ m^2 s^{-1} the molecualr viscosity (Apel, 1988). The Reynolds number indicates the range of scales of turbulence in the flow. The higher the Reynolds number, the greater the range of scales. Three-dimensional turbulent energy typically cascades from the largest to the smallest scale, where kinetic energy is damped by viscosity and dissipated (Thorpe, 2005). Experiments on flows through a pipe suggest a value of $O(10^3)$ as the "transition" Reynolds number, where the flow behaviour goes from laminar to turbulent (Whitehead and Wang, 2008; Engineering Toolbox 2009).

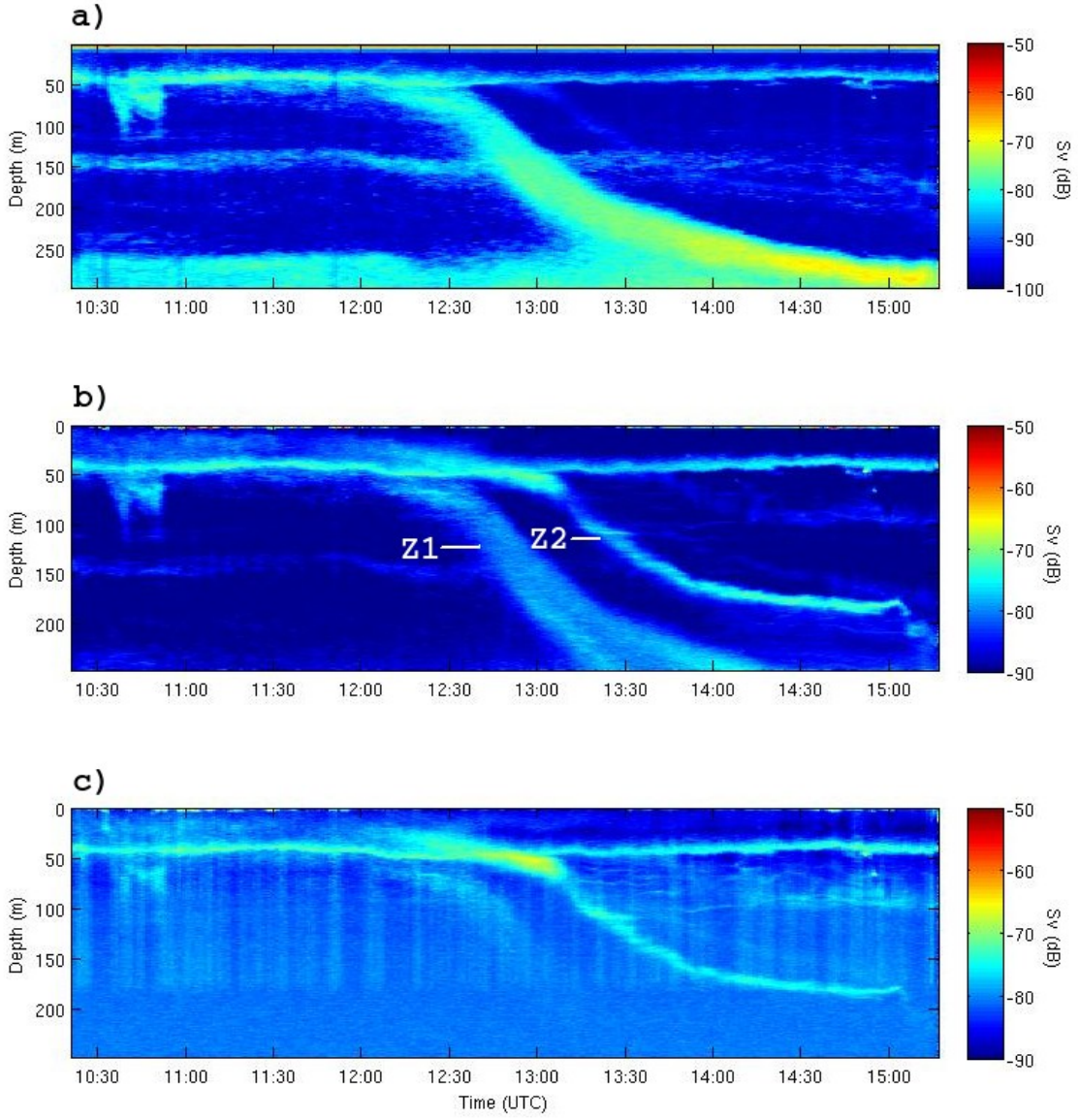

Figure 3.4. Acoustic backscatter at Station S, 177 km south of Ocean Station P, sampled on June 11, 2007 during dawn descent. Sunrise is at 1331 UTC. Shown at frequencies (a) 38, (b) 120, (c) 200 kHz. Two distinct migrating layers are present in addition to the non-migrating surface layer. Layer labeled Z1 (b) migrates downward first, followed by layer Z2 approximately 40 minutes later. Volume-backscattering strength of layer Z1 decreases with increasing frequency, whereas it increases with frequency in layer Z2.

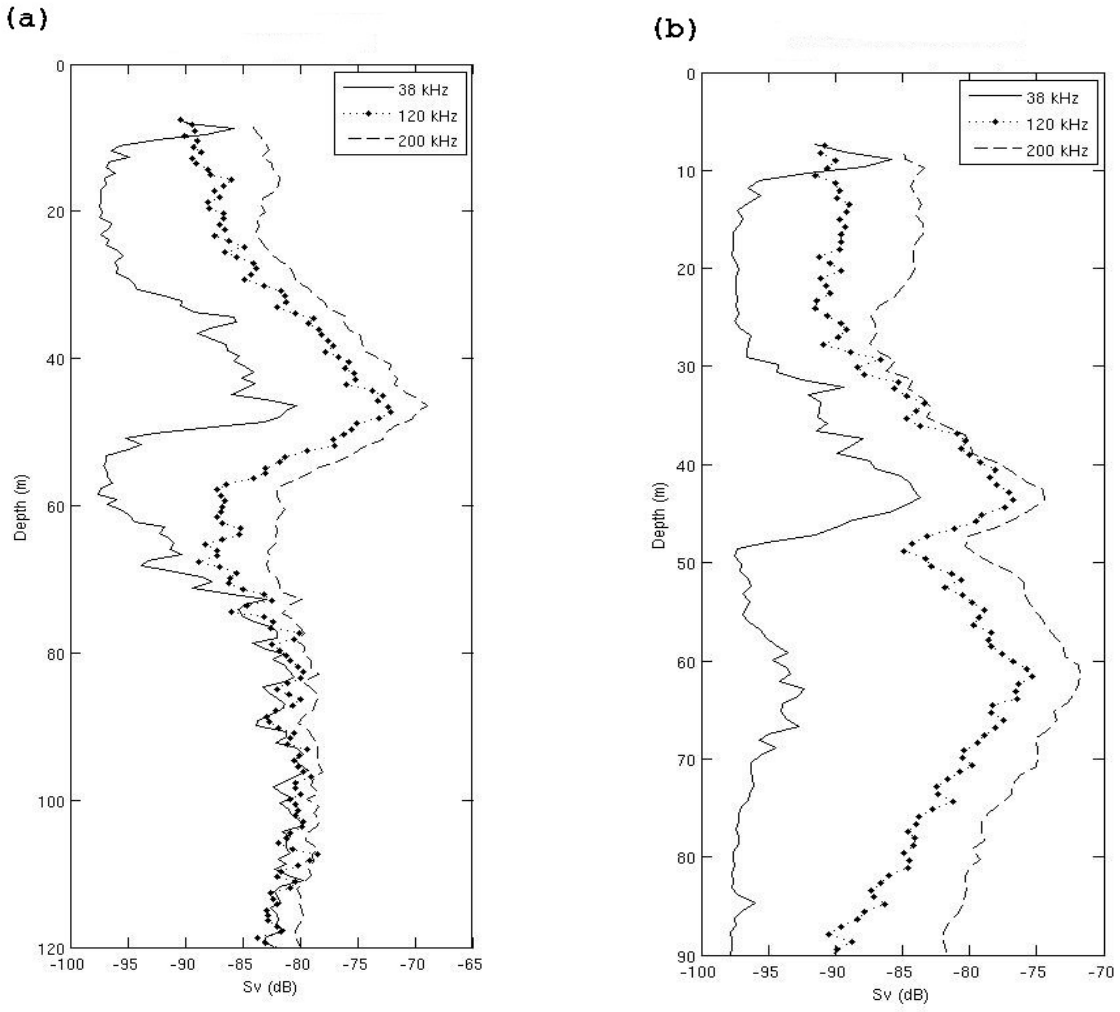

Figure 3.5. Profiles of volume scattering strength at Station S during dawn descent at 38, 120 and 200 kHz. (a) One-minute-averaged profile at 1244 UTC showing the surface layer between 30 and 50 m and the first migrating layer (Z1) between 80 and 120 m. (b) One-minute-averaged profile at 1307 UTC showing the surface layer between 35 and 50 m and the second migrating layer (Z2) between 50 and 70 m.

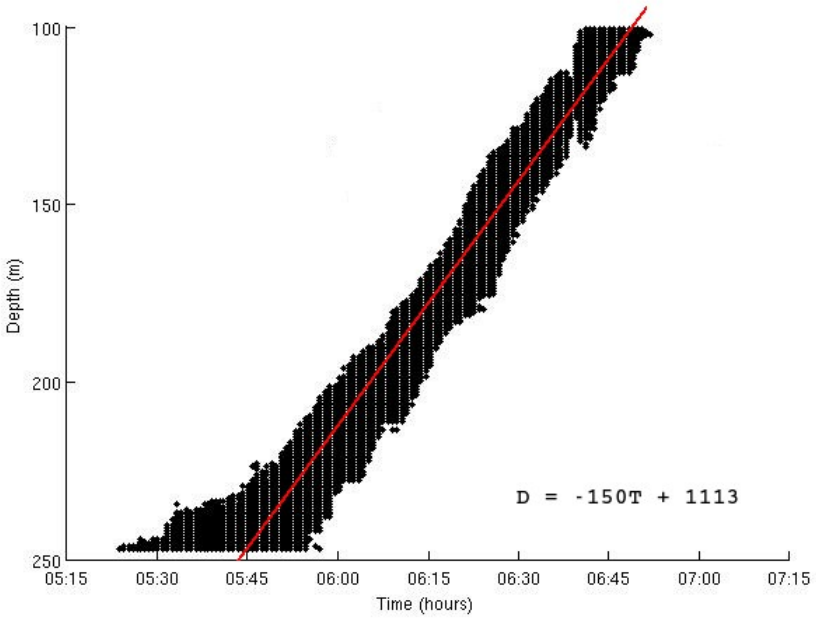

Figure 3.6. Migration rate determined using the volume-scattering strength with a threshold of -80 dB for the time-series *OSPJun06Dusk*. Volume backscattering data is averaged over 1 minute and 1 meter. In the equation shown, D is in meters and T in hours, corresponding to a swimming speed of 4.2 cm/s.

Huntley and Zhou (2004) related the Reynolds numbers associated with swimming marine organisms to their mass as:

$$Re_c = 1.46 \times 10^5 M^{0.63} \quad (3.3)$$

at cruising speed and

$$Re_e = 6.69 \times 10^5 M^{0.52} \quad (3.4)$$

at escape speed (Huntley and Zhou, 2004). These relations hold for organisms of mass ranging from 5.2×10^{-16} kg (bacteria *Escherichia coli*) to 6.4×10^4 kg (blue whale). Using a transition Reynolds number of 10^3, they find that, at cruising speed, the transition to

turbulence occurs for animals in the size range of small fishes and large crustaceans (M ~ 10^{-3} kg) whereas, at escape speed, the transition Reynolds number applies to animals with a body mass two orders of magnitude smaller, such as large copepods, euphausiids and larval fish (M ~ 10^{-5} kg).

Here, we estimate Reynolds numbers for euphausiids and myctophids. The migration rate is not representative of the instantaneous swimming speed of these organisms but of the overall movement upward of the aggregation, so is not used in the Reynolds number estimates. Typical swimming speeds of 5-10 cm/s have been observed for euphausiids (De Robertis et al., 2003). The average length of the main euphausiid found in our net tow (*T. inspinata*) is 1.71 cm, resulting in a Reynolds number ranging from 855 to 1710. This represents a higher range as euphausiids are frequently found to swim at speeds ranging from 0 to 5 cm/s, even during dusk ascent (De Robertis et al., 2003). Myctophids found at OSP are commonly 20-60 mm in length depending on their age (Trevorrow, 2005). Trevorrow (2005) finds an average length of 28 mm to be the best fit to his acoustical analysis for myctophid length at Station P. Here we use a swimming speed of 2.8 cm/s (Baird, 1995) for myctophids, corresponding to one body length per second, leading to a Reynolds number of 855. This likely represents a lower range value, corresponding to myctophids' cruising speed.

3.3 Physical characteristics

The water column at Ocean Station P and Station S is characterized by two pycnoclines (figure 3.7). At 50 m, a seasonal thermocline forms in spring due to increased solar radiation. A permanent pycnocline regulated by salinity lies between 100 and 120 m. A temperature inversion is observed between 50 and 100 m, where a layer of cold water overlies warmer, saltier water underneath. This layer is the remnant of the winter mixed-layer from the previous winter (Ueno et al., 2007).

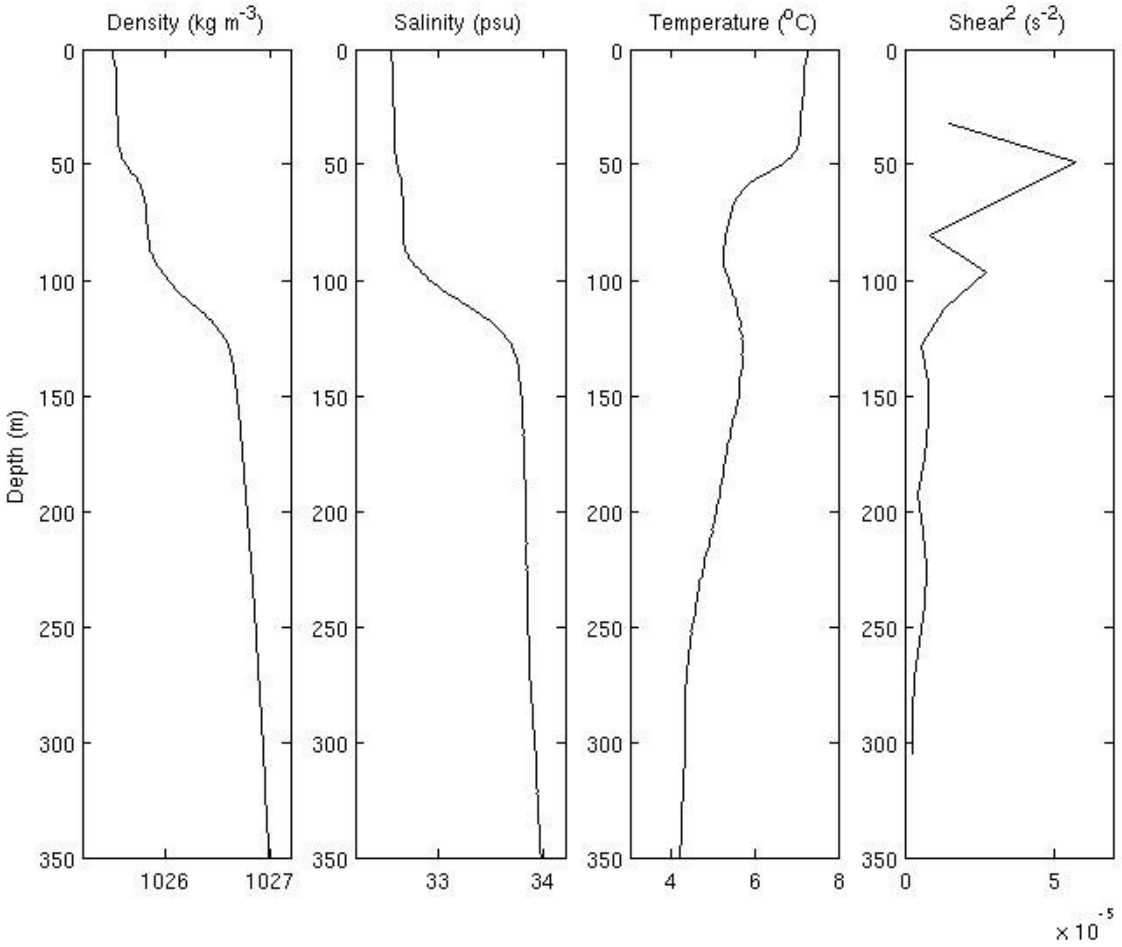

Figure 3.7. Density, salinity and temperature profiles averaged over the entire Ocean Station P and Station S datasets, between June 06 to 11 2007. The last profile on the right is the shear obtained from the hull-mounted ADCP and also averaged over the entire datasets.

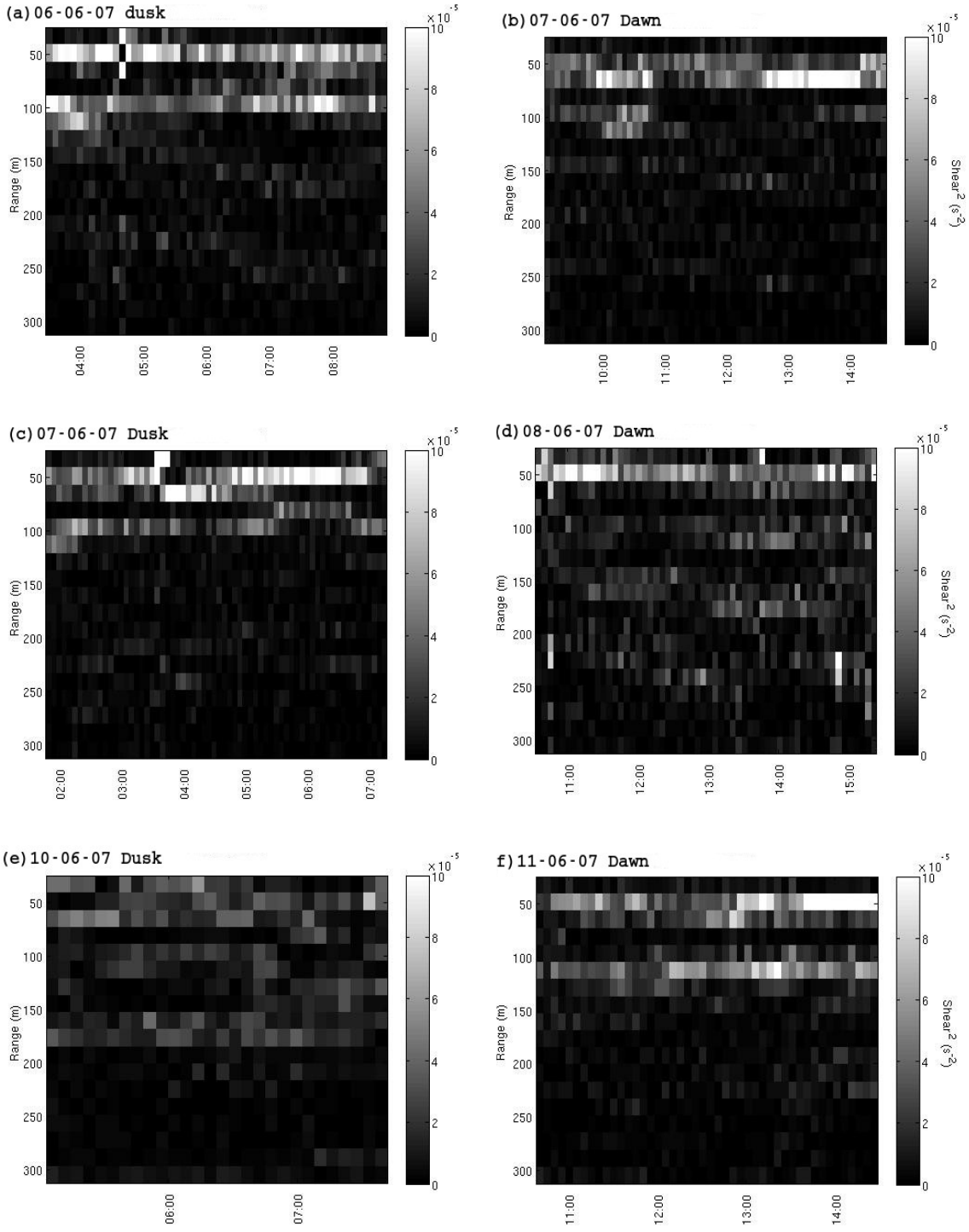

Figure 3.8. Hull-mounted ADCP 16-m shear variance at Ocean Station P (a-d) and Station S (e-f). Data was temporally averaged over 5 minutes. Time on the horizontal axis is in UTC.

The ADCP shear reveals two main features at Ocean Station P and Station S (figure 3.8). The highest shear (~10 x 10^{-3} s^{-1}) was consistently observed in the 48- and 64-m depth bins, which correspond to the depth of the seasonal thermocline. A second region of high shear (~7 x 10^{-3} s^{-1}) was observed in the 96- and 112-m depth bins, which corresponds to the top of the permanent pycnocline.

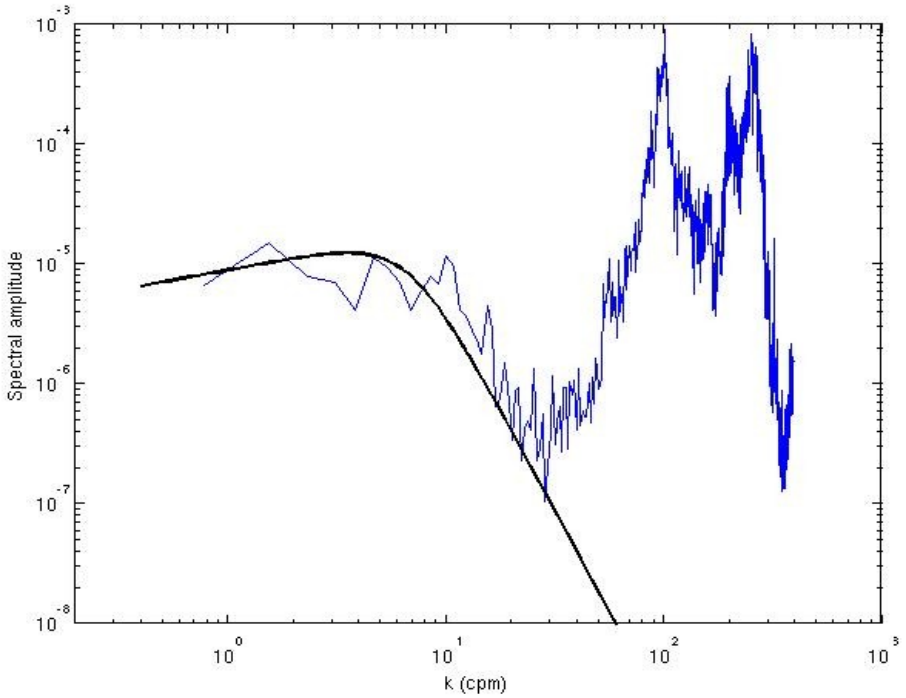

Figure 3.9. Example of shear spectrum at Ocean Station P, time-series *OSPJun11Dawn*, profile 53. Depth interval is from 57 to 61 m. This spectrum corresponds to a dissipation rate of 1.16 x 10^{-9} W kg^{-1}. The black line represents the shape of the equivalent Nasmyth spectrum. At k > 30 cpm, noise, most likely due to instrument vibration, dominates the signal.

Dissipation rates at Ocean Station P and Station S rarely exceeded 10^{-8} W kg^{-1}. The background turbulence level was 10^{-10} W kg^{-1}. A 10^{-11} W kg^{-1} noise level was chosen from the lowest values in our time-series. At high dissipation rate, microstructure shear spectra match the universal spectrum both at high and low wavenumber, covering vertical scales

ranging from 0.02 to 1 m (figure 3.9). This result differs from that of Gregg and Horne (2009) for which the shear spectra at low wavenumber within fish aggregations did not correspond to the universal spectrum. Microstructure temperature spectra are well-correlated with theoretical Batchelor (1959) spectra between 0.02 and 1 m (figure 3.10).

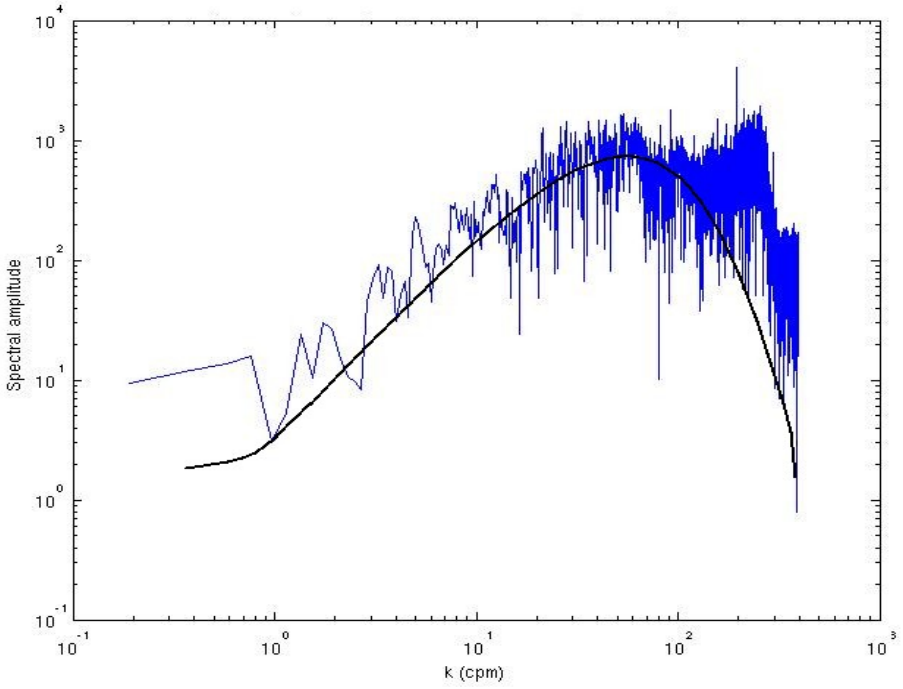

Figure 3.10. Example of temperature gradient spectrum at Ocean Station P, time-series *OSPJun11Dawn*, profile 53. Depth interval is 111 to 115 m. The black line is an approximation of the shape of the equivalent Batchelor spectrum. Noise is observed in the signal at k > 100.

We compared estimates of variables derived from microstructure shear and temperature gradient. Dissipation rate estimates can be obtained from both variables through two different methods (fitting spectra to the Nasmyth and Batchelor spectra, respectively) which both require several assumptions about the structure of the turbulence at small scales (such as isotropy) (Kokcsis et al., 1999) that cannot always be verified. A comparison between the two variables (shear and temperature-gradient) is a good indication of the validity of our estimates of dissipation rate.

Since the microthermistor data do not resolve the high-wavenumber rolloff, the temperature variance dissipation rate χ_T cannot be estimated without assumptions so a proxy for χ_T (χ'_T), the rate of loss of temperature variance, was estimated using the microstructure temperature data (Thorpe, 2005):

$$\chi'_T = 6\,\kappa_T \left\langle \frac{dT^2}{dz} \right\rangle \tag{3.5}$$

where κ_T is the molecular thermal diffusivity coefficient (1.4 x 10^{-7} m^2 s^{-1}, Thorpe 2005). Microstructure temperature was averaged over 2 cm before calculating the temperature gradient. The temperature sensors sample at a scale of 0.25 cm, but the spectra were well resolved down to a scale of 2 cm. χ_T is the only adjustable parameter in the calculation of the turbulent kinetic energy dissipation using the Batchelor method (Batchelor, 1959; Dillon and Caldwell, 1980).

A significant Spearman correlation coefficient was found between χ'_T and the kinetic energy dissipation rate ε in both datasets (significance $p < 0.05$, figure 3.11). In other words, high dissipation rates coincided with high microstructure temperature gradients in contrast to the findings of Gregg and Horne (2009) for aggregations of small fish.

Turbulent mixing in the surface mixed-layer can originate externally from the sea surface or internally from below. From the sea surface, energy for turbulence is driven by winds and surface buoyancy flux. Shear within or at the base of the mixed-layer, and breaking internal waves at the base of the mixed layer, introduce energy from below (Thorpe, 2005). The pycnocline is a region of strong density gradient, separating the surface mixed-layer from the deep water below. Diffusivities of 1.1 x 10^{-5} m^2 s^{-1} (Ledwell et al., 1993) and 5 x 10^{-6} m^2 s^{-1} (Gregg et al., 1989) have been reported in the highly stratified pycnocline and thermocline below the surface mixed-layer. The surface mixed layer,

however, is intermittently highly turbulent with diapycnal diffusivities that can reach 10^{-2} m^2 s^{-1} (DeSzoeke and Springer, 2003). In the deep ocean, observations support a diapycnal diffusivity of 10^{-5} m^2 s^{-1} (Moum and Osborn, 1986; Gregg, 1987).

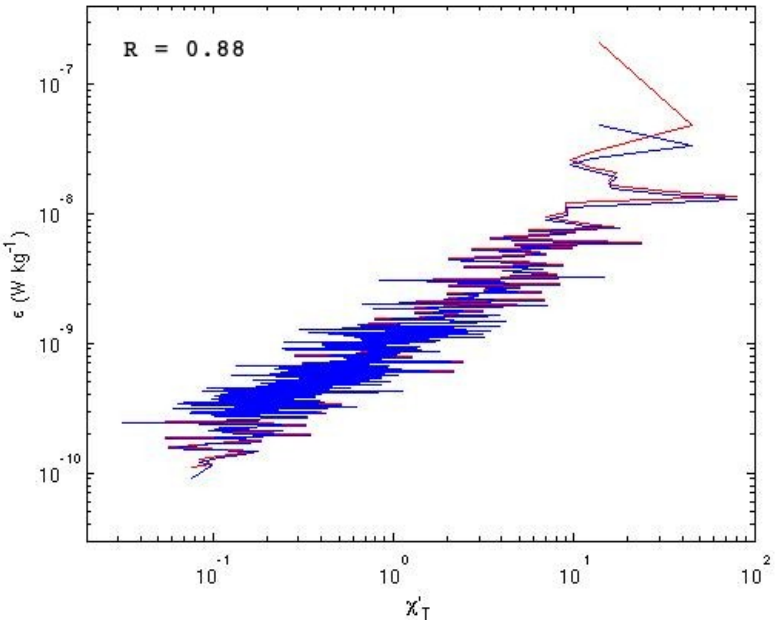

Figure 3.11. Correlation between χ'_T and the kinetic energy dissipation rate ε for the entire Ocean Station P and Station S datasets. Data outside the 45-250 m interval were excluded. Red and blue lines represent the upper and lower limits of the 68 % confidence interval, respectively, corresponding to one standard deviation.

We calculate a value for the diapycnal diffusivity K_ρ

$$K_\rho = \frac{\Gamma \varepsilon}{N^2} \tag{3.6}$$

where Γ is the so-called mixing efficiency, here assumed to be 0.2 (Osborn, 1980; Oakey, 1982). Mean diapycnal diffusivity in the 20-50 m surface mixed layer is 1.87 x 10^{-2} m^2 s^{-1}. Below 50 m, diapycnal diffusivities are several orders of magnitude smaller (5-8 x 10^{-6} m^2 s^{-1}). Values are slightly lower (1.26 x 10^{-6} m^2 s^{-1}) within the permanent halocline

(figure 3.12). Our dissipation rates are not proportional to the buoyancy frequency as is often the case in the open-ocean (Gregg and Sanford, 1988), thus K_ρ is not independent of N in this dataset.

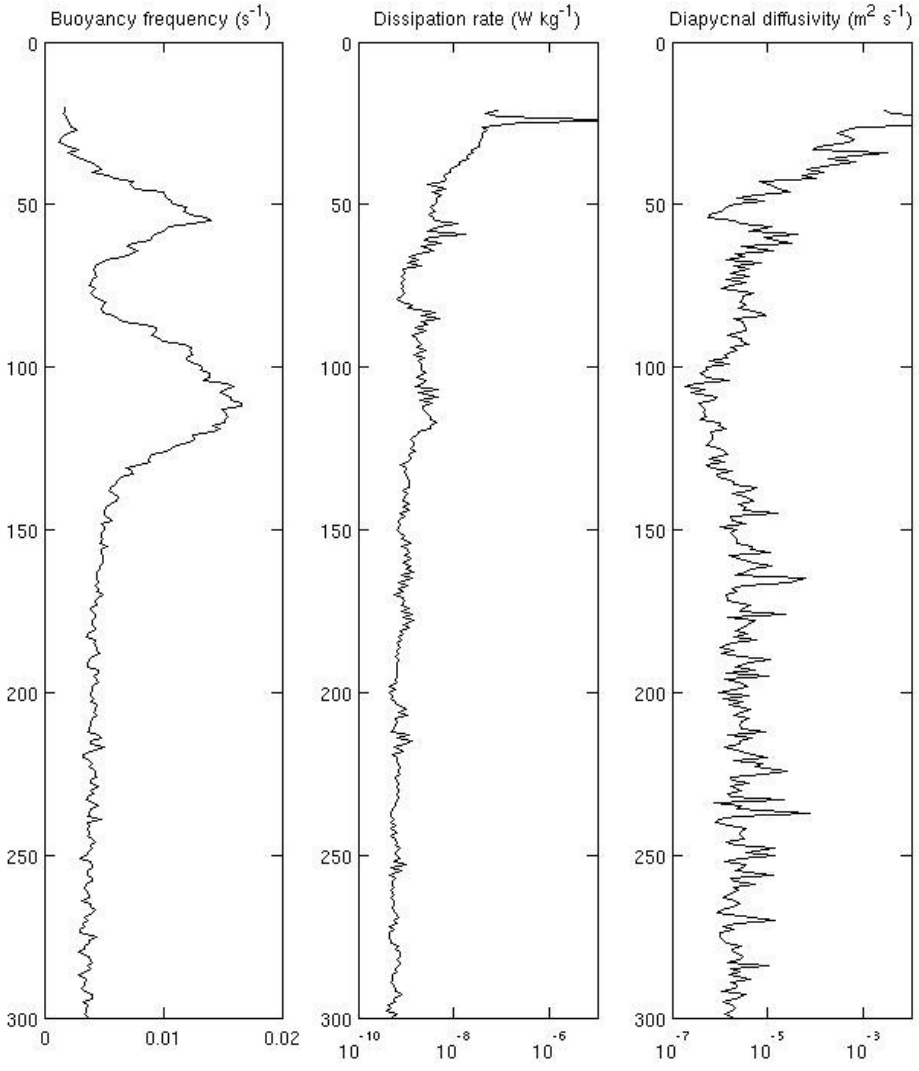

Figure 3.12. Buoyancy frequency, dissipation rate and diapycnal diffusivity profiles at Ocean Station P and Station S using mean value of the entire datasets at each meter. Diapycnal diffusivity is calculated from the averaged buoyancy frequency and dissipation rate profiles.

Diapycnal diffusivities were similar inside and outside the migratory layer (3.6 x 10^{-6} and 4.2 x 10^{-6} m^2 s^{-1}, respectively), but were orders of magnitude higher in the near-surface zooplankton layer (1.3 x 10^{-2} m^2 s^{-1}) (figure 3.13). This increased diapycnal diffusivity is likely due to surface processes rather than swimming zooplankton.

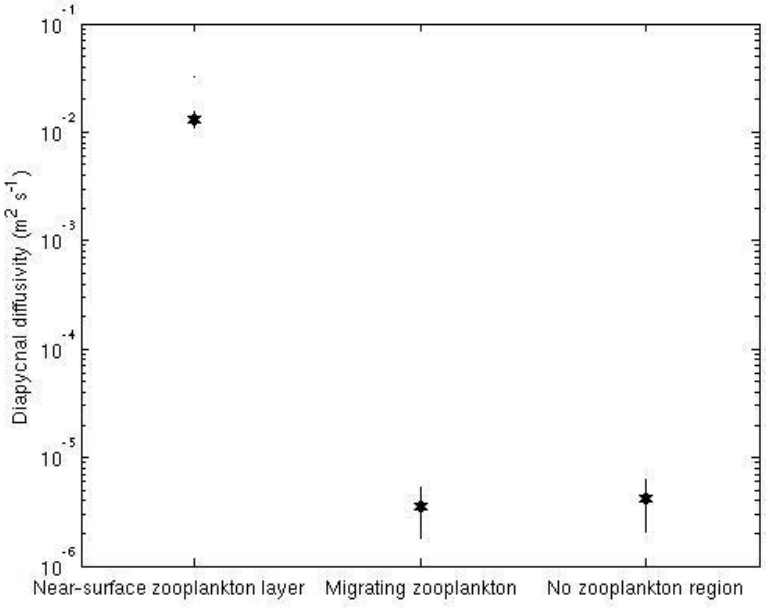

Figure 3.13. Diapycnal diffusivities per region at Ocean Station P and Station S. Each star is the mean diffusivity within one given region. Error bars represent the standard deviation of the resulting mean for each time-series. *Near-surface zooplankton layer* includes the depth interval from 20 to 60 m. *Migrating zooplankton* and *No zooplankton region* are located within the 60-250 m depth range.

3.4 Dissipation rates outside and inside the migratory layer

In order to compare mean dissipation rates outside and inside zooplankton aggregations, the water column was separated into three regions and the dissipation rate distributions within them were compared. The “Surface Layer” (SL) encompasses the 20-60 m depth range, including the non-migrating surface zooplankton layer but excluding the migratory layer. The “Migratory Layer” (ML) encompasses the depth interval ranging from 60 to 250 m, which includes the migratory layer. Finally, the “No Zooplankton” layer (NZ) encompasses the depth range from 60-250 m but includes only those areas of the water column where no zooplankton were detected by the echosounder.

Probability density functions of the dissipation rate were not log-normal (figure 3.14), in contradiction with lognormal theory proposed by Gurvich and Yaglom (1967). Yamazaki and Lueck (1990) give a brief review of the lognormal theory. Two critical assumptions were made in Gurvich and Yaglom's theory: dissipation rates must be identically distributed (statistically homogeneous) and mutually independent. Identically distributed means that the data must come from a single population, i.e. the observed turbulence must be caused by a single process. This assumption conflicts with our initial hypothesis of krill-generated turbulence. In addition, most of our probability density functions encompass at least partially a region of high temperature or density gradient, as the regions were determined following zooplankton presence/absence rather than water characteristics. Thus, the condition of statistical homogeneity is not satisfied. In addition, as pointed out by Yamazaki and Lueck (1990), the mutual independence condition fails at small scales in all situations.

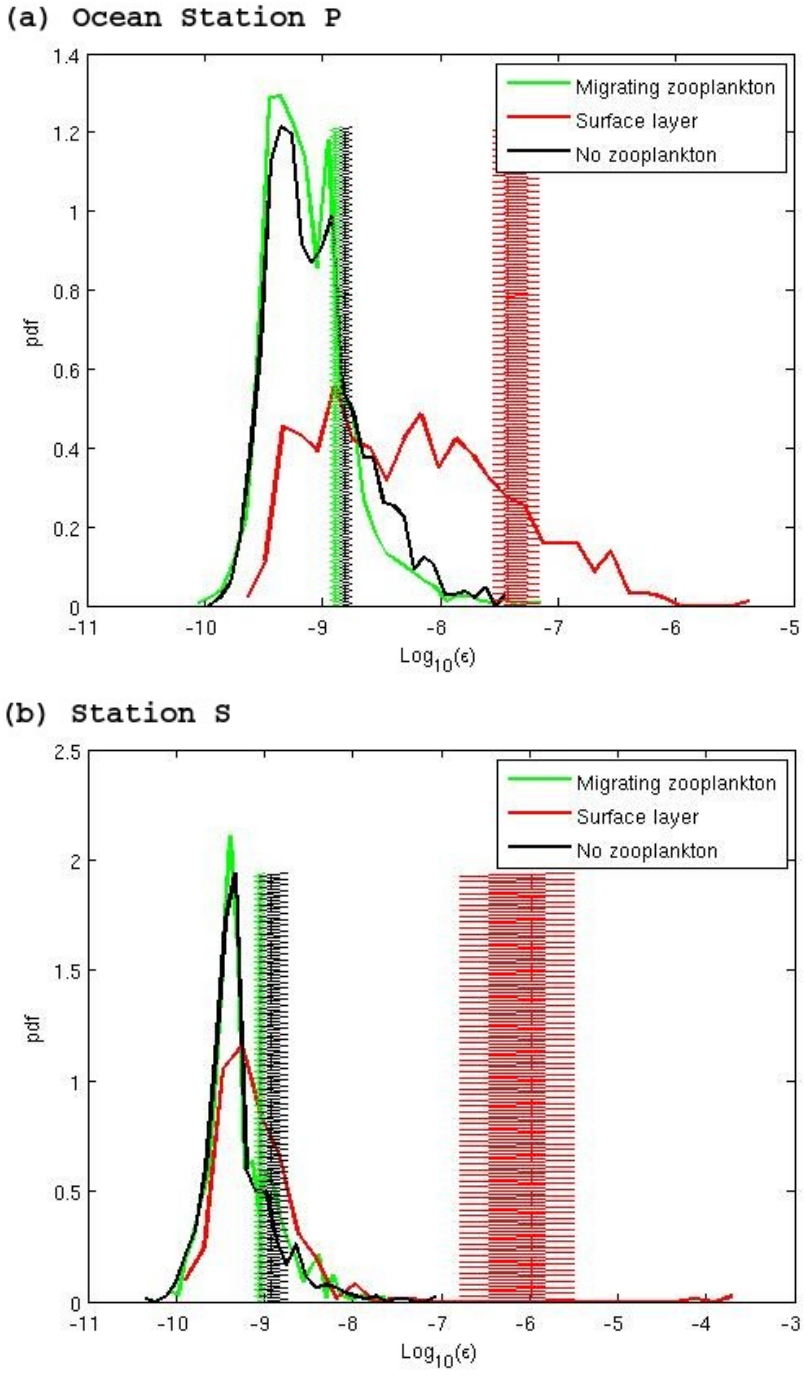

Fig 3.14. Probability density functions of the dissipation rate for the entire time series at (a) Ocean Station P and (b) Station S, differentiating between the surface layer (20-60 m), and the regions including and excluding the migration layer(s) (60-250 m). June 06-11

2007. Vertical columns represent 95% bootstrap confidence interval.

Confidence intervals were calculated at 95% using the bootstrap method with 1000 iterations. Probability density functions (figure 3.14) show that, at both Ocean Station P and Station S, dissipation rates within and outside the migration layer are not significantly different, and that these two regions have dissipation rates significantly lower than those in the surface layer. Mean dissipation rates above 60 m are highly variable (table A2.1.2) but are consistently 1 to 4 orders of magnitude higher than the two other regions (both located between 60 and 250 m). Higher dissipation rates in this region are likely caused by near-surface processes such as wind-generated mixing and surface cooling/heating. No pattern was observed in the standard deviations and skewness of the distributions (table A2.1.3).

In two of the time-series (*OSPJun07Dusk, SSJun11Dawn,* table A2.1.2), no significant difference was observed between the SL and the ML and NZ layers. In these time-series, the mean dissipation rate was much lower in the surface layer than in the remaining time-series (table A2.1.2), suggesting that atmospherically-forced turbulence was low during this period. The migrating zooplankton region was never significantly higher than any of the two regions in all the time-series.

3.5 Correlating acoustic intensity and shear to dissipation rate

Correlations between dissipation rate, volume-backscattering strength and 16-m shear were examined to understand to what extent swimming zoooplankton and internal wave shear contribute to diapycnal mixing in the open ocean.

Volume-backscattering strength from the 120-kHz frequency of the EK60 echosounder was used for the correlations. Backscattering data were averaged temporally over one minute, and vertically over 2 meters. Shear data (from the ADCP) were averaged over

five minutes since a one-minute average was still overly noisy. With a vertical resolution of 16 m, ADCP shear data were not averaged spatially. Only the time interval covering the migration period was considered in the statistics. Data were analyzed statistically between the depth intervals of 15 to 250 m, differentiating between the 15-60 m and 60-250 m depth ranges. Data were sorted in order of increasing dissipation rate before averaging over 10 datapoints. The Spearman coefficient of correlation was used. This is the non-parametric equivalent of the Pearson coefficient of correlation and uses ranks instead of numerical values to perform the test. The assumptions for the parametric test are (i) linearity of the relation between the variables and (ii) normality of the variables. In the present case, although the condition for linearity of the relations was generally met, the dissipation rate distributions did not satisfy the condition for normality. Spearman's rank correlation coefficient is calculated as follows:

$$r = 1 - \frac{6 \Sigma d_i^2}{n(n^2 - 1)}$$

where

$d_i = x_i - y_i$ is the difference between the ranks of the corresponding values X_i and Y_i (Wolfram MathWorld, 2009).

Statistical analyses showed a significant correlation ($p < 0.05$, $r = 0.3$ to 0.8) between dissipation rate and 16-m shear below 60 m at Ocean Station Papa and Station S (figure 3.15, table A2.1.4). This correlation increases ($r = 0.5$ to 0.8) when the 15-60 m surface layer is included.

A good correlation can also be seen between dissipation rate and scattering volume in many of the scatterplots (figures A2.1.2, A2.1.3). However, this correlation occurs mainly in the surface region where high dissipation rate, high shear and strong backscattering are all coincident. Below 60 m, the correlation between volume backscattering and dissipation rate never exceed $r = 0.4$ (table A2.1.4), suggesting that we can identify no

unambiguous turbulence events generated by marine organisms at Ocean Station P.

Lagged correlations were analyzed statistically as well. A direct correlation between dissipation rate and backscattering may be biased by the mismatch between the occurrence of turbulence and the source location if the source is an isolated target moving with time, such as a marine organism. High dissipation rates will be detected in the wake of the swimming organism instead of the organism's location at the time of measurement. Thus, decaying turbulence can still be detected without its matching source if the source has moved. A turbulent event could therefore be detected by the VMP minutes after it was initiated, and a correlation would not be observed between the location of the turbulence event and the zooplankton aggregation at a given time. Averaging the data over time and space is likely to decrease this bias but it could also attenuate the volume-backscattering in the case of isolated targets. The fact that we are dealing with aggregations instead of isolated targets reduces the likelihood of such a mismatch.

The time that it takes for turbulence to dissipate depends upon the energy input, the scale of the turbulent patch, the Richardson number and ultimately the kinematic viscosity (Tennekes and Lumley, 1972; Venayagamoorthy and Stretch, 2006; Hwang et al., 2006). In a stratified fluid, it also depends on the buoyancy frequency. According to Venayagamoorthy and Stretch (2006), mixing rates and overturning motions tend to become insignificant at times longer than one to two buoyancy periods. To account for decaying turbulence, we performed another set of correlations and used one buoyancy period as the upper time lag to which a turbulence event can last. For each dissipation rate value, we selected the highest volume backscattering strength within a buoyancy period $2\pi/N$.

Overall, the resulting lagged correlations did not result in stronger correlations (table A2.1.4) and do not suggest an unambiguous relation between swimming zooplankton and turbulence. This is in agreement with the relatively low abundance (compared to Saanich Inlet) of marine organisms present at the study site and suggests that finescale shear is

responsible for the observed turbulence at Ocean Station P and Station S. Biologically-generated turbulence at these sites was not evident in our data.

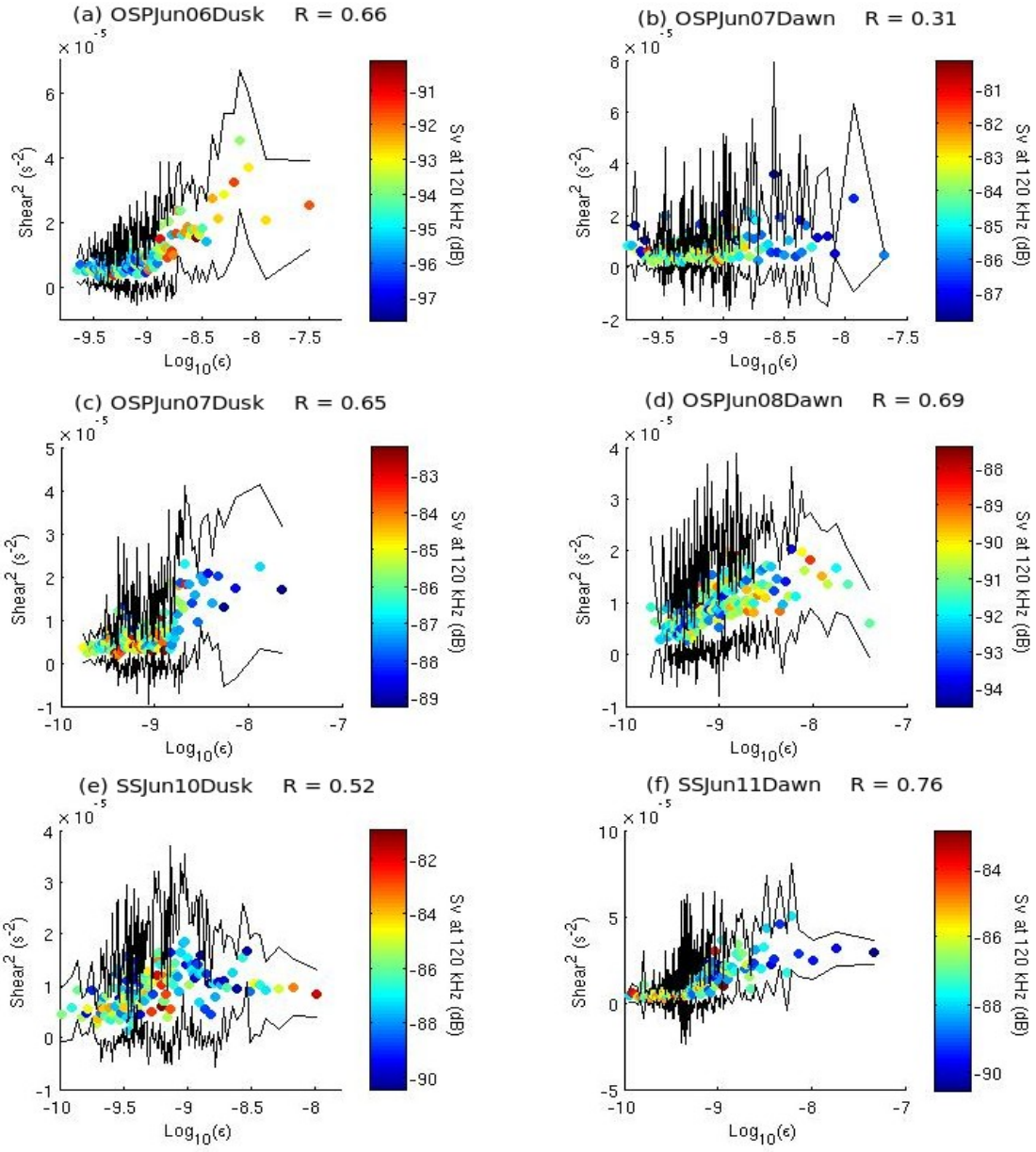

Figure 3.15. Scatterplots showing dissipation rate as a function of 16-m shear (Y-axis) and volume-scattering strength (colorbar), excluding the surface layer above 60 m and below 250 m for all time-series collected at Ocean Station P (a-d) and Station S (e-f) between June 06-11, 2007. p = 0.00 for all time-series. Black lines are the upper and

lower limit of the 68 % confidence interval, corresponding to one standard deviation. See figure A2.1.4 for correlations between volume-backscattering and shear in the surface layer (20-60 m).

It appears that, at Ocean Station P and Station S, the observed turbulence values were not correlated with the presence of swimming organisms. Turbulence events were positively correlated with the surface layer (20-60 m), as well as regions of high shear. Turbulence in the upper ocean likely originates from surface processes such as wind shear and cooling. High-shear at ~50 m and ~ 100 m is the likely source of turbulence at depth as can be observed in the correlations (figure 3.15) as well as in figure A2.1.1 where higher turbulence is consistently observed around 100-m depth. This strongly suggests that turbulence at Ocean Station P and Station S is driven by fine-scale shear.

Chapter 4
Results and Analysis: Saanich Inlet

Profile time-series of microstructure dissipation rate ε and acoustic backscatter were collected over 11 dawns and dusks in Saanich Inlet during June 2006, May 2007 and May 2008. Data were analyzed using methods described in the previous chapter. Two time-series collected during April 2005 by Kunze et al. (2006) were likewise re-analyzed and some of the statistical results are mentioned in this chapter. ADCP current shear measurements were collected during May 2008 and are used to diagnose the absence of shear-related turbulence in the inlet.

4.1 Physical characteristics

The upper water column in Saanich Inlet is characterized by a strong pycnocline extending from the near-surface to approximately 20 m, and a halocline extending from 60 to 80 m (figure 4.1). Buoyancy frequency is of approximately 2 x 10^{-2} s^{-1} in the surface pycnocline between 20 and 80 m, and about 1 x 10^{-2} s^{-1} between 80 and 120 m (figure 4.1). Diapycnal diffusivities, assuming a 0.2 mixing efficiency, average 1.1 x 10^{-5} m^2 s^{-1} between 20 and 80 m and decrease to 1.3 x 10^{-6} m^2 s^{-1} between 80 to 160 m. ADCP data collected in May 2008 indicate that 4-m shear was generally low during these measurements, averaging 4.5 x 10^{-3} s^{-1} throughout the water column (figure 4.2). Higher shear features (9-10 x 10^{-3} s^{-1}) were sometimes observed near the surface (figure 4.2, upper panel).

At high dissipation rates, microstructure shear spectra matched the universal spectrum both at high and low wavenumber, covering vertical scales ranging from 0.01 to 1 m (figure 4.3). Microstructure temperature gradient (figure 4.3) is well-correlated with

dissipation rates ($p < 0.05$, figure 4.4). The 2006 dataset has the strongest correlation between the two variables. Dissipation rate noise level is 10^{-10} W kg^{-1} in the three datasets. Values of 10^{-7} W kg^{-1} are frequently observed at depth but dissipation rates of order 10^{-6} W kg^{-1} are always observed in the upper 35 m, whereas values of order 10^{-5} W kg^{-1} observed in May 2008 were almost entirely observed in the upper 20 m, suggesting that they are related to surface processes.

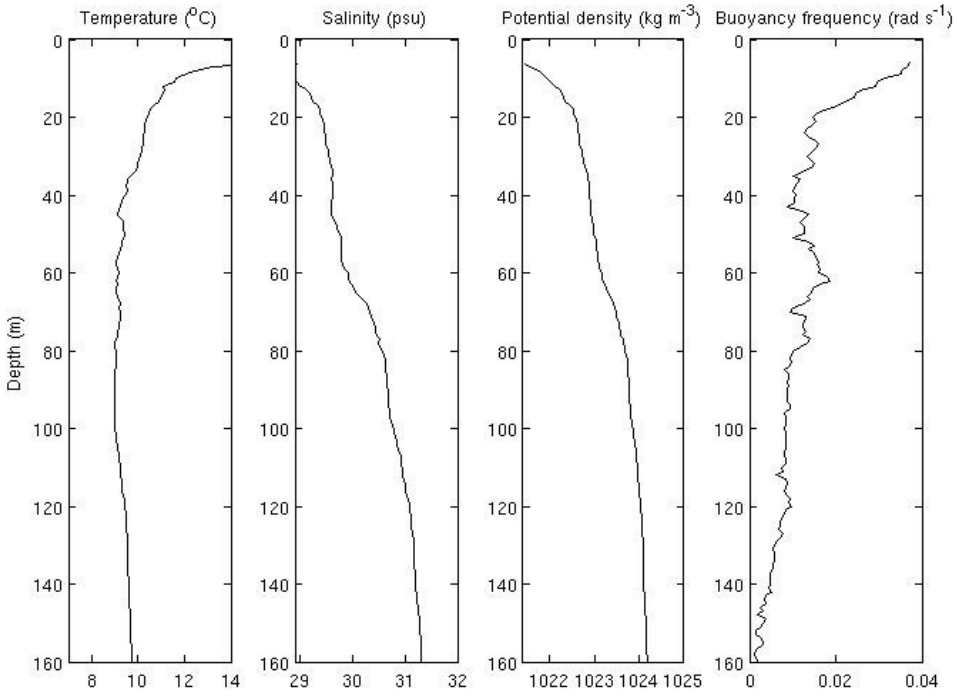

Figure 4.1. Typical temperature, salinity, potential density and buoyancy frequency profiles in Saanich Inlet. Taken from the averaged data collected in June 2006. Density profile is regulated by salinity. The density gradient is higher above 20-m depth as well as between 60 and 80 m, resulting in a higher buoyancy frequency in these depth intervals.

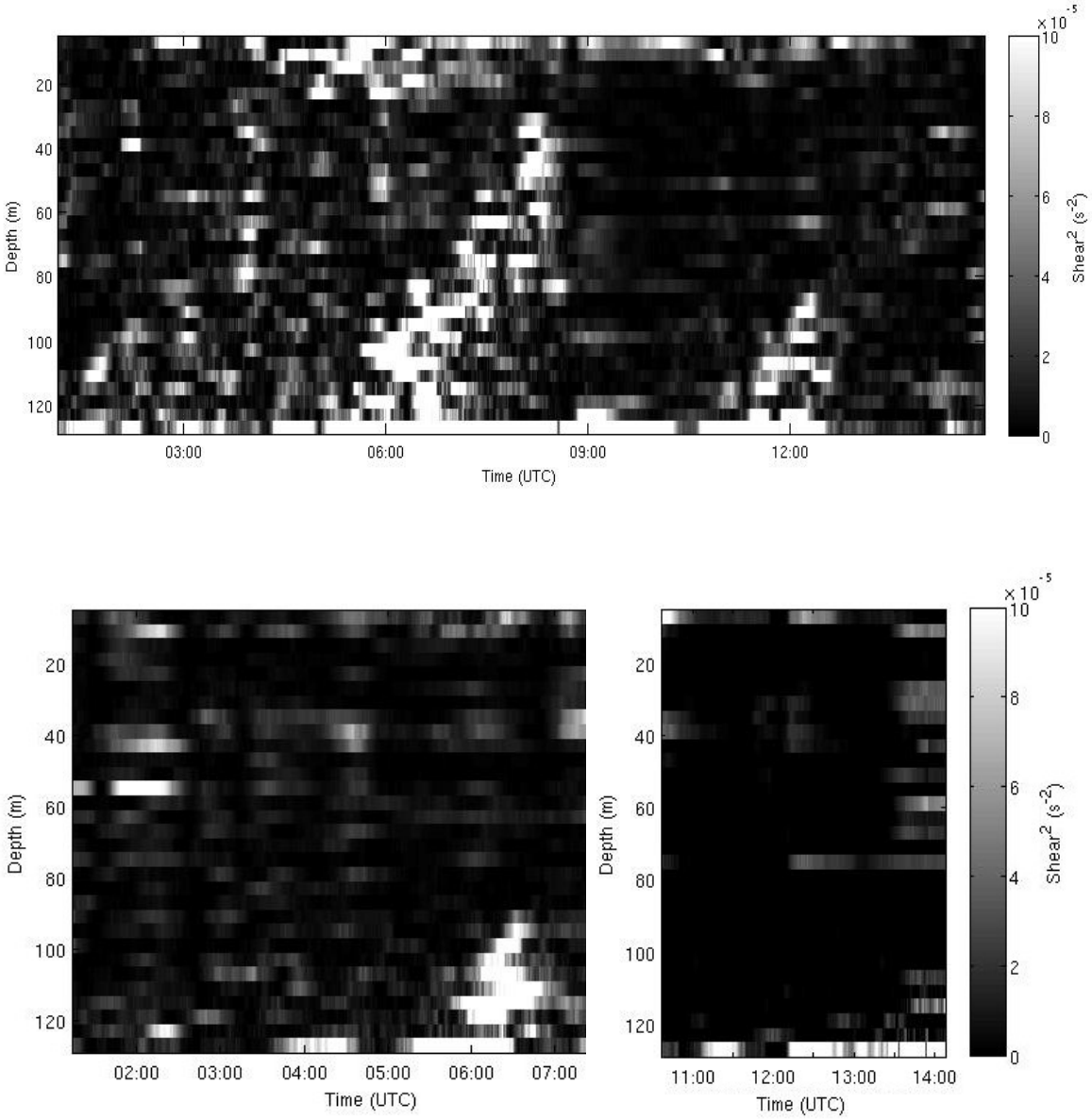

Figure 4.2. 4-m ADCP shear data collected in Saanich Inlet between May 07, 1800 PDT and May 09, 0700 PDT. (upper panel): May 07 at dusk and May 08 at dawn; (lower left): May 08 at dusk; (lower right): May 09 at dawn. Shear averages 2 x 10^{-5} s^{-2}. Higher shear features appear near the surface (upper panel). The white diagonal bands appear to be noise but the source is unknown.

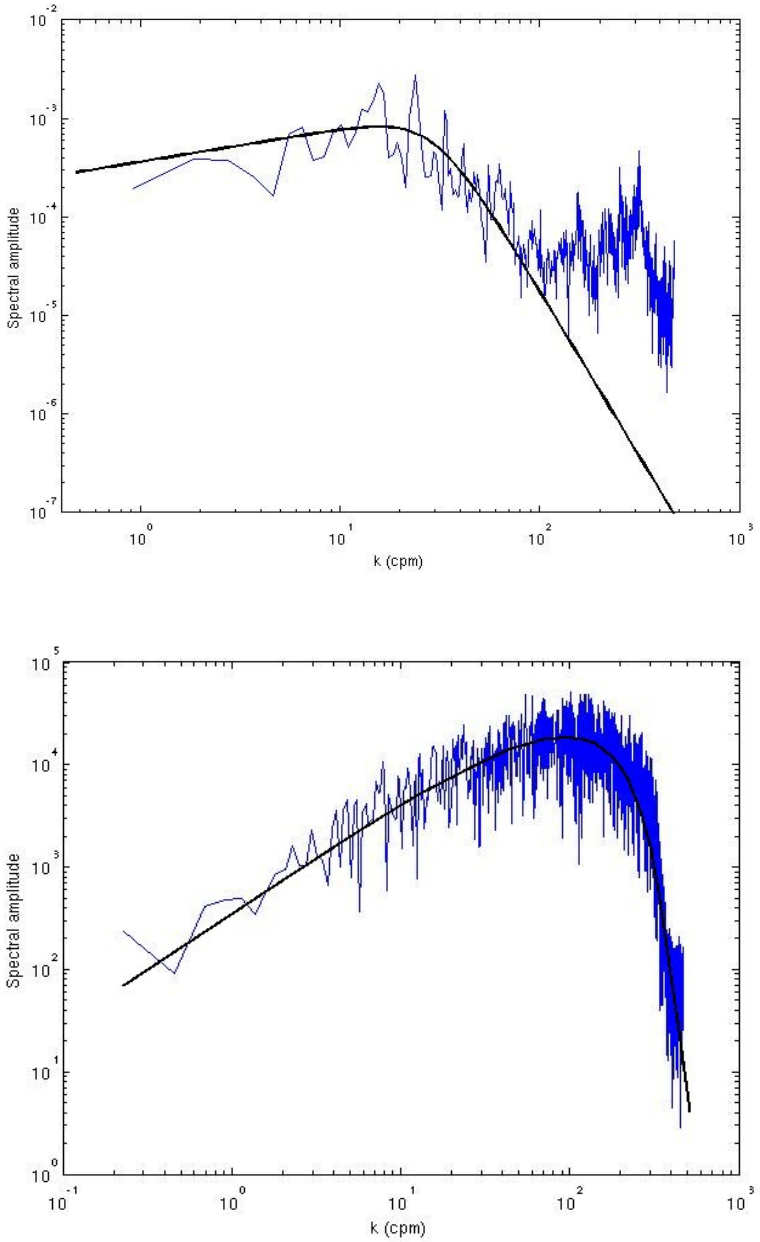

Figure 4.3. (upper panel): Example of a shear variance spectrum from the 2006 dataset in Saanich Inlet. Taken from time-series *SI06Jun09Dusk*, profile 45 at 04:05 UTC between 35 and 39 m. The black line represents the Nasmyth spectrum for a dissipation rate of 10^{-8}. (lower panel): Example of temperature gradient spectrum from the 2006 dataset in Saanich Inlet. Time-series *SI06Jun09Dusk*, profile 35. Depth interval is 28 to 32 m. The black line is an approximation of the shape of the Batchelor spectrum.

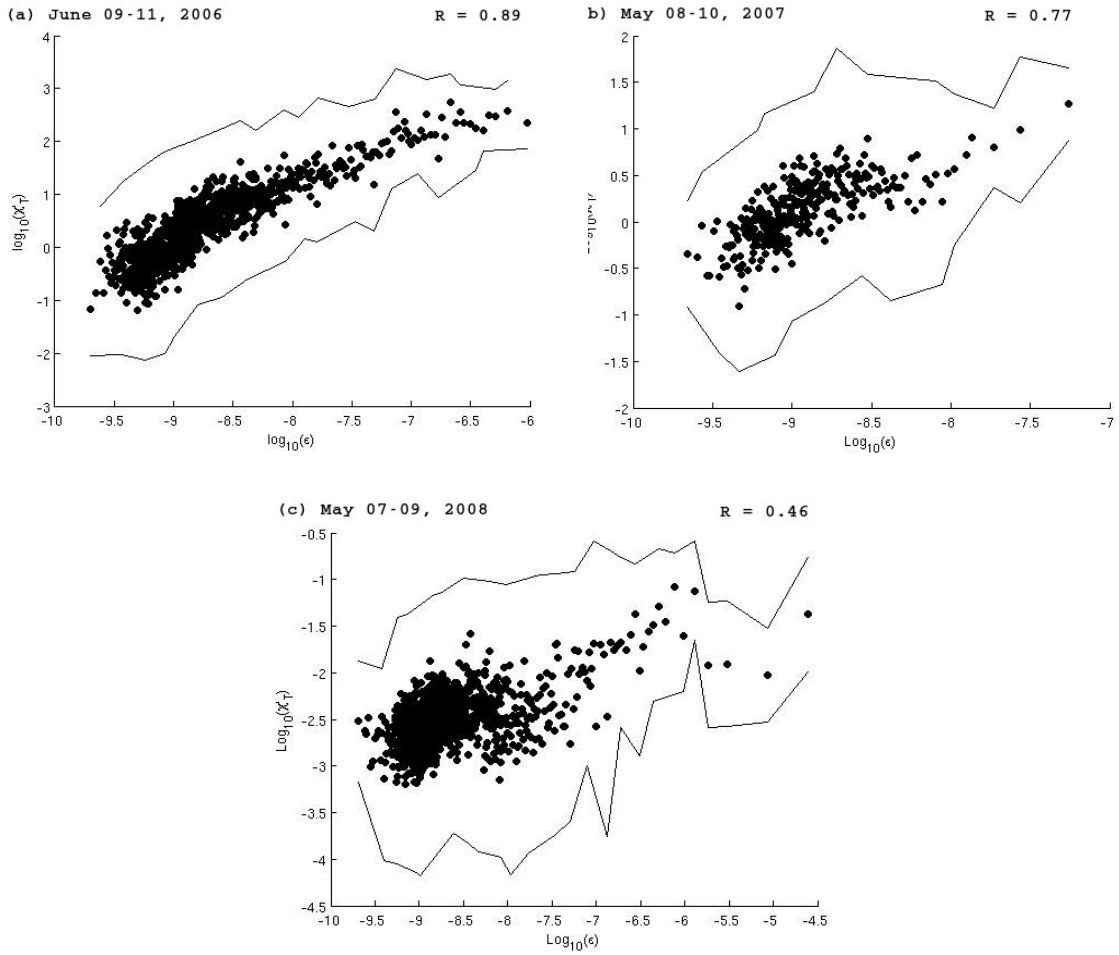

Figure 4.4. Correlation between χ'_T and the dissipation rate ε for the three datasets collected in Saanich Inlet in (a) 2006; (b) 2007 and (c) 2008. Datapoints outside the 20-120 m interval were excluded. For all three datasets, p = 0.0.

ADCP data collected in Saanich Inlet during May 2008 allow us to examine the influence of shear on the observed dissipation rates (figure 4.5). A wide range of shear values is observed at dissipation rates of 10^{-8} W kg^{-1} and lower. This high variation is due to the noisy features constituting the white bands in figure 4.2, but also to undersampling at high dissipation rate. At dissipation rates higher than 10^{-8} W kg^{-1}, 4-m shear averages 4.5 x 10^{-3} s^{-1}. The correlation between shear and dissipation rate was not significant in Saanich Inlet (p = 0.71, figure 4.5) suggesting that internal wave shear does not dominate turbulence production.

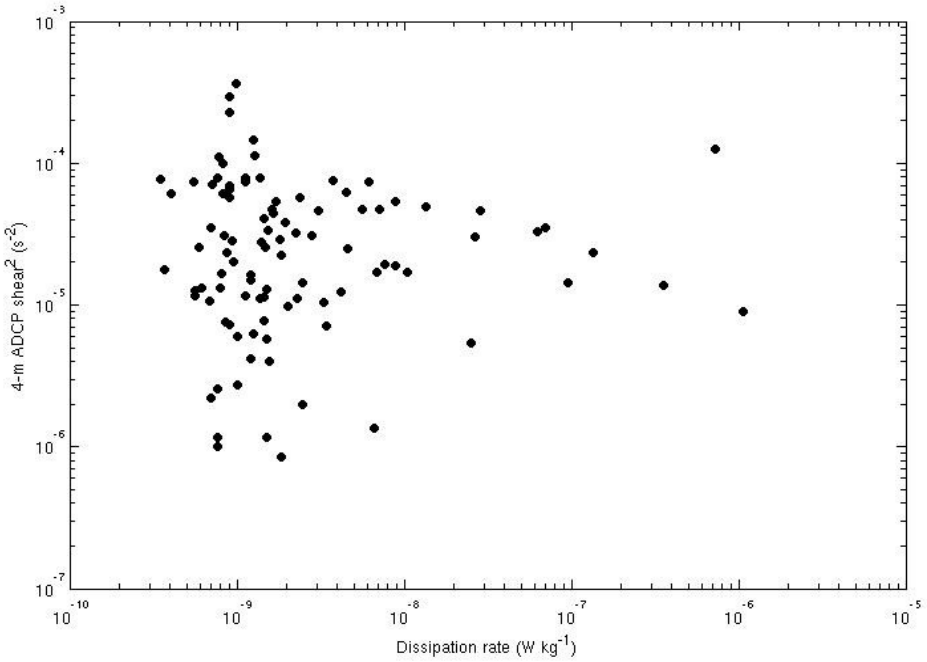

Figure 4.5. Correlation between dissipation rate and 4-m ADCP shear in Saanich Inlet, May 2008.

4.2 Acoustic characterization of the aggregations and species identification

In all time-series (*SI06Jun09-11, SI07May08-10, SI08May07-09*), a strong migratory layer was observed in the acoustic data, which migrated to the surface at dusk and downward to approximately 100-m depth at dawn. The thickness of the migrating layer ranged from 20 to 50 m, sometimes appearing to spread nearly throughout the whole water column (figure 4.6). Volume-backscattering strength was higher at the surface at night than within the migration period (up to -40 and -52 to -68 dB, respectively) suggesting that the organisms that constituted the migrating layer spread out during migration and aggregated at the surface. It is also possible that fish joined the aggregation at the surface, as has been observed in previous studies (Greenlaw, 1979). In June 2006, a second, more diffuse layer was observed to migrate 20 m below the main layer, appearing

to swim at the same average speed and joining the main group at the surface, or staying slightly below the main layer between 20 and 40 m (figure 4.6).

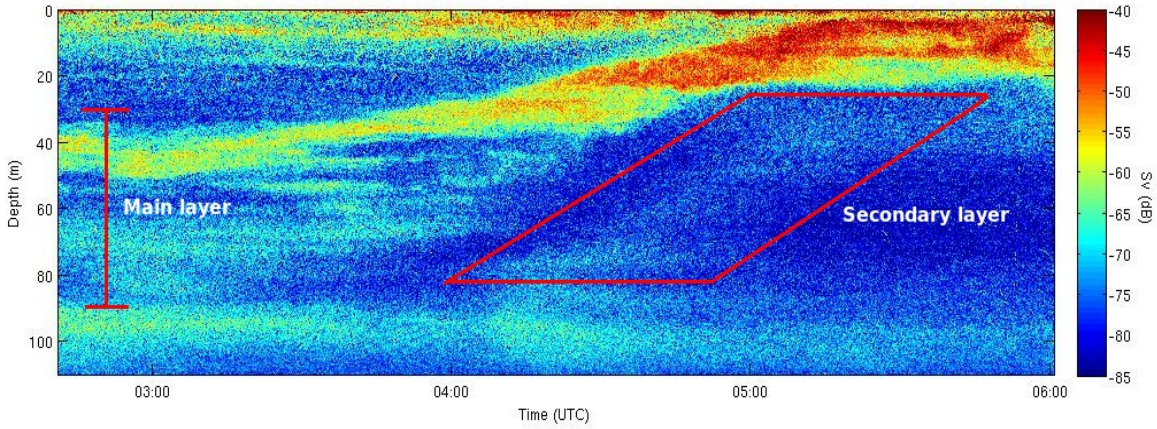

Figure 4.6. Example of backscattering data in Saanich Inlet, June 09 2006. The main layer spread almost throughout the entire water column, between 30 and 100 m at the beginning of the upward migration. A smaller, more diffuse acoustic layer is observed as well, starting its migration atround 0410 UTC, approximately 40 minutes after the main layer.

Acoustical analysis in Saanich Inlet is limited by the use of a single-beam, single-frequency 200-kHz echosounder (MacLennan and Simmonds, 1992), meaning that: 1) sizes and species cannot be determined from the acoustic data; 2) abundance estimates can be attempted only if a monospecific distribution is assumed. Because no net tows were collected in Saanich Inlet during our measurements, we rely on previous knowledge to determine which organisms compose the acoustic backscattering signal. Fortunately, the physics, biochemistry and ecosystem dynamics of Saanich Inlet have been studied extensively and a large literature is available (e.g. Greenlaw, 1979; Parsons et al., 1983; DeRobertis et al., 2003; Gargett et al., 2003; Beveridge, 2007). An instrumental platform has been deployed on the seafloor of Saanich Inlet and has been collecting real-time data of water properties, ADCP shear and bioacoustics since 2006 (VENUS, 2009). A large number of studies have shown that the euphausiid species *E. pacifica* is the dominant

acoustic scatterer in Saanich Inlet and dominates the daily migrating zooplankton layer (Greenlaw, 1979; Mackie and Mills, 1983; DeRobertis, 2002). The current analysis follows this assumption.

Typical target strength for a 15-mm long euphausiid individual is -79 dB (Trevorrow et al., 2005). Using (3.1) leads to densities ranging from 13 to 501 m^{-3} in the migratory layer, reaching 7940 m^{-3} at the surface at night, assuming a monospecific population of *E. pacifica*. These results, however, are quite uncertain, especially near the surface where acoustic backscattering could be dominated by planktivorous fish (Greenlaw, 1979). However, they are not in contradiction with previous studies of euphausiids abundance in Saanich Inlet. Concentrations of 50 to 500 m^{-3} were observed at the surface at night and abundances of up to 10 000 m^{-3} were observed around 100-m depth during the day (Mackie and Mills, 1983).

4.3 Swimming speed and turbulence

The vertical migration period was quite long compared to Ocean Station P and Station S migration periods, lasting between 60 and 90 minutes, from about 2030 to 2200 PDT at dusk and from 0430 to 0600 PDT at dawn during June 2006, and from approximately 2020 to 2120 PDT at dusk and 0500 to 0600 PDT at dawn during May 2007 and 2008 (figure A2.2.2, A2.2.3, A2.2.4). A higher abundance of predators in Saanich Inlet could explain this difference in migration period with Ocean Station P assuming that both aggregations are composed of *E. pacifica*.

Migration rates averaged around 1.6 cm/s, with a maximum of 3.1 cm/s during downward migration on May 2007 (time-series *SI07May10Dawn*), and minimum of 0.69 cm/s during upward migration on June 2006 (time-series *SI06Jun09Dusk)*. As previously mentioned, these migration rates cannot be used to infer swimming speeds of individuals.

Euphausiids in Saanich Inlet do not swim directly upward or downward when migrating. During dusk migration, De Robertis et al. (2003) found that swimming euphausiids migrate at an angle $\sim< 60^{o}$ relative to horizontal. The increased metabolic costs resulting from such a behaviour are thought to be offset by a reduction in vulnerability to visual predators (De Robertis et al., 2003); most euphausiids (including *E. pacifica*) possess ventral photophores which produce a downward-directed luminescence, serving as a camouflage from predators below. These photophores would no longer be downward-directed if the zooplankters were to swim vertically.

A number of studies discuss swimming speeds of individual euphausiids. De Robertis et al. (2003) found highly variable swimming speeds during dusk ascent in Saanich Inlet, ranging from 0 to 17 cm/s. Although a large proportion of the euphausiids were observed to swim within the range 5-10 cm/s, the majority were found to swim at very low speed (close to 0 cm/s). These highly variable swimming speeds are reflected in a range of possible Reynolds number. Typical euphausiid lengths in Saanich Inlet range from 12 to 22 mm (De Robertis et al., 2003). This leads to Reynolds numbers ranging from 0 to 3740. Torres (1984) notes Reynolds numbers ranging from 121.4 to 2429 for individual *E. pacifica* of 17 mm, with swimming speed ranging from 1 to 20 cm/s. Swimming euphausiids vary between a non-turbulent and a turbulent swimming behaviour (Yen, 2000).

Considering *E. pacifica* aggregations in Saanich Inlet and taking the average migration rate as a value for u in (17), with the aggregation thickness as a representative vertical length-scale, the resulting Reynolds number is 3.2×10^{5}. This is a much higher value and suggests that, as an ensemble, the aggregation could produce significant mixing, while individuals might not.

4.4 Dissipation rate levels in the presence/absence of zooplankton

Mean dissipation rates were calculated for each time-series according to different parameters (high/low backscatter, regions of migrating/non-migrating zooplankton versus regions without zooplankton) and statistical results are presented in this section. Mean volume-backscattering at high/low dissipation rate was also calculated, as well as coefficients of correlation between dissipation rate and volume-backscattering. Results are presented at the end of this section.

Estimates of mean dissipation rates at high and low volume-backscattering strength show significantly higher dissipation rates (approximately two-fold) at high backscatter in 8 out of 11 time-series (figure 4.7, table A2.2.2), suggesting that turbulence and presence of zooplankton in the water column are correlated. Thresholds for high and low backscatter were determined from the distributions of the volume-backscattering for each time-series. Figure A2.2.5 shows probability density functions of dissipation rates at high and low backscatter for the three datasets (2006, 2007, 2008). Similarly to the probability density functions of dissipation rates at Ocean Station P and Station S, PDFs in Saanich Inlet are not log-normal.

Mean volume-backscattering strengths were significantly higher at high dissipation rates in 5 out of the 11 time-series, with a 2 to 12 dB difference using a dissipation rate threshold of 10^{-8} W kg^{-1}. Data collected in April 2005 by Kunze et al. (2006) showed higher backscatter at high dissipation rate in the two time-series collected (figure 4.7).

Correlations were performed between volume-backscattering strength and dissipation rates in the depth range of 30-120 m. The acoustic data was averaged over 1 minute and 1 m. Spearman coefficients indicate that the correlations were generally good, except for the 2008 dataset (figures A2.2.6. A2.2.7, A2.2.8, table A2.2.6). Apart for this dataset, correlations were all significantly correlated ($p < 0.05$).

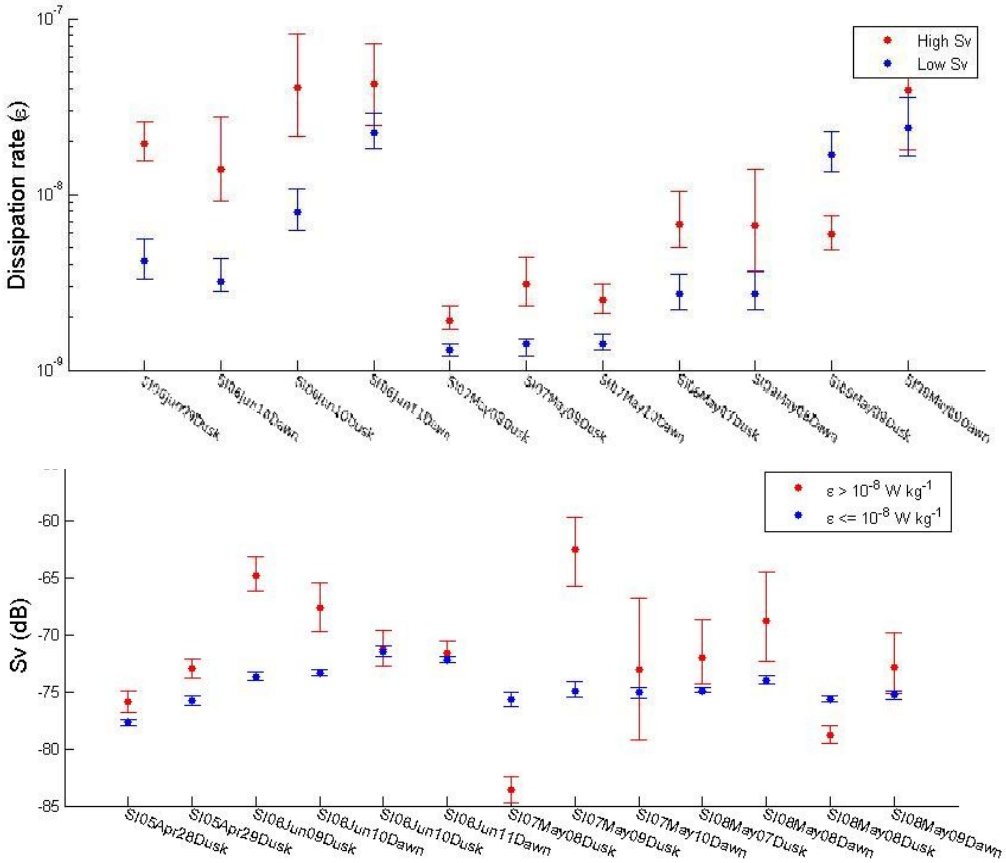

Figure 4.7. (upper panel): Mean dissipation rate at high and low volume-backscattering for each time-series collected in 2006, 2007 and 2008. Volume-backscattering thresholds used are -67 dB in 2006; -67 dB in 2007 and -70 dB in 2008. Thresholds were chosen in accordance to the volume-backscattering distribution function to distinguish between the absence and presence of marine zooplankters. Only data in the 30-120 m depth range were used. (lower panel): Mean volume-backscattering strength at high and low dissipation rate, using a dissipation rate threshold of 10^{-8} W kg^{-1}. Data from Kunze et al. (2006) collected in April 2005 are included. Only data in the 30-120 m depth range were used.

Correlations taking into account a possible mismatch between the occurrence of turbulence and the source's location in time (see sections 3.4 and 3.5) resulted in stronger coefficients of correlation (using a maximum time lag of one buoyancy period) in five time-series only, and did not change the overall results, meaning that positive correlations were generally more positively correlated using a time lag, and non-correlated interactions were still uncorrelated (table A2.2.6).

A number of other correlations were examined, such as the temporal and spatial gradients of volume-backscattering as a function of the dissipation rate, as well as the second derivative of the volume-backscattering ($dSv^2/dzdt$) as a function of the dissipation rate, but they did not show any significant correlation.

Analyses differentiating between mean dissipation rates in regions including and excluding the migratory layer were also performed. The water column was separated into three regions (figure 4.8): the region including the migration layer (ML); the region excluding the migration region, where acoustic backscatter was very low, i.e., where no marine organisms were detected by the echosounder (NZ), and a deep layer excluding the migration period but where a strong acoustic backscatter indicated the presence of non-migrating zooplankton (DL). This latter region is consistently observed before dusk migration and after dawn migration. Dissipation rates shallower than 30-40 m (depending on time-series) were excluded. In every case, the depth interval used to calculate the probability density function was the same for all regions to eliminate the effects of a possible dependence of dissipation rate on depth. Region-averaged dissipation rates were estimated for each dataset as well as for each time-series.

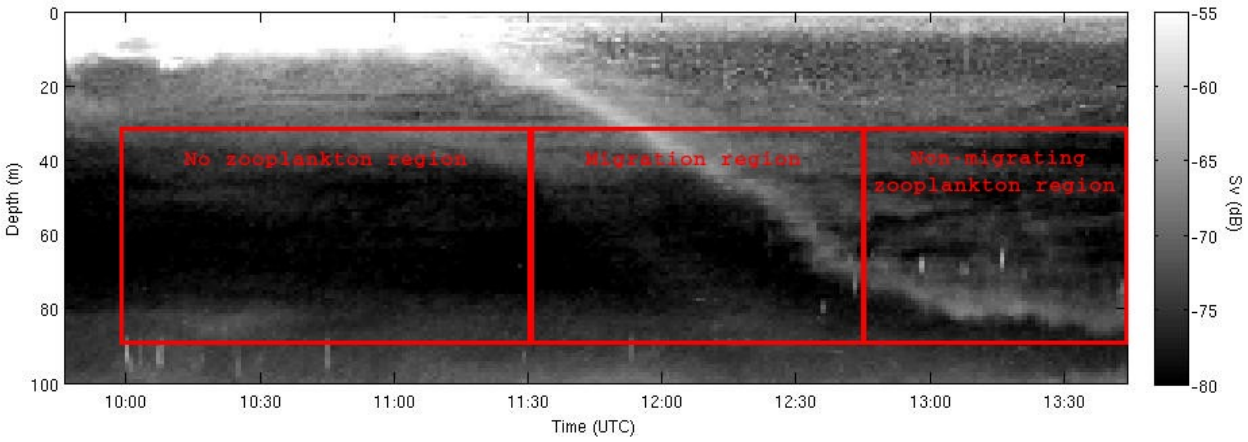

Figure 4.8. Example of selection of the three regions (ML, DL, NZ) used to compare dissipation rates distributions.

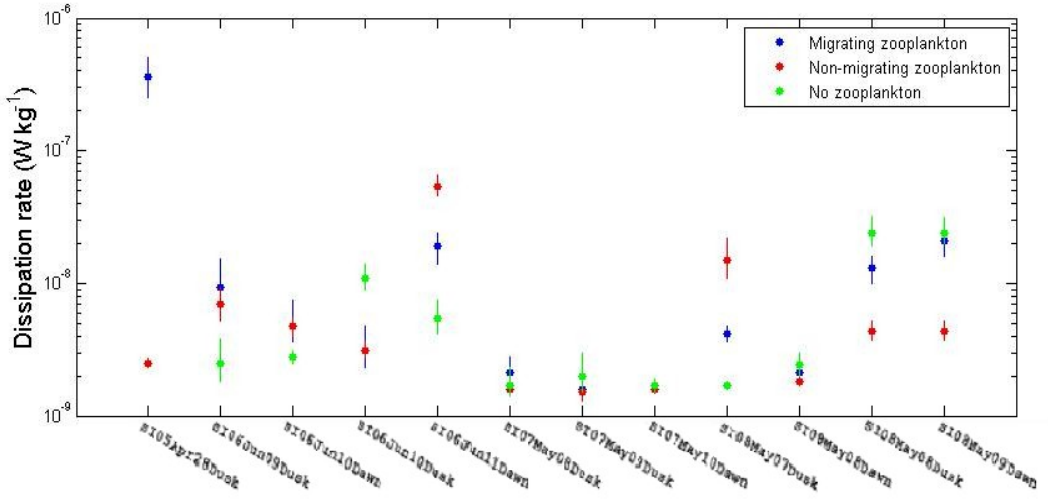

Figure 4.9. Mean dissipation rate per region (migrating zooplankton, non-migrating zooplankton, no zooplankton regions) for each time-series of datasets 2006, 2007 and 2008. Mean dissipation rates in regions of migrating and non-migrating zooplankton are also shown for measurements collected in April 2005 (Kunze et al., 2006). Confidence intervals were calculated using the bootstrap method.

Results are highly variable and lead to no definite conclusion (figure 4.9). Data collected in April 2005 by Kunze et al. (2006) is the only time-series to show a significantly higher dissipation rate during the migration period. Three out of four time-series collected in June 2006 show significantly higher dissipation rates where zooplankton were present. Mean dissipation rates in May 2007 were similar in all three regions. Fish were detected in the acoustic data throughout this dataset. Mean dissipation rates in May 2008 were highly variable, showing no dominant pattern. Some of the measurements collected in 2006 and 2008 (table A2.2.3) suggest that, in Saanich Inlet, regions of non-migrating zooplankton contribute as much to turbulence as regions of migrating zooplankton. No patterns were observed in the standard deviations and skewness of the distributions between the three regions (tables A2.2.4, A2.2.5).

Chapter 5
Discussion and Conclusion

5.1 Summary

Measurements at Ocean Station P and Station S suggested turbulence generated by finescale shear. Reynolds numbers of the largest individuals found at these two stations indicate that turbulence production is possible but no unambiguous zooplankton-generated turbulence was observed. If aggregating zooplankters must act together to generate turbulence at a significant scale, densities of swimming marine organisms in these open ocean waters are likely too low to contribute even partly to turbulence processes. In the case of turbulence generated by individuals, it would be very difficult to detect such scattered signals in the natural environment.

In Saanich Inlet, there were indications of zooplankton-generated turbulence, but the observations are highly variable. Background turbulence was very low (~10^{-10} W kg^{-1}) but dissipation rates of up to 10^{-6} W kg^{-1} were observed in 73 of the 376 profiles collected. A relation between the dissipation rate and volume-backscattering was observed in many time-series. On 11 time-series of dawn and dusk, 8 showed moderate to strong correlations between dissipation rate and backscatter. Mean dissipation rates were significantly higher (approximately two-fold) at high backscatter for nearly every time-series (8 out of 11) when using volume-backscattering thresholds of -67 (2006 and 2007 datasets) and -70 dB (2008 dataset). Using a dissipation rate threshold of 10^{-8} W kg^{-1}, mean volume-backscattering strengths were significantly higher by 2 to 12 dB at high dissipation rate in 5 out of 11 time-series. Over all time-series collected, dissipation rates in the presence of zooplankton averaged 1.4 x 10^{-8} W kg^{-1} whereas the average in the absence of zooplankton was 0.7 x 10^{-8} W kg^{-1}. Typical mid-inlet nitrate gradients in the upper 35 m averaged 0.79 μmol $m^{-3}m^{-1}$ (data not shown), resulting in a two-fold increase

in nitrate flux in the presence of zooplankton (0.06 μmol N m^{-2} day^{-1} in the presence of zooplankton; 0.03 μmol N m^{-2} day^{-1} in the absence of zooplankton).

Overall, mean dissipation rates per region were not significantly different between the ML, DL and NZ regions (mean dissipation rates in the ML and/or DL layers were significantly higher than the ones in NZ region in four out of eleven time-series) but suggested that regions of non-migrating zooplankton included at least as much turbulence events than the regions of migrating zooplankton.

Although data collected above 30 m have been excluded in the analysis due to the possible influence of surface processes on turbulence, it is worth noting that dissipation rates often (6 times out of 10) seemed higher when zooplankters were feeding near the surface relatively to when the aggregation was located at depth (figures A2.2.1, A2.2.2 and A2.2.3). This also corresponds to a day/night pattern and therefore could be related to seabreeze and surface cooling/heating.

5.2 Discussion

Results suggest that other sources of turbulence were likely present in Saanich Inlet in addition to the observed biologically-generated turbulence because high dissipation rates were also observed in areas where no marine organisms were detected. Wind- and tide-generated turbulence are known to be very low in Saanich Inlet (Parsons et al., 1983, Gargett et al., 2002), but they cannot be entirely excluded when interpreting the results. Experimental work on zooplankton aggregations in water tanks would allow great insights on the subject of biologically-generated turbulence by eliminating non-zooplankton-related turbulence. In Saanich Inlet, a front located just outside the inlet in Satellite Channel is thought to be responsible for the advection of surface nitrate from the well mixed waters of Prevost Passage into the inlet, resulting in the observed high productivity. This influx would occur every spring tide and be responsible for peaks in

primary production observed every neap tide in Saanich Inlet (Parsons et al., 1983). The timing of our measurements relative to the lunar- and daily tidal-cycles varies (figure A2.2.1) and, unfortunately, our data are insufficient to address a relation between dissipation rates and these variables. Also, a valid analysis of zooplankton-generated turbulence was not possible in the surface waters where surface heating/cooling in addition to winds may well dominate turbulence production.

Zooplankton have a wide range of swimming behaviours which likely impact their ability to generate turbulence in ways that we do not fully understand. For instance, bigger individuals generally swim more rapidly (De Robertis et al., 2003), but there is evidence (Huntley and Zhou, 2004; Catton et al., unpublished) that the magnitude of the turbulence generated by marine organisms is not dependent solely on their size. It has also been demonstrated that *E. pacifica* maintain a depth that keeps them at the same irradiance level which they were exposed to during the day (Boden and Kampa, 1965). Thus, their migration speed, as well as the depth at which they settle at the surface at night, will vary according to a number of factors including times of sunset and sunrise, cloud cover and the lunar cycle. In addition, individual euphausiids swim in periodic bursts followed by short periods of rest (De Robertis et al., 2003). There is also evidence that migrating euphausiids in Saanich Inlet swim somewhat randomly within the aggregation with a net movement upward (De Robertis et al., 2003). Presence of predators, or even turbulence itself, can also trigger escape responses (Yen et al., 2000), resulting in an increased swimming speed for short intervals. This behaviour may explain the non-recurrence of the Kunze et al. (2006) result in our data. It makes it very difficult, perhaps even impossible with the type of measurements that we used, to relate the occurrence of turbulence to the swimming speed of zooplankton because an individuals' swimming speed may not be correlated with the migration rate of the aggregation.

Catton et al. (unpublished) mention some interesting points about the synchronization of swimming zooplankton within an aggregation. Using four swimming *Euphausia superba* in a water tank, they note that, if the individuals are swimming in a way that each of them

is located in or near the wake of the previous individual, water particles are carried from the first to the last individual. In the context of a zooplankton aggregation, this would bring the water particles from the top to the bottom of the aggregation, generating a density overturn at a scale of the aggregation. However, this requires synchronized swimming. An aggregating species is defined as one composed of a unique species in the same size class, swimming as a whole in the same direction; thus, they likely meet the requirement of synchronized swimming. However, it is arguable that *E. pacifica* swarms found in Saanich Inlet do not qualify as an aggregating species since De Robertis et al. (2003) showed that euphausiids in Saanich Inlet adopt a very random swimming behaviour, swimming at different speeds in all directions, with only a general trend upward during dusk migration. The type of analysis that we used do not allow detection of turbulence generated at the scale of an individual euphausiid. It can only be used to relate O(1-m) turbulence to the overall movement of the aggregation at a given time and location. The technique we used to estimate dissipation rates uses 4-m intervals to derive a shear spectrum. Well-resolved spectra include scales ranging from 0.01 to 1 m. This implies that, whenever a high dissipation rate is obtained, it is occurring at a scale much larger than that of an individual krill. Therefore, our method is not suited to detect turbulence by individual krill but rather at an aggregation scale, so is better-suited to detecting turbulence generated by krill acting as a group. From this point of view, the aggregation's density and the aggregating behaviour of a marine species will influence its ability to generate turbulence and mixing.

A good example of aggregating zooplankton species is *E. superba*, which is large (~0.8-7 cm) and very abundant in Antarctic waters (Zhou and Dorland, 2004). It qualifies as a schooling species and has been shown to always orient uniformly and exhibit synchronized swimming (Hamner et al., 1983). It would be very interesting to investigate krill-generated turbulence in the Southern Ocean where this species is commonly found in extremely high abundance [densities of 20 000 to 30 000 m^{-3} have been observed (Hamner et al., 1983)] in coastal shelf regions of the Antarctic Peninsula (Zhou and Dorland, 2004). *E. superba* is the world's largest species of krill and is known to exhibit

daily vertical migrations. Swarms generally range from 17 to 307 m in horizontal length, and from 6 to 50 m in thickness, but can reach thousands of meters in length (Zhou and Dorland, 2004; Hamner et al., 1983).

Biologically-generated turbulence is a very intermittent phenomenon and a systematic positive response was not to be expected. As mentioned earlier, a number of factors can influence its occurrence which are not yet understood. It appears that a very high density of swimming organisms is required to generate turbulence on a significant scale, but it is not the only condition. The level of synchronization between swimming organisms within an aggregation is likely to be another important factor.

5.3 Conclusion

This study constitutes, to our knowledge, the first search for biologically-generated turbulence in the deep ocean. In addition, our 11 time-series of zooplankton-generated turbulence in Saanich Inlet constitute the most comprehensive dataset to date. Our study showed a sharp difference in turbulence profiles collected in the deep ocean and a coastal inlet. Turbulence at Ocean Station P and Station S was well-correlated with O(16-m) shear features at 50- and 100-m depth, confirming our initial hypothesis that turbulence at this location originates mostly from internal wave shear. ADCP data collected during May 2008 in Saanich Inlet found low current-shear with no dominant pattern. Observed turbulence was uncorrelated with O(1-m) shear. Statistical analyses performed on the 2006, 2007 and 2008 datasets showed that turbulence dissipation rates were significantly higher in the presence of marine organisms in eight of the eleven time-series collected with a confidence interval of 95%. When the difference was significant, turbulent dissipation rates were a factor of 2-3 higher when backscatter was high compared to low. These turbulence events occurred at scales of more than 1 m as they were positively detected by our dissipation rate estimation technique, implying that they were generated

by groups of swimming zooplankton acting together rather than individual zooplankters. Given the small fraction of time that the backscatter layer migrates, migrating backscatter layers would not contribute much to the average dissipation rate and average mixing in Saanich Inlet. However, the fact that the mean dissipation rate was generally significantly higher at high volume-backscattering, but not specifically during the migration period, suggests that zooplankton-generated turbulence occurred in the inlet but was not consistently associated with the migrating zooplankton. At depths where krill swarms rest during the day, swimming non-migrating zooplankton may double or triple the mixing rate.

APPENDIX 1

A1 Acoustics theory

The volume backscattering strength (S_v) is the logarithmic equivalent of the volume backscattering coefficient (Clay and Medwin, 1977)

$$S_v = 10\log_{10}(s_v) \quad \text{(dB)} \tag{A1.1}$$

where s_v, the volume backscattering coefficient, is calculated by

$$s_v = \Sigma \frac{\sigma_{bs}}{V} \quad (\text{m}^{-4}). \tag{A1.2}$$

V is the insonified volume, and

$$\sigma_{bs} = R^2 \left(\frac{I_{bs}}{I_i} \right) \quad (\text{m}^2\ \text{m}^{-3}) \tag{A1.3}$$

is the backscatter cross-section. R is the range from the transducer, I_{bs} the backscattered intensity and I_i, the incident intensity at the target.

The volume backscattering strength is therefore a ratio of the volume averaged backscattered intensity to the incident sound wave (Iida et al., 1996) and has decibels (dB) as units. To determine S_v from the voltage or counts output of the echosounders, we use the SONAR equation:

$$S_v = 20\log(C) - G_{TVG} - RS - SL + 20\log(R) + 2\alpha R - 10\log\left(c\tau\frac{\psi}{2}\right) - 20\log(K) \qquad \text{(A1.4)}$$

where C is the acoustic count; G_{TVG} is the time varied gain (dB); RS is the transducer receiving sensitivity (dB re 1 μPa at 1m); SL is the source level (dB re 1 μPa at 1m); R is the range from the transducer (m); α(S,T,p) is the absorption coefficient (dB m-1) which is dependant on salinity, temperature and pressure; c is the speed of sound in seawater (~1480 m s-1); τ is the pulse length; ψ is the equivalent beam angle (steradians) and K is the calibration constant (dB).

Transducer constants for ASL Water Column Profiler are as follows: Source Level, 213.5 dB re 1 μPa at 1m; Receiver Sensitivity, -191 dB re 1 μPa at 1m; Equivalent Beam Angle, 0.01531 steradians; Calibration Constant, 144.25. For Simrad EK60, they are: Source Level, 21.98 dB re μPa at 1m; Receiver Sensitivity, -150 dB re 1 μPa at 1m; Equivalent Beam Angle, 0.0079 steradians; Calibration Constant, 501.19.

Equation (3.1) can be derived from (Clay and Medwin, 1977)

$$TS = 10\log(\sigma_{bs}) \qquad \text{(A1.5)}$$

where

$$\sigma_{bs} = \frac{s_v}{N} \qquad \text{(A1.6)}$$

which leads to

$$TS = 10\log\left(\frac{s_v}{N}\right) = 10\log(s_v) - 10\log(N) \qquad \text{(A1.7)}$$

we then obtain, using (A1.1):

$$TS = S_v - 10\log\ (N) \tag{A1.8}$$

which leads to equation (3.1).

APPENDIX 2

A2.1 Ocean Station P and Station S

Dataset	Location	Date (PDT)	Start time (UTC)	End time (UTC)	Profile numbers	Comments
OSPJun06Dusk	OSP	Jun-06-07	07-Jun-07 04:39:15	07-Jun-07 06:44:30	00-06	*Wind 16 knts SW*
OSPJun07Dawn	OSP	Jun-07-07	07-Jun-07 11:36:14	07-Jun-07 14:35:29	07-19	*Wind 16 knts*
OSPJune07Dusk	OSP	Jun-07-07	08-Jun-07 05:22:47	08-Jun-07 07:26:53	20-28	*Wind 14 knts*
OSPJun09Dawn	OSP	Jun-09-07	09-Jun-07 11:08:26	09-Jun-07 14:22:05	29-40	*Wind up to 30 knts*
SSJun10Dusk	SS	Jun-10-07	11-Jun-07 05:30:31	11-Jun-07 07:41:44	41-50	*Wind 5 knts Very strong acoustic signal at 18 kHz*
SSJun11Dawn	SS	Jun-11-07	11-Jun-07 11:06:24	11-Jun-07 14:19:17	51-62	*Wind 4 knts*

Table A2.1.1 Time-series collected at Ocean Station P (OSP) and Station S (SS) with the starting and ending times of the VMP deployments, and the profile numbers. At both stations, ADCP and multi-frequency bioacoustic data was also collected.

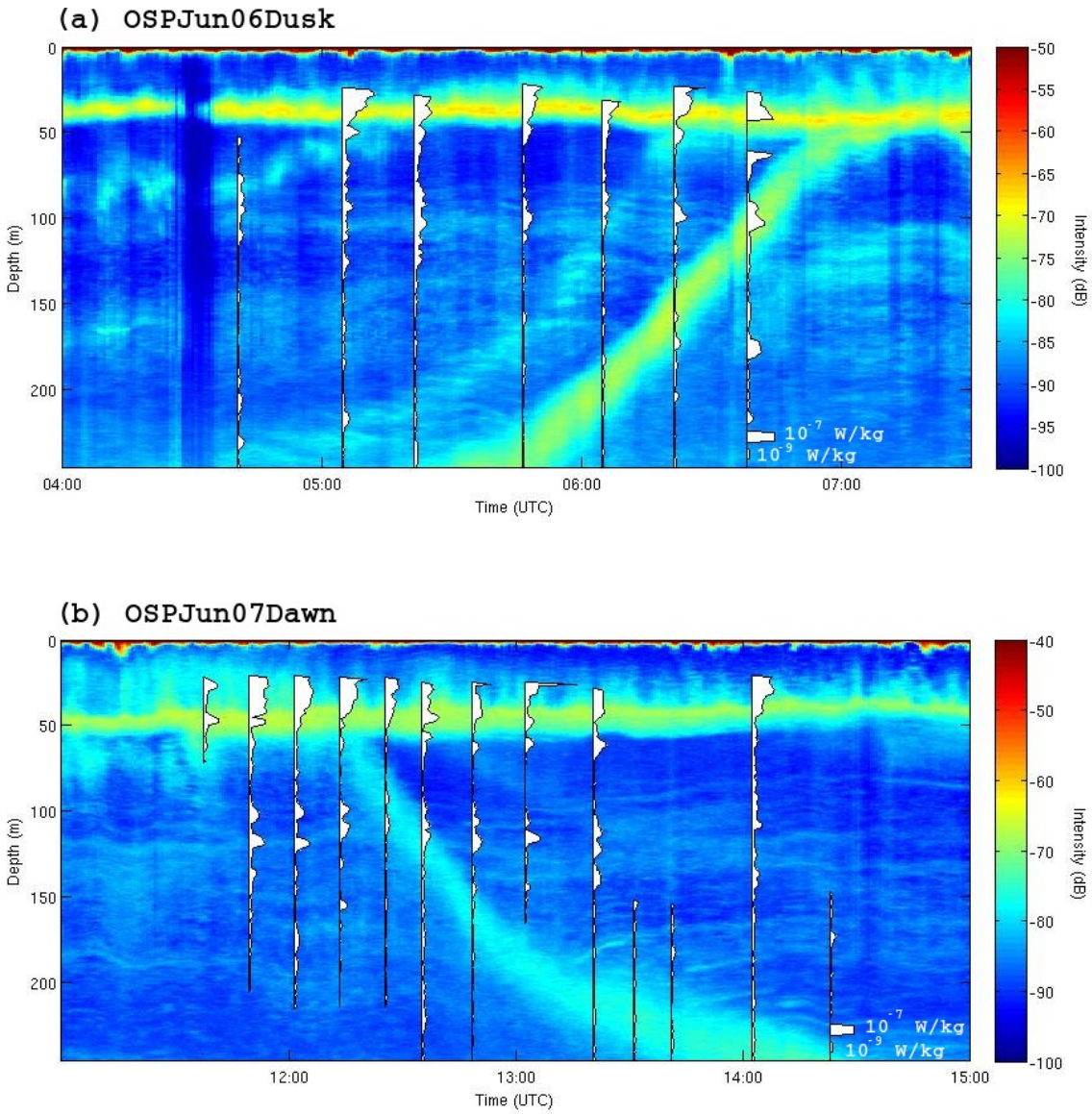

Figure A2.1.1. Volume-backscattering and dissipation rates collected at Ocean Station P (a-d) and Station S (e-f), using frequency of 120 kHz. (a) *OSP07Jun06Dusk*; (b) *OSP07Jun07Dawn;* (c) *OSP07Jun07Dusk*; (d) *OSP07Jun09Dawn*; (e) *OSP07Jun10Dusk*; (f) *OSP07Jun11Dawn*.

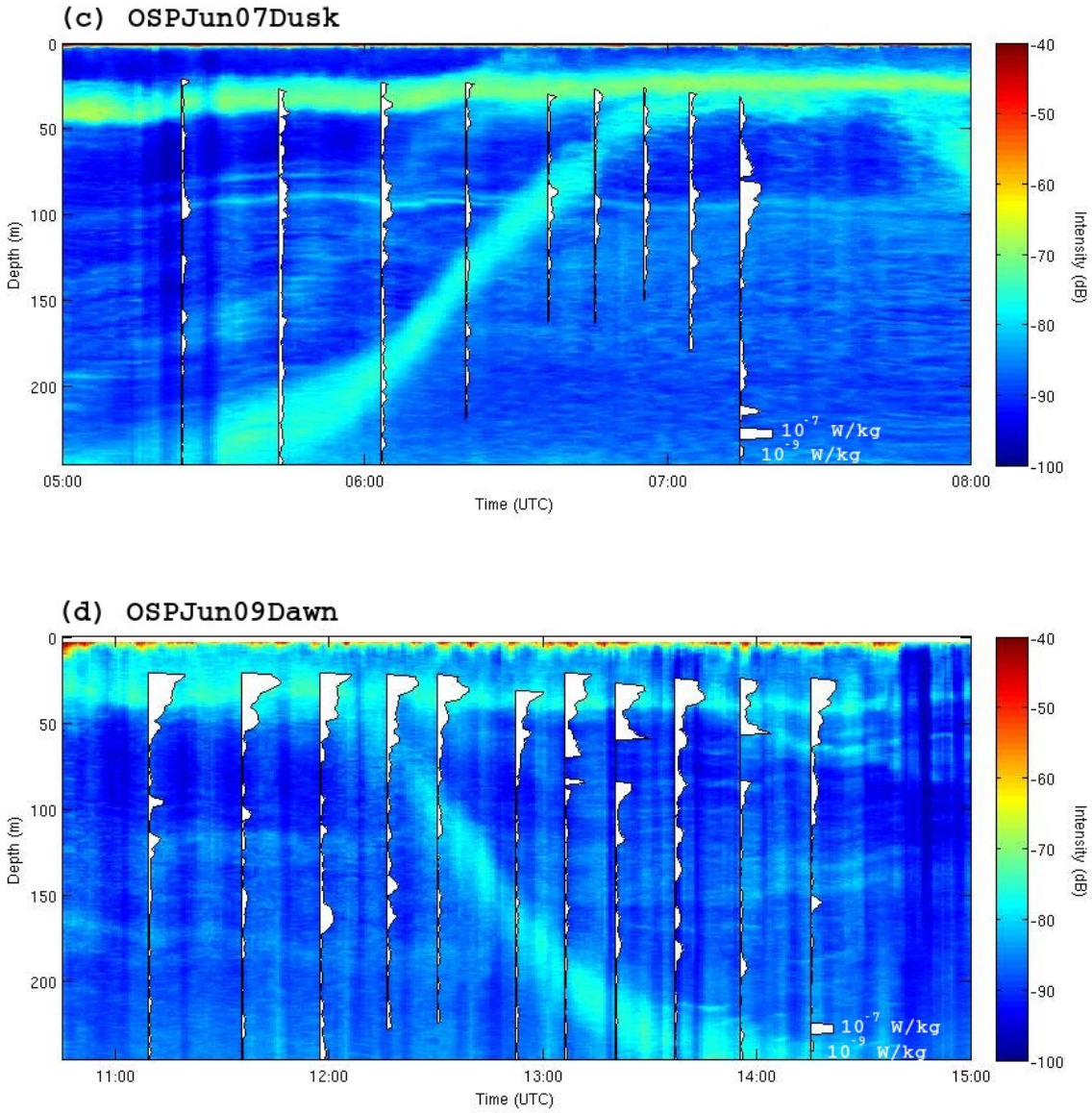

Figure A2.1.1. Continued

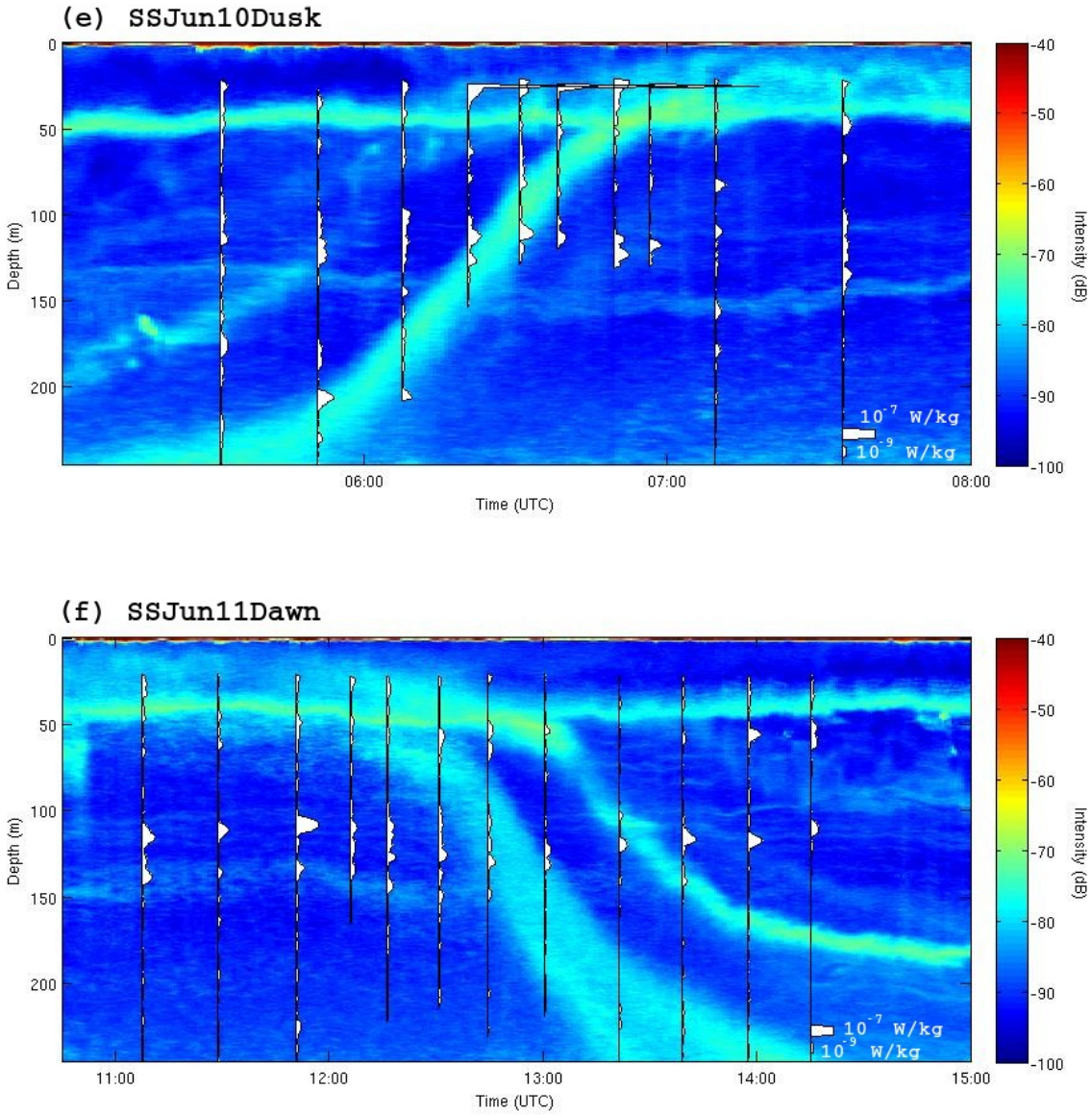

Figure A2.1.1. Continued.

Dataset	Mean dissipation rate (x 10^{-9} W kg^{-1})		
	ML	**NZ**	**SL**
OSPJun06Dusk	1.46 (1.13-2.13)	1.15 (1.03-1.31)	18.5 (13.3-28.5)
OSPJun07Dawn	0.93 (0.85-1.1)	2.1 (1.8-2.6)	37.4 (11.4-161.4)
OSPJun07Dusk	1.0 (0.93-1.09)	1.2 (1.03-1.55)	1.2 (1.06-1.4)
OSPJun09Dawn	1.8 (1.5-2.2)	1.8 (1.5-2.3)	76.3 (61.8-95.5)
SSJun10Dusk	1.03 (0.88-1.25)	0.74 (0.64-0.91)	2334 (358-7154)
SSJun11Dawn	0.79 (0.69-1.1)	1.5 (1.03-2.6)	1.1 (0.92-1.5)
OSPJun06-08	1.29 (1.2-1.5)	1.56 (1.4-1.8)	38.0 (28.5-67.6)
SSJun10-11	0.88 (0.79-1.0)	1.18 (0.90-1.8)	1040 (160-3245)

Table A2.1.2. Dissipation rate means per region for each time-series at Ocean Station P and Station S with 95% confidence intervals (in brackets) as obtained using the bootstrap method. ML = Migration Layer; SL = Surface Layer (20-60 m); NZ = No Zooplankton region.

(a)

Parameter	ML	NZ	SL
Skewness	12.8 (10.8-16.0)	6.5 (5.6-7.6)	20.0 (15.4-22.9)
Standard deviation (10^{-9})	3.4 (2.6-4.7)	2.9 (2.4-3.7)	198.4 (72.7-435.6)

(b)

Parameter	ML	NZ	SL
Skewness	7.6 (5.7-11.1)	14.3 (9.3-21.2)	13.4 (5.4-20.5)
Standard deviation (10^{-9})	1.6 (1.2-2.3)	5.4 (2.5-9.5)	13169 (3270-24110)

Table A2.1.3. Skewness and standard deviation of the distribution of dissipation rates per region. ML = Migration layer; NZ = No Zooplankton; SL = Surface Layer (20-60 m).Numbers in brackets correspond to the 95% confidence interval as obtained from the bootstrap method. Distributions include (a) all datasets from Ocean Station P only; (b) all datasets from Station S only.

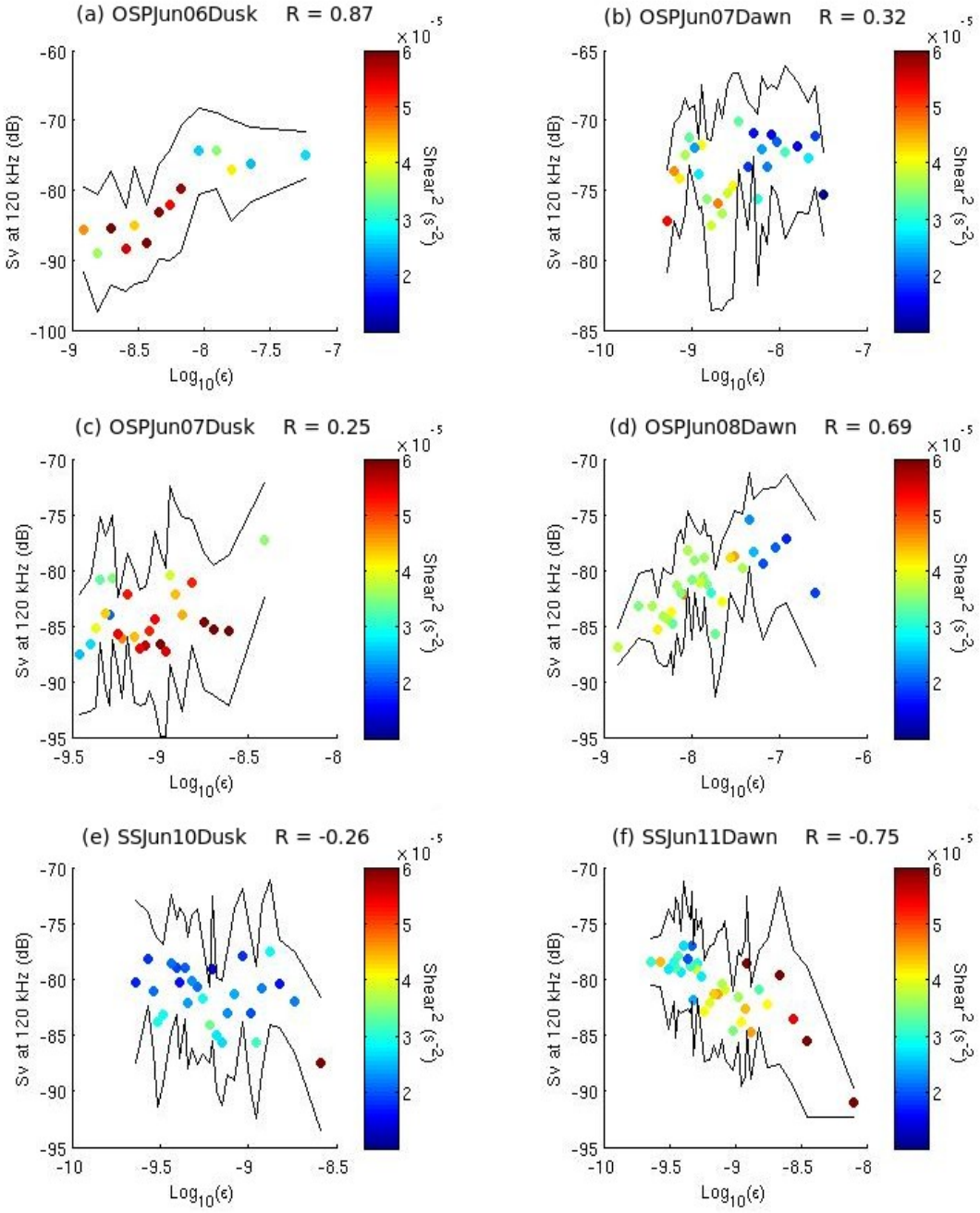

Figure A2.1.2. Dissipation rate as a function of the volume backscattering between 20 and 60 m. This depth interval excludes the migratory zooplankton layer but includes the near-surface zooplankton layer. Colour represents ADCP shear (see colorbar). Black lines are the upper and lower 68 % confidence interval corresponding to one standard deviation.

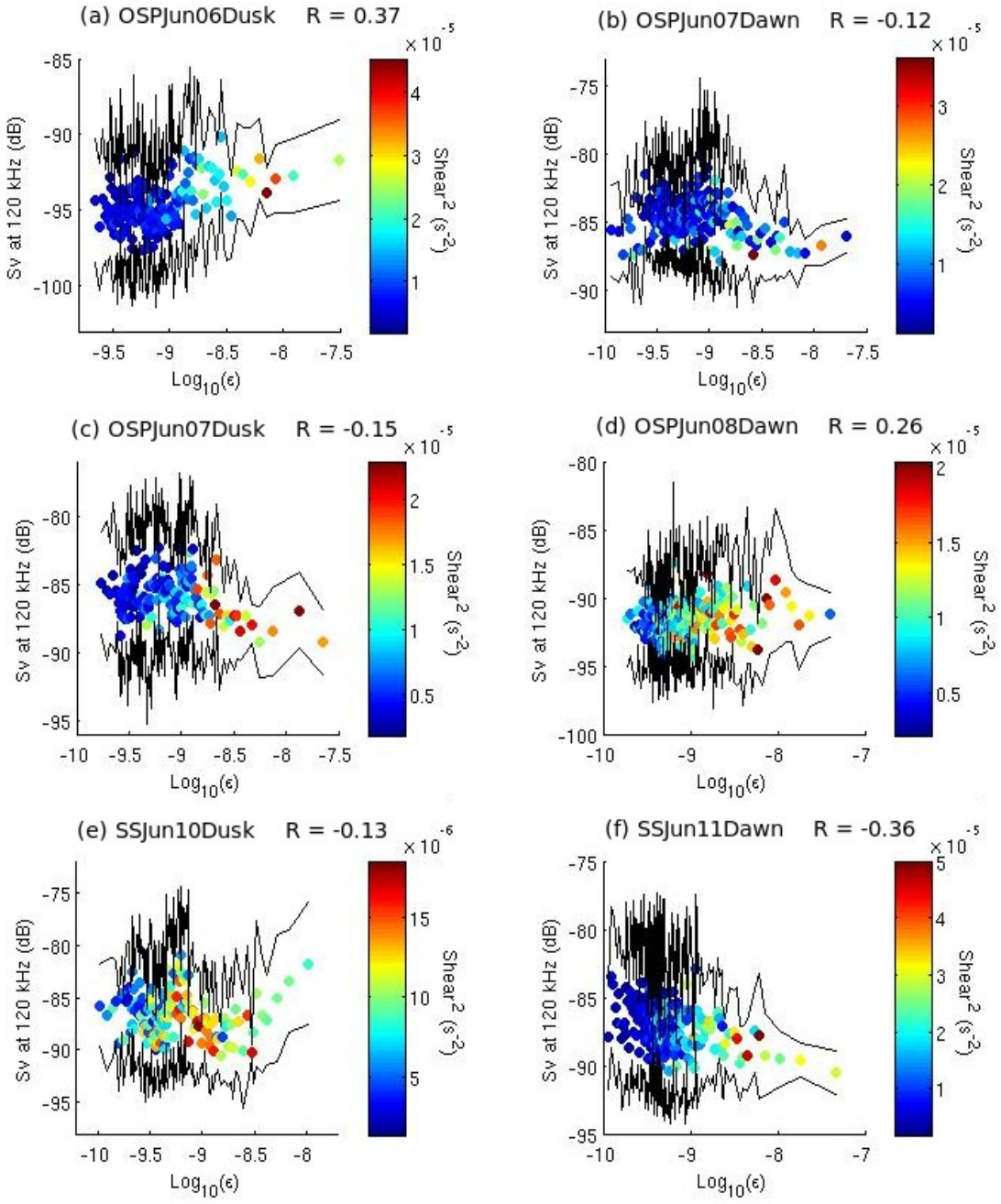

Figure A2.1.3. Dissipation rate as a function of the volume backscattering between 60 and 300 m. This depth interval includes the migratory zooplankton layer but excludes the near-surface zooplankton layer. Colour represents ADCP shear (see colorbar). Black lines are the upper and lower 68 % confidence interval corresponding to one standard deviation.

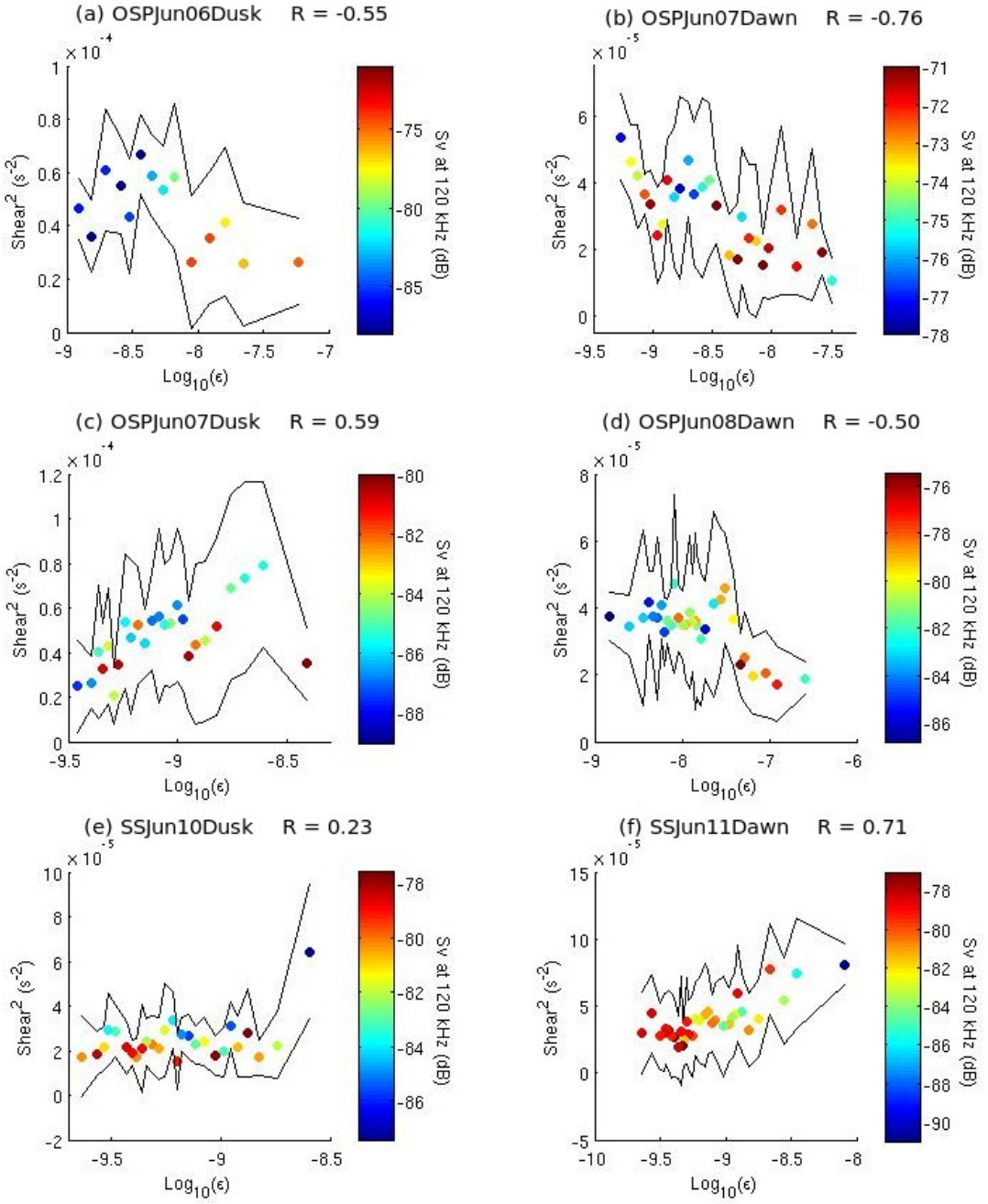

Figure A2.1.4. Dissipation rate as a function of the ADCP 16-m shear between 20 and 60 m. This depth interval excludes the migratory zooplankton layer but includes the near-surface zooplankton layer. Colour represents volume backscattering strength (see colorbar). See figure 3.15 for the scatterplots of the dissipation rate as a function of ADCP shear between 60 and 300 m. Black lines are the upper and lower 68 % confidence interval corresponding to one standard deviation.

Dataset	**Spearman coefficient**		
	ε – Sv (*unlagged*)	**ε – Sv** (*lagged*)	**ε - shear^2**
OSPJun06Dusk	0.37	0.35	0.66
OSPJun07Dawn	-0.12	-0.17	0.31
OSPJun07Dusk	-0.15	0.72	0.65
OSPJun08Dawn	0.26	0.46	0.69
SSJun10Dusk	-0.13	-0.19	0.52
SSJun11Dawn	-0.36	-0.35	0.76

Table A2.1.4. Spearman coefficients evaluating the correlation between dissipation rate and volume-backscattering strength (ε – Sv) using lagged and unlagged data, and dissipation rate and shear variance (ε - shear^2), for Ocean Station P and Station S. Unlagged correlations were estimated using the higest backscatter found within a time interval corresponding to one buoyancy period $2\pi/N$ before the time each dissipation rate was measured. Data averaged over 10 datapoints in order of increasing dissipation rate is used. Acoustic data is taken from the 120 kHz frequency. Volume backscattering strength is averaged over 1 m and 1 minute at the depth and time each dissipation rate value was taken. Depth range 60-250 m.

A2.2 Saanich Inlet

Dataset	Date (PDT)	Start time (UTC)	End time (UTC)	Profile numbers	Comments
SI06Jun09Dusk	Jun-09-06	10-Jun-06 02:50:21	10-Jun-06 05:51:02	33-57	*Full moon*
SI06Jun10Dawn	Jun-10-06	10-Jun-06 10:04:51	10-Jun-06 13:50:16	58-89	*Full moon*
SI06Jun10Dusk	Jun-10-06	11-Jun-06 02:59:29	11-Jun-06 06:13:07	90-116	*Full moon*
SI06Jun11Dawn	Jun-11-06	11-Jun-06 10:12:12	11-Jun-06 13:38:03	117-143	*Full moon*
SI07May08Dusk	May-08-07	09-May-07 02:36:14	09-May-07 04:36:08	09-25	
SI07May09Dusk	May-09-07	10-May-07 02:35:17	10-May-07 05:11:44	26-47	
SI07May10Dawn	May-10-07	10-May-07 11:22:38	10-May-07 13:54:43	48-68	
SI08May07Dusk	May-07-08	08-May-08 01:36:19	08-May-08 09:50:39	04-53	*Thermistor not working*
SI08May08Dawn	May-08-08	08-May-08 09:54:25	08-May-08 14:35:08	54-88	*Thermistor changed*
SI08May08Dusk	May-08-08	09-May-08 01:40:40	09-May-08 06:15:51	89-132	
SI08May09Dawn	May-09-08	09-May-08 10:42:00	09-May-08 12:50:10	137-154	

Table A2.2.1 Time-series collected in Saanich Inlet with the starting and ending times of the VMP profiling, and the profile numbers. At both stations, ADCP and multi-frequency bioacoustic data was also collected with each dataset.

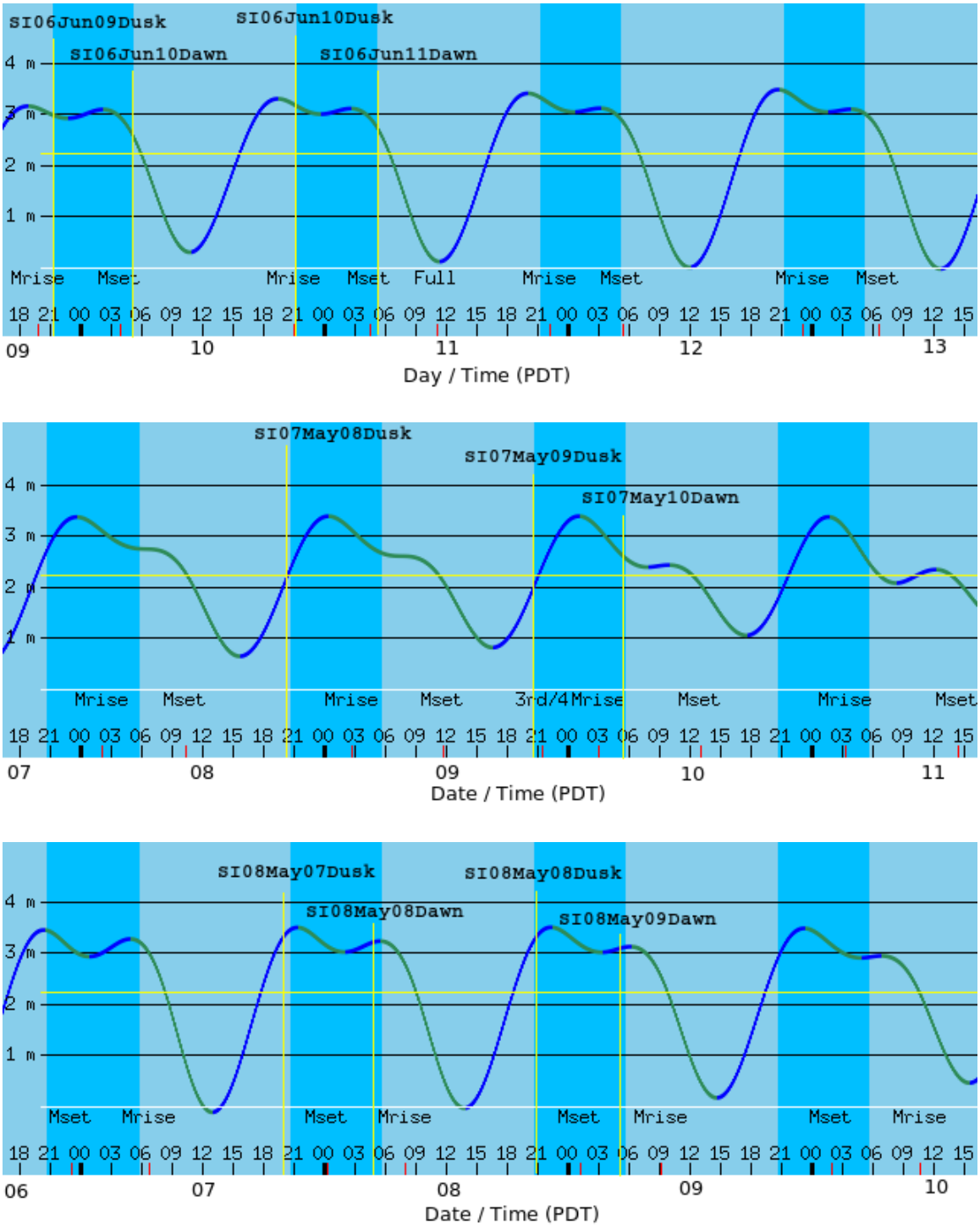

Figure A2.2.1. Tidal cycle in Saanich Inlet during field measurements in June 2006, May 2007 and May 2008. Vertical yellow lines indicate dusk/dawn measurement periods. Moon cycle information is included at the bottom of each graph. June 2006 measurements were collected during full moon.

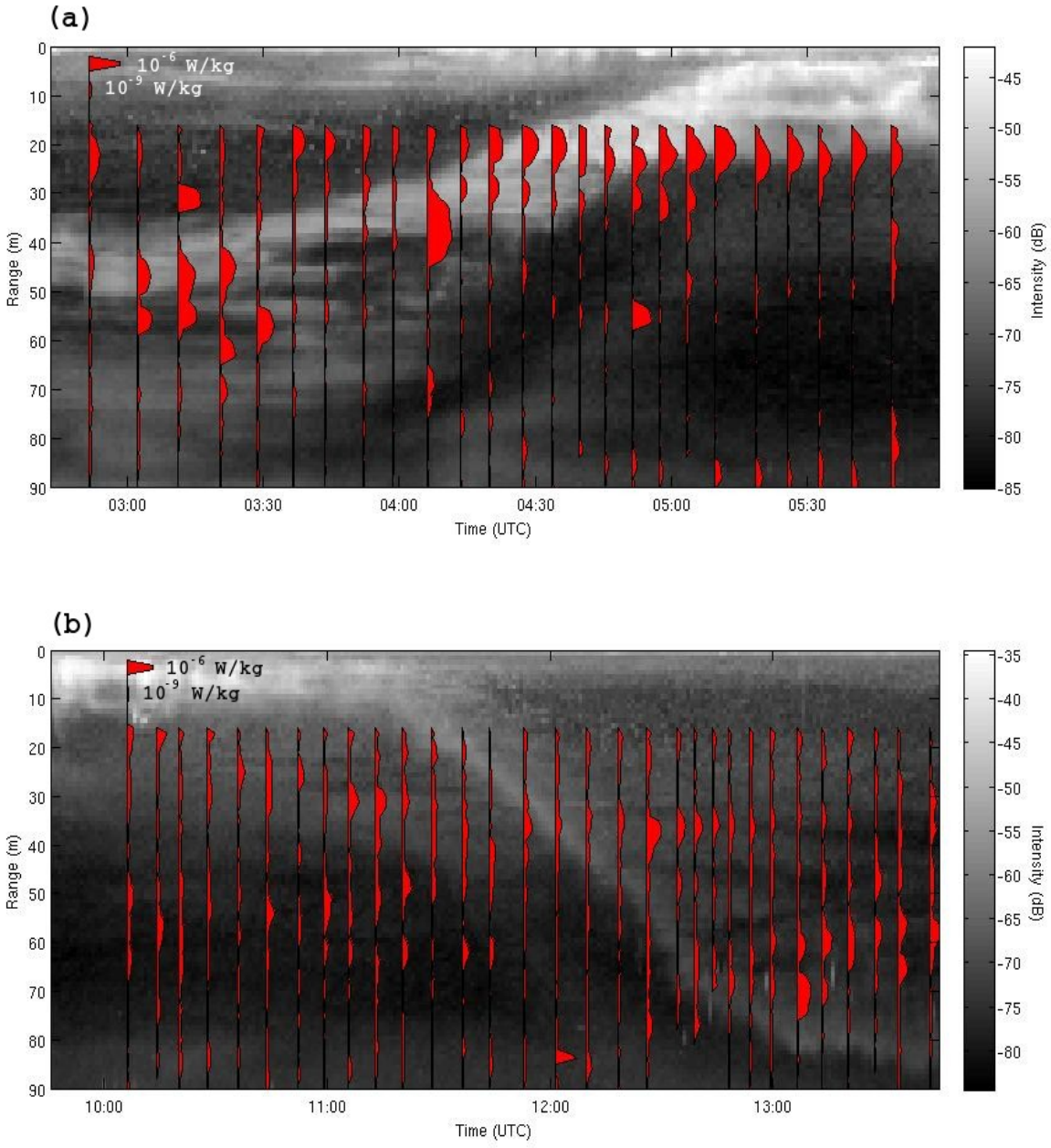

Figure A2.2.2. Volume-backscattering strength and dissipation rates collected in Saanich Inlet in June 2006. Echosounder frequency is 200 kHz. (a) *SI06Jun09Dusk*; (b) *SI06Jun10Dawn*; (c) *SI06Jun10Dusk*; (d) *SI06Jun11Dawn*.

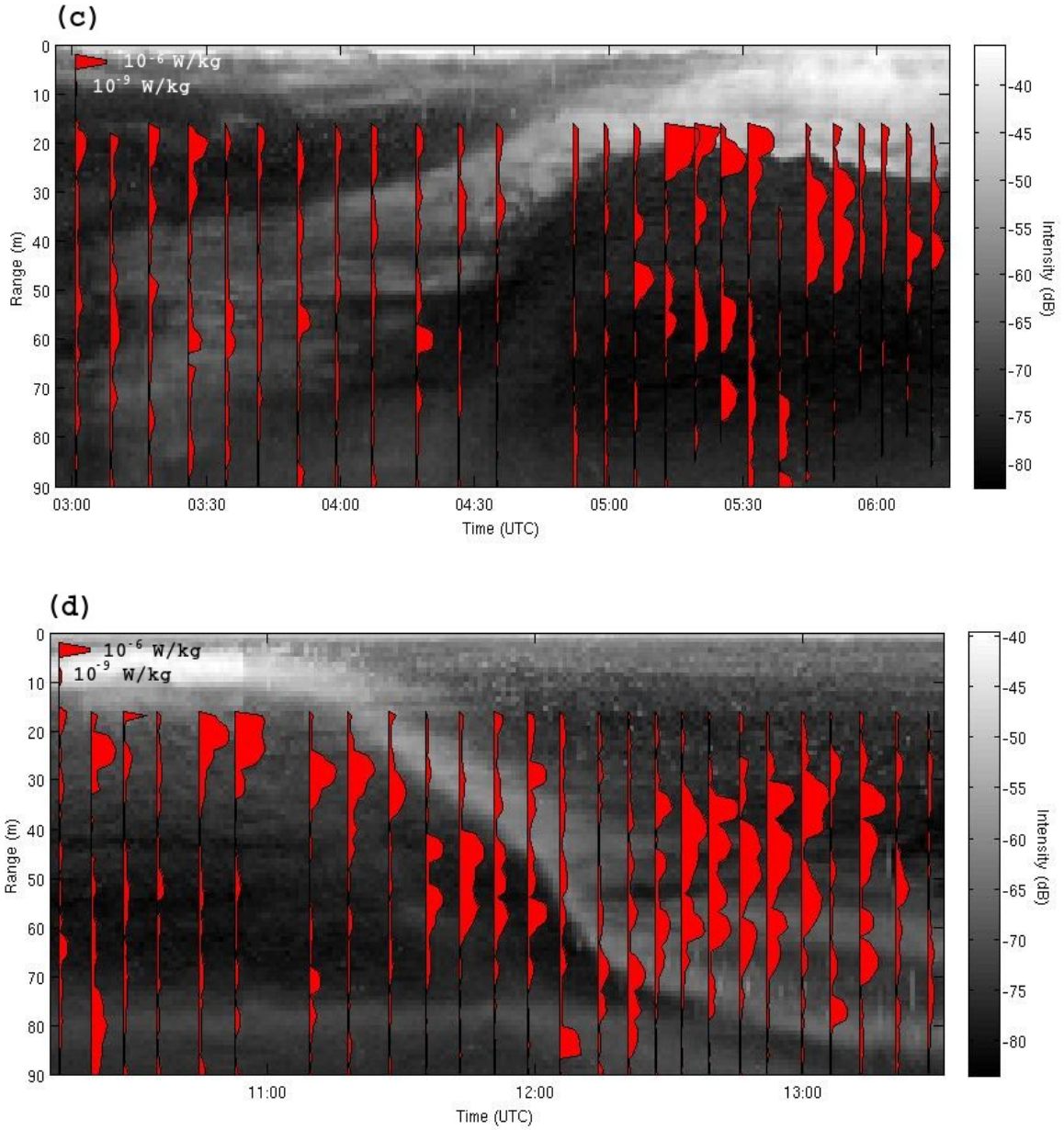

Figure A2.2.2. Continued.

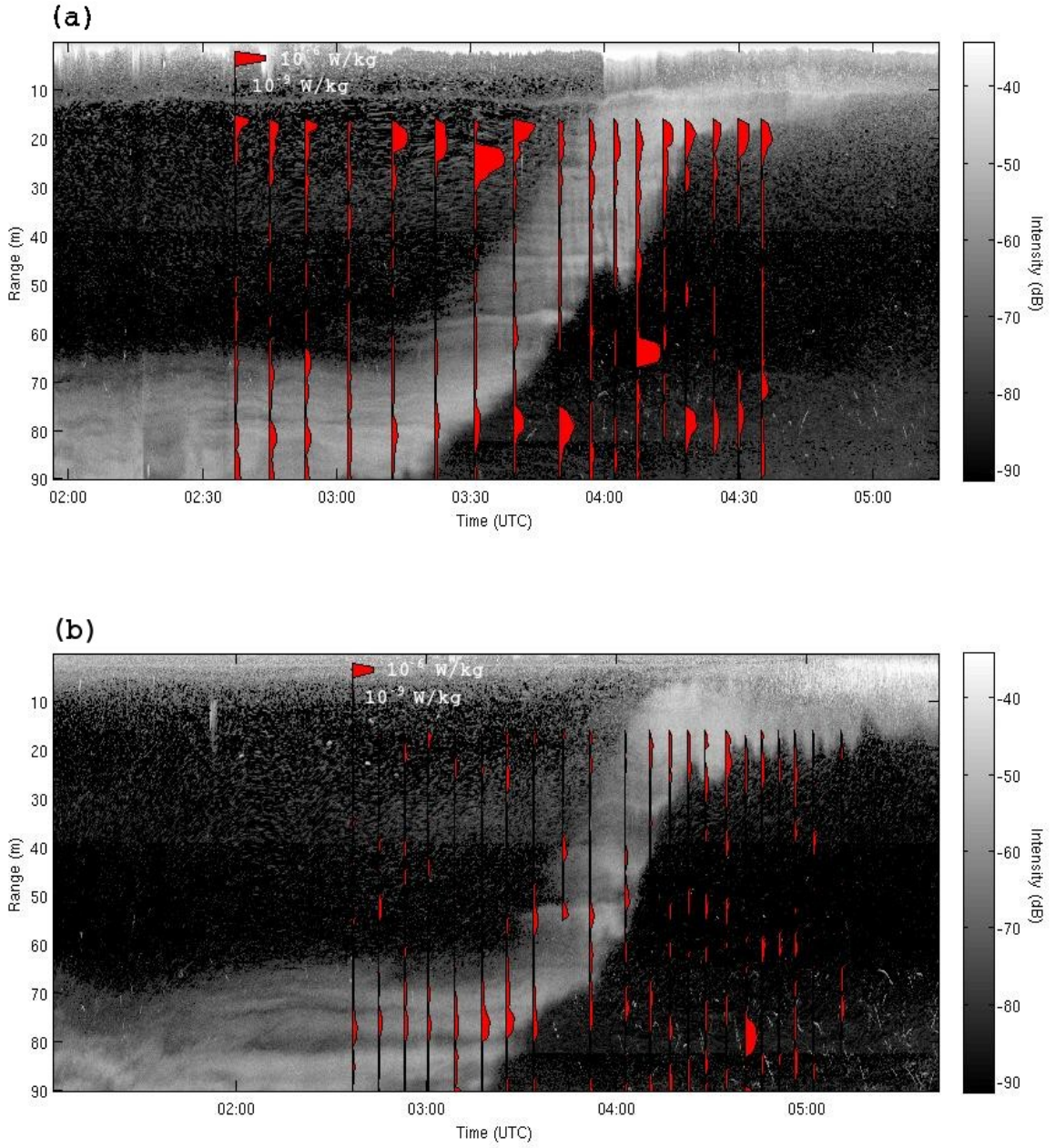

Figure A2.2.3. Volume-backscattering strength and dissipation rates collected in Saanich Inlet in May 2007. Echosounder frequency is 200 kHz. (a) *SI07May08Dusk*; (b) *SI07May09Dusk*; (c) *SI07May10Dawn.*

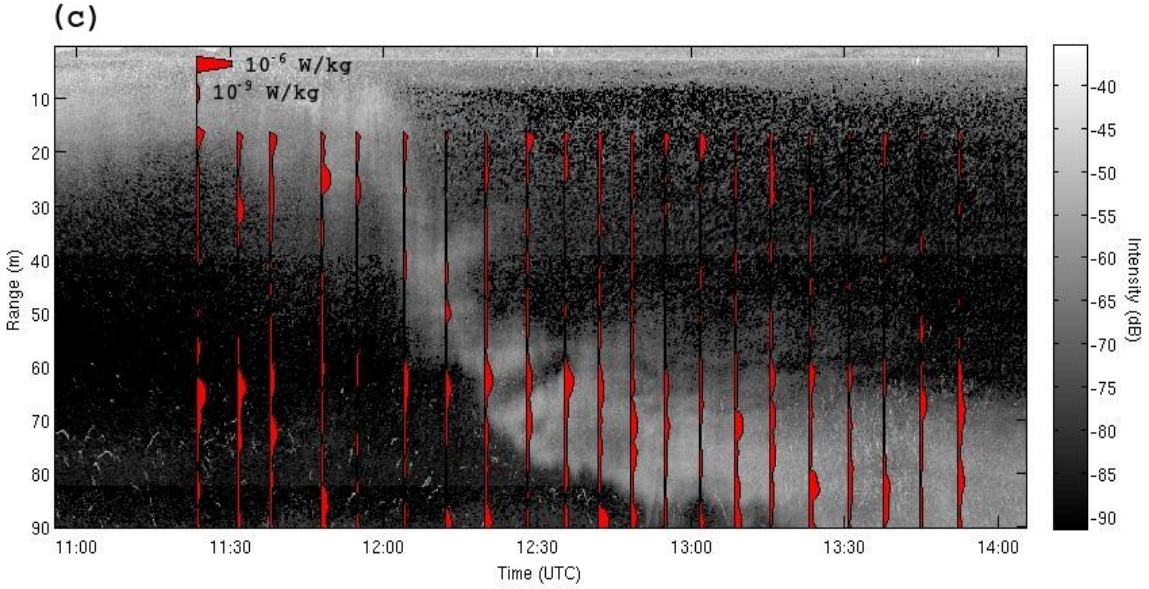

Figure A2.2.3. Continued.

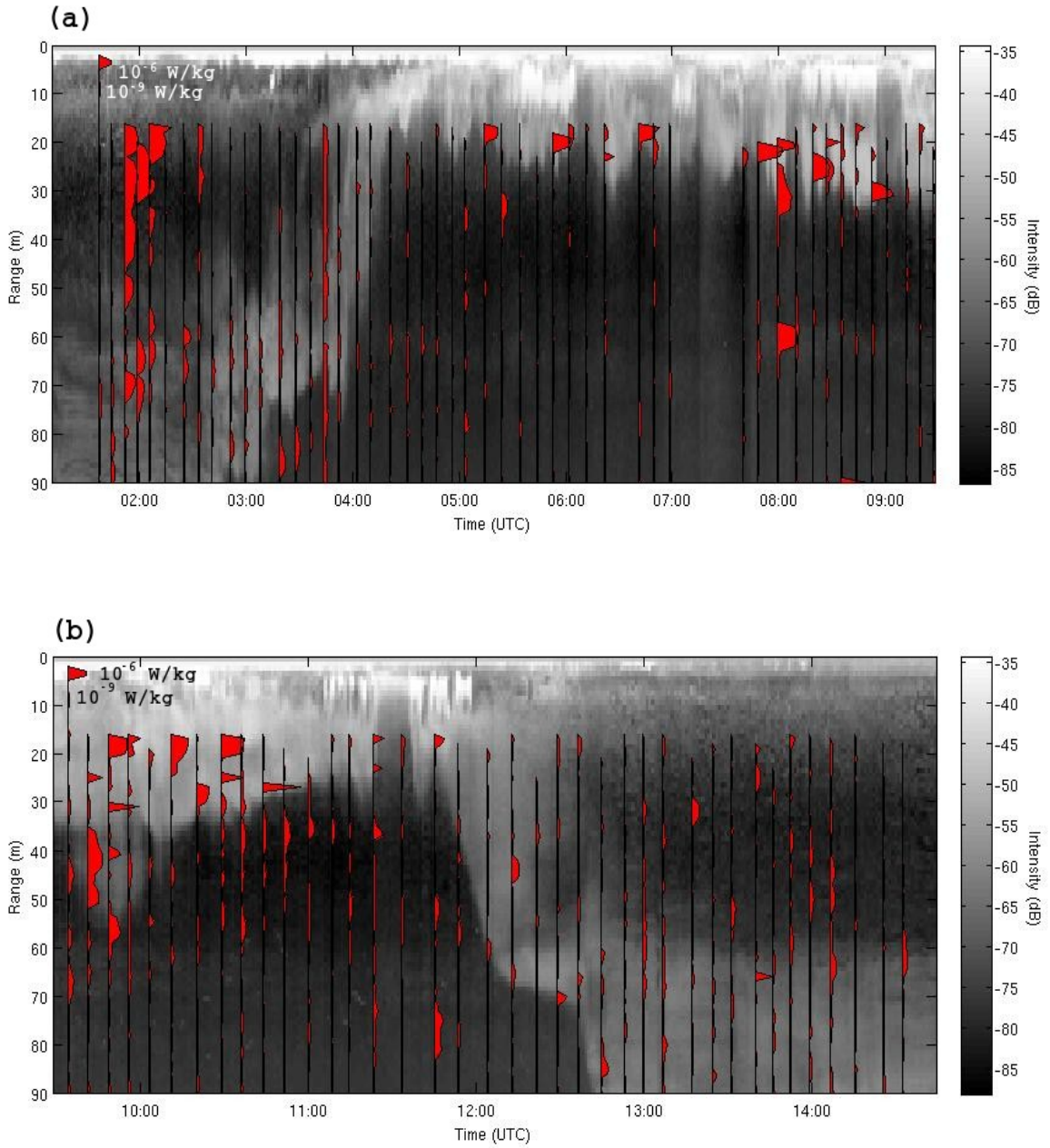

Figure A2.2.4. Volume-backscattering strength and dissipation rates collected in Saanich Inlet in May 2008. Echosounder frequency is 200 kHz. (a) *SI08May07Dusk*; (b) *SI08May08Dawn*; (c) *SI08May08Dusk; (d) SI08May09Dawn.*

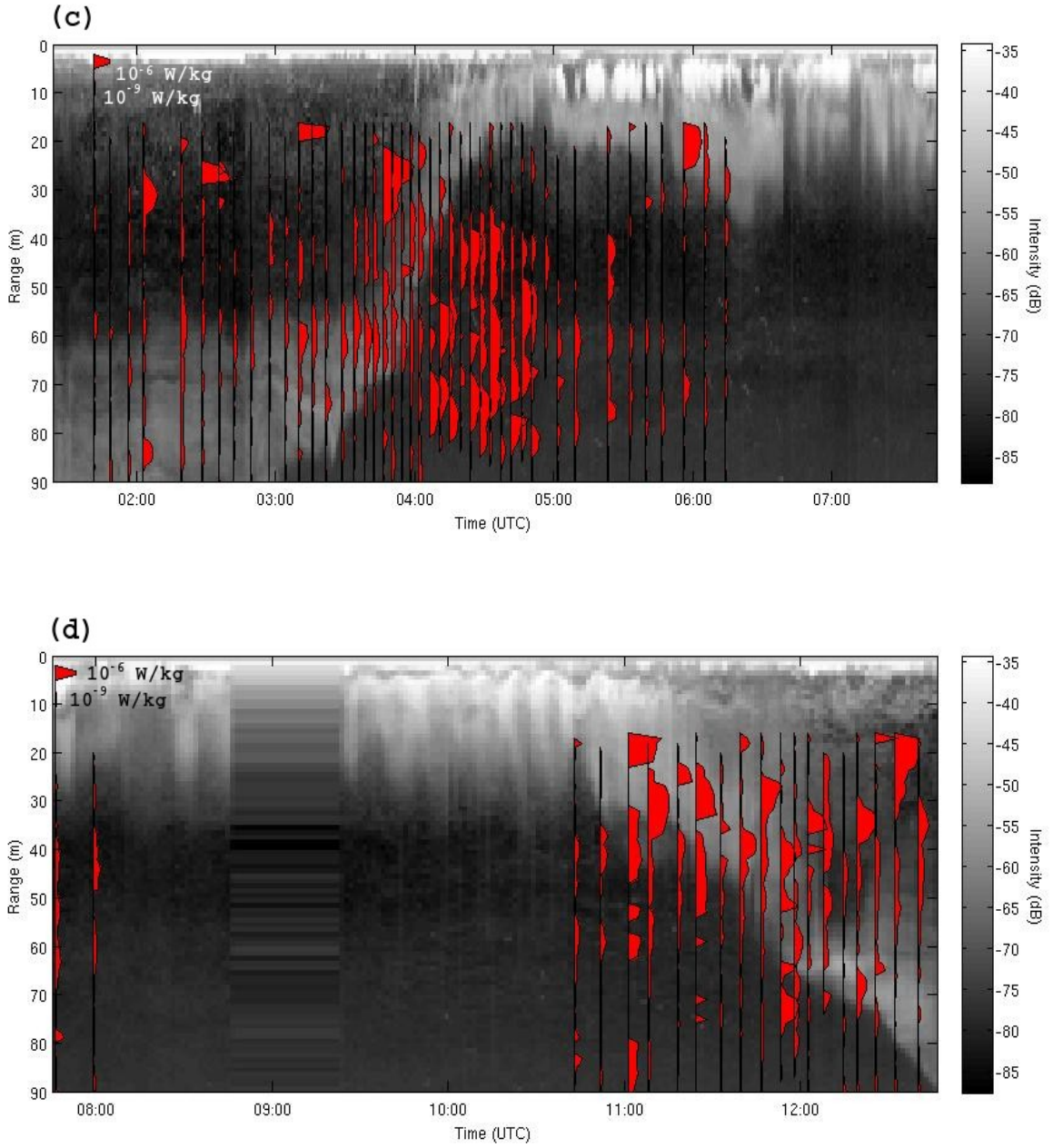

Figure A2.2.4. Continued.

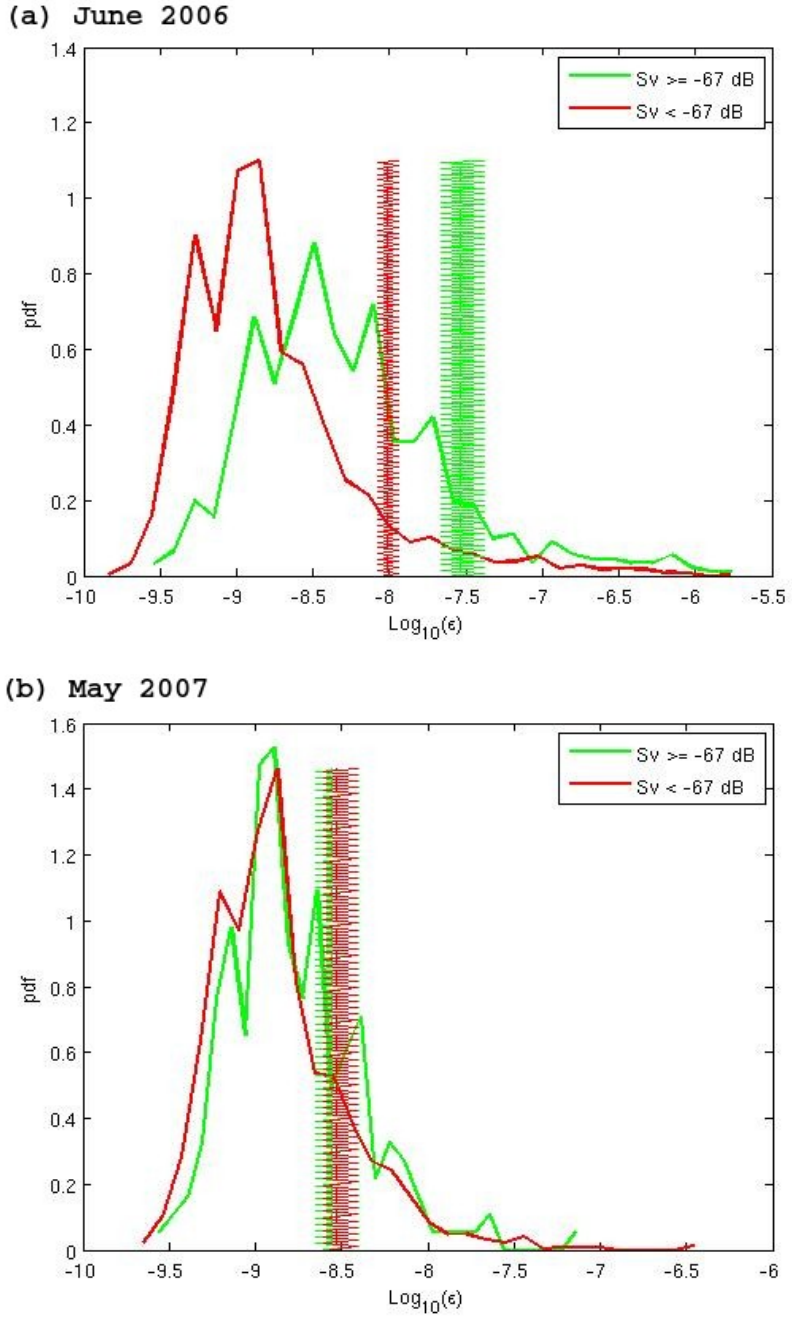

Figure A2.2.5. Probability density functions of the dissipation rate at high and low backscattering intensity. Volume backscattering thresholds used are (a) -67 dB; (b) -67 dB and (c) -70 dB. Thresholds were chosen in accordance to the volume backscattering distribution function to distinguish between the absence and presence of marine zooplankters. Vertical lines represent the mean of the distribution and horizontal stripes the mean's confidence intervals at 95% calculated using the bootstrap method (Emery and Thomson, 2001).

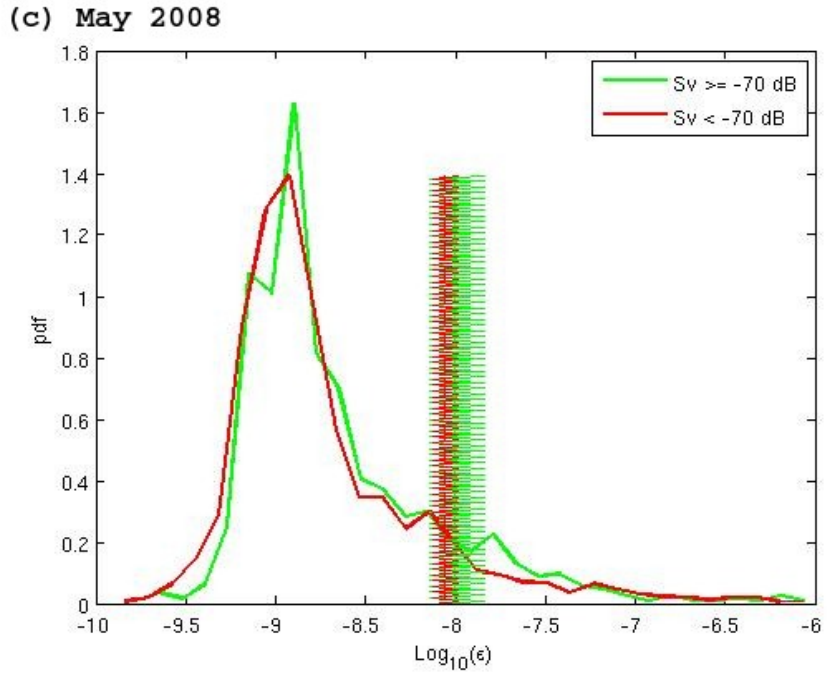

Figure A2.2.5. Continued.

Time-series	Dissipation rate mean (x 10^{-9} W kg^{-1})		Skewness		Sv threshold
	Low Sv	High Sv	Low Sv	High Sv	
SI06Jun09-11	9.7(8.4-11.6)	29(21.7-41.2)	1.6	1.05	-67
SI07May08-10	2.9(2.48-3.88)	2.8(2.26-3.96)	1.4	0.94	-67
SI08May07-09	8.7(7.5-10.2)	9.9(7.3-14.4)	1.73	1.62	-70

Table A2.2.2. Dissipation rate means at high and low backscatter with 95 % confidence interval as obtained using the bootstrap method (Emery and Thomson, 2001), and skewness of the probability density functions for the three time-series (2006, 2007 and 2008) in Saanich Inlet.

Dataset	Mean dissipation rate (x 10^{-9} W kg^{-1})		
	ML	**DL**	**NZ**
SI05Apr28Dusk	357.9(251.8-505.6)	2.5(2.3-2.7)	N/A
SI06Jun09Dusk	9.3 (5.4-15.4)	6.9(5.2-9.4)	2.5(1.8-3.8)
SI06Jun10Dawn	4.7(3.6-7.5)	4.7(4.0-5.5)	2.8(2.5-3.1)
SI06Jun10Dusk	3.1(2.3-4.8)	3.1(2.8-3.6)	11(9-14)
SI06Jun11Dawn	19(14-24)	54(46-65)	5.4(4.2-7.5)
SI06Jun09-11	9 (7-11)	18 (16-22)	5.6 (4.9-6.4)
SI07May08Dusk	2.1(1.6-2.8)	1.6(1.5-1.8)	1.7(1.4-2.3)
SI07May09Dusk	1.6(1.4-1.9)	1.5(1.3-2.0)	2.0(1.5-3.0)
SI07May10Dawn	1.6(1.5-1.8)	1.6(1.5-1.7)	1.7(1.5-1.9)
SI07May08-10	1.8 (1.6-2.2)	1.6(1.5-1.7)	1.9 (1.6-2.3)
SI08May07Dusk	4.2(3.6-4.8)	15(11-22)	1.7(1.6-1.8)
SI08May08Dawn	2.1(1.7-2.6)	1.8(1.7-2.0)	2.4(2.0-3.0)
SI08May08Dusk	13(10-16)	4.3(3.7-5.2)	24(19-32)
SI08May09Dawn	21(16-29)	4.3(3.7-5.2)	24(20-31)
SI08May07-09	7.4(6.3-9.0)	8.2(6.4-12.3)	8.6(7.2-11.0)

Table A2.2.3. Dissipation rate means per region for each time-series in Saanich Inlet with 95% confidence intervals (in brackets) as obtained using the bootstrap method. ML = Migration Layer; DL = Deep Layer (non-migrating zooplankton); NZ = No Zooplankton region. Depth intervals included in the analysis are: SI06: 30-90 m; SI07: 30-100 m; SI08: 35-100 m.

Time-series	Skewness		
	ML	**DL**	**NZ**
SI06Jun09-11	7.6 (6.6-9.0)	7.5 (6.4-9.1)	7.7 (6.8-8.9)
SI07May08-10	11.2 (8.9-15.6)	8.1 (4.1-11.6)	12.6 (9.9-17.6)
SI08May07-09	11.2(9.2-14.1)	21.9 (13.4-34.5)	21.2 (11.7-31.4)

Table A2.2.4. Skewness of the distribution functions of the dissipation rates of each dataset (2006, 2007, 2008) for each region represented in figure 4.9. Numbers in brackets correspond to the 95% confidence interval as obtained from the bootstrap method.

Time-series	Standard deviation (x 10^{-8})		
	ML	**DL**	**NZ**
SI06Jun09-11	3.6 (3.0-4.4)	7.0 (5.9-8.6)	1.9 (1.6-2.3)
SI07May08-10	0.40 (0.28-0.61)	0.20 (0.16-0.30)	0.61 (0.41-0.91)
SI08May07-09	2.8 (2.1-3.8)	6.0 (3.6-11.1)	4.9(3.4-8.7)

Table A2.2.5. Standard deviation of the distributions of the dissipation rate per region for each dataset (2006, 2007, 2008). Numbers in brackets correspond to the 95% confidence interval as obtained from the bootstrap method.

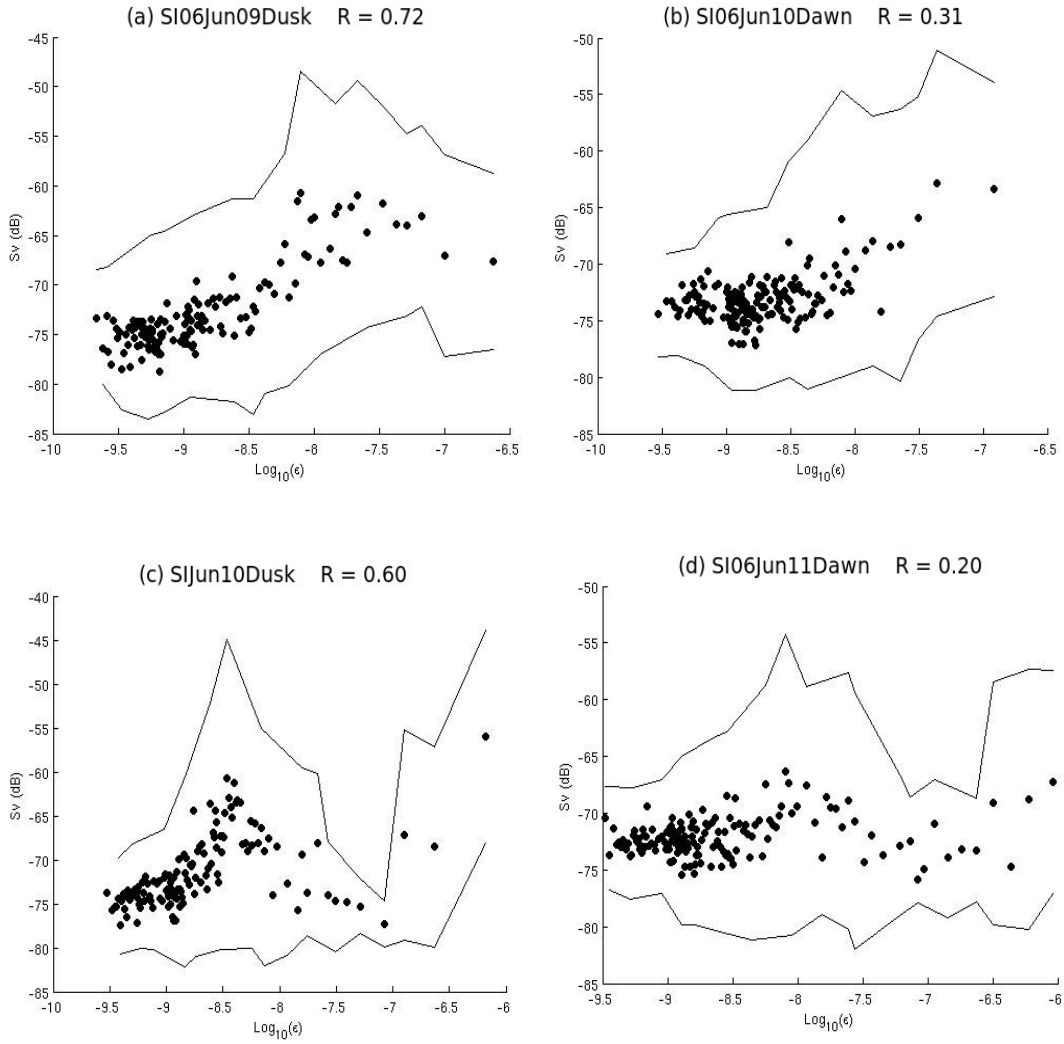

Figure. A2.2.6. Correlation between dissipation rates and volume-backscattering strength in Saanich Inlet, June 2006. Data above 30 m and below 60 m are excluded. Raw data was averaged over 10 datapoints in order of increasing dissipation rate. Volume backscattering strength is averaged over 1 m and 1 minute at the depth and time each dissipation rate value was taken. Solid lines represent the standard deviation of each averaged datapoint, corresponding to a 68% confidence interval.

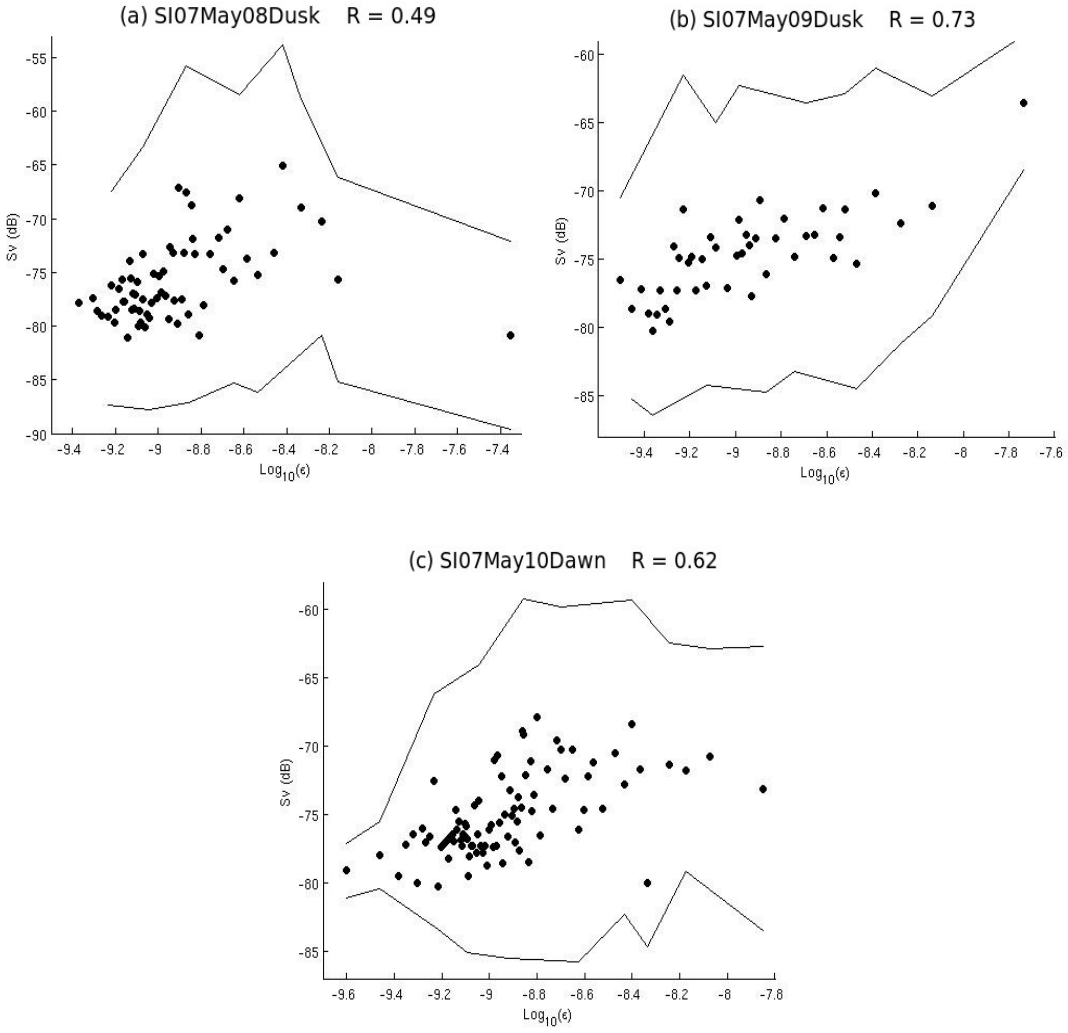

Figure A2.2.7. Correlation between dissipation rates and volume-backscattering strength in Saanich Inlet, May 2007. Data above 30 m and below 60 m are excluded. Raw data was averaged over 10 datapoints in order of increasing dissipation rate. Volume backscattering strength is averaged over 1 m and 1 minute at the depth and time each dissipation rate value was taken. Solid lines represent the standard deviation of each averaged datapoint, corresponding to a 68% confidence interval.

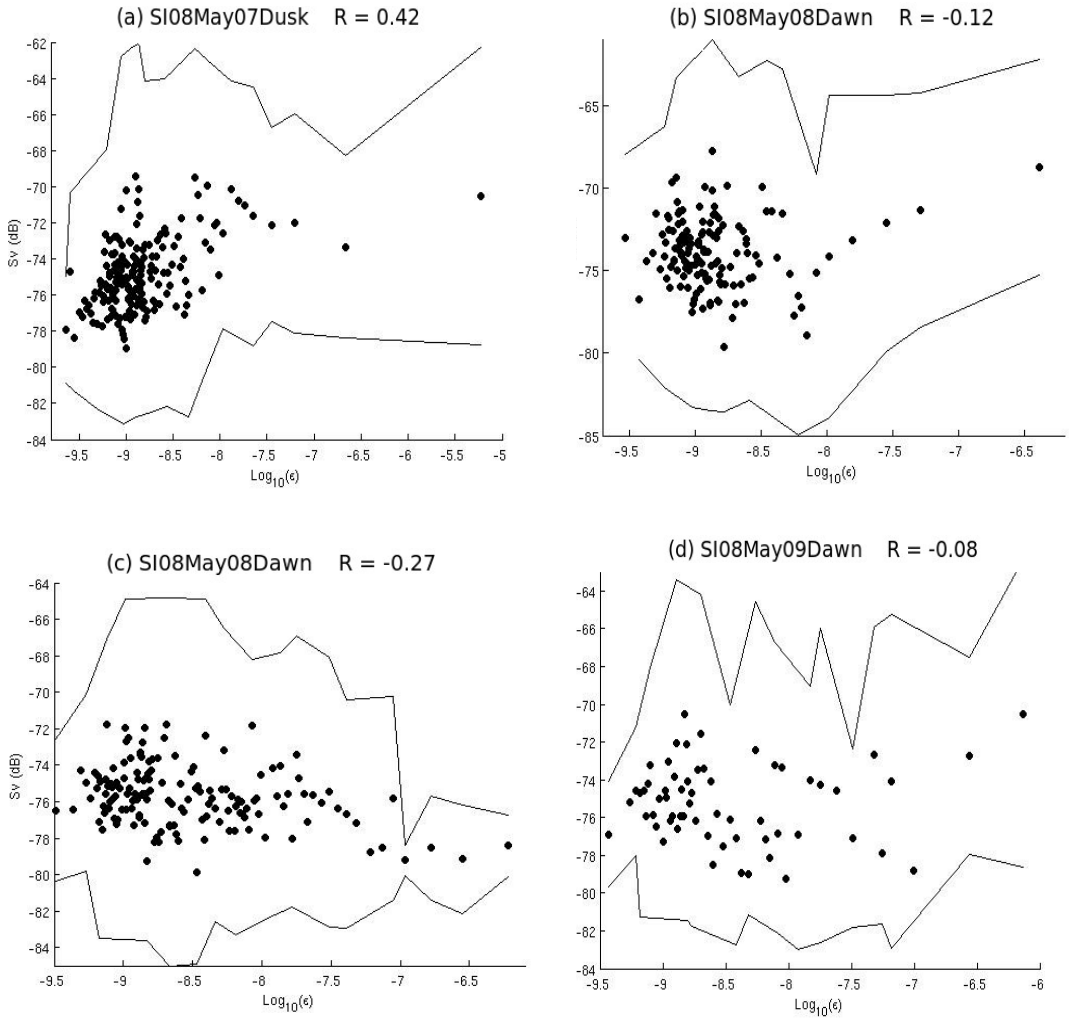

Figure A2.2.8. Correlation between dissipation rates and volume-backscattering strength in Saanich Inlet, May 2008. Data above 30 m and below 60 m are excluded. Raw data was averaged over 10 datapoints in order of increasing dissipation rate. Volume backscattering strength is averaged over 1 m and 1 minute at the depth and time each dissipation rate value was taken. Solid lines represent the standard deviation of each averaged datapoint, corresponding to a 68% confidence interval.

	Spearman coefficient	
Dataset	**Unlagged**	**Lagged**
SI06Jun09Dusk	0.72	0.75
SI06Jun10Dawn	0.31	0.07
SI06Jun10Dusk	0.60	0.52
SI06Jun11Dawn	0.20	0.03
SI07May08Dusk	0.49	0.62
SI07May09Dusk	0.73	0.68
SI07May10Dawn	0.62	0.67
SI08May07Dusk	0.42	0.47
SI08May08Dawn	-0.12	0.17
SI08May08Dusk	-0.27	-0.25
SI08May09Dawn	-0.08	-0.13

Table A2.2.6. Spearman coefficients evaluating the correlation between dissipation rates and volume-backscattering strength using lagged and unlagged data. Lagged correlations were estimated using the highest backscatter found within a time interval corresponding to one buoyancy period $2\pi/N$ before the time each dissipation rate was measured. Data averaged over 10 datapoints in order of increasing dissipation rate is used. Volume-backscattering strength is averaged over 1 m and 1 minute at the depth and time each dissipation rate value was taken. Depth range 30-120 m.

REFERENCES

Apel, J.R. (1988). Principles of Ocean physics. International geophysics series. Academic Press Inc., San Diego. Vol. 38, 634p.

Batchelor, G.K. (1959). Small-scale variation of convected quantities like temperature in turbulent fluid. Journal of Fluid Mechanics, 5, 113-139.

Baird, R.C. and G.Y. Jumper (1995). Encounter models and Deep-Sea fishes: numerical simulations and the mate location problem in *Sternoptyx diaphana* (Pisces, Sternoptychidae). Deep-Sea Research I, 42(5), 675-696.

Beveridge, I.A. (2007). Acoustic observations of zooplankton distribution in Saanich Inlet, an intermittently anoxic fjord. Msc Thesis, University of Victoria.

Boden, B.P. and E.M. Kampa (1965). An aspect of euphausiid ecology revealed by echo sounding in a fjord. Crustaceana, 9, 155-173.

Boyd P.W., P.J. Harrison and B.D. Johnson (1999). The Joint Global Ocean Flux Study (Canada) in the NE Subarctic Pacific. Deep-Sea Research II , 46, 2345-2350.

Catton, K.B., D.R. Webster, S. Kawaguchi and J. Yen (Unpublished). Krill aggregation behavior as a mechanism for mixing in the ocean.

Catton, K.B., D.R. Webster and J. Yen (2008). Can krill mix the ocean? ASLO, Orlando, Fl, Abstract ID:209.

Clay, C.S. and H. Medwin (1977). Acoustical Oceanography: principles and applications. John Wiley and Sons, New York, 544p.

Denman, K.L. and A.E. Gargett (1995). Biological-physical interactions in the upper ocean: The role of vertical and small scale processes. Annual Reviews of Fluid Mechanics, 27, 225-255.

DeRobertis A. (2002). Small-scale spatial distribution of the euphausiid *Euphausia pacifica* and overlap with planktivorous fishes. Journal of Plankton Research, 24(11), 1207-1220.

De Robertis A., C. Schell and J.S. Jaffe (2003). Acoustic observations of the swimming behavior of the euphausiid *Euphausia pacifica* Hansen. ICES Journal of Marine Science, 60, 885-898.

DeSzoeke, R.A. and S.R. Springer (2003). A diapycnal diffusion algorithm for isopycnal ocean circulation models with special application to mixed layer. Ocean Modelling, 5, 297-323.

Dewar, W.K., R.J. Bingham, R.L. Iverson, D.P. Nowacek, L.C. St-Laurent and P.H. Wiebe (2006). Does the marine biosphere mix the ocean? Journal of Marine Research, 64, 541-561.

Dillon, T.M. and D.R. Caldwell (1980). The Batchelor spectrum and dissipation in the upper ocean. Journal of Geophysical Research, 85, 1910-1916.

Emery, W.J. and R.E. Thomson (2001).Data Analysis Methods in Physical Oceanography. Elsevier, 2nd edition, Amsterdam, Netherlands. 638p.

Engineering Toolbox. [cited 2009 Apr 8]. The Engineering ToolBox [Internet]. Available from: http://www.engineeringtoolbox.com.

Freeland, H., K. Denman, C.S. Wong, F. Whitney and R. Jacques (1997). Evidence of change in the winter mixed layer in the Northeast Pacific Ocean. Deep-Sea Research I, 44(12), 2117-2129.

Gargett, A.E., D. Stucchi and F. Whitney (2003). Physical processes associated with high primary production in Saanich Inlet, British Columbia. Estuarine, Coastal and Shelf Science, 56, 1141-1156.

Goldblatt R.H., D.L. Mackas and A.G. Lewis (1999). Mesozooplankton community characteristics in the NE subarctic Pacific. Deep-Sea Research II, 46, 2619-2644.

Greenlaw, C.F. (1979). Acoustical estimation of zooplankton populations. Limnology and Oceanography, (24)2, 226-242.

Gregg, M.C. (1987). Diapycnal mixing in the thermocline. Journal of Geophysical Research, 92, 5249-5286.

Gregg, M.C. (1989). Scaling turbulent dissipation in the thermocline. Journal of Geophysical Research, 94, 9896-9698.

Gregg, M.C. and J.K. Horne (2009). Turbulence, Acoustic backscatter and pelagic Nekton in Monterey Bay. Journal of Physical Oceanography, 39, 1097-1114.

Gregg, M.C. and T.B. Sanford (1988). The dependence of turbulent dissipation on stratification in a diffusively stable thermocline. Journal of Geophysical Research, 93, 12381-12392.

Gurvich, A.S. and A.M. Yaglom (1967). Breakdown of eddies and probability distributions for small-scale turbulence. Physics of Fluids, 10(9P2), S59-S65.

Hamme, R. and S.R. Emerson (2006). Constraining bubble dynamics and mixing with dissolved gases: Implications for productivity measurements by oxygen mass balance. Journal of Marine Research, 64, 73-95.

Hamner, W.M., P.P. Hamner, S.W. Strand and R.W. Gilmer (1983). Behavior of Antarctic krill, Euphausia superba: chemoreception, feeding, schooling and molting. Science, 220(4595), 433-435.

Hobson, L. A. (1983). Phytoplankton crops, bacterial metabolism and oxygen in Saanich Inlet, a fjord in Vancouver Island, British Columbia. Sedimentary geology, 36, 117-130.

Huntley, M.E. and M. Zhou (2004). Influence of animals on turbulence in the sea. Marine Ecology Progress Series, 273, 65-79.

Hwang, J.H., H. Yamazaki and C.R. Rehman (2006). Buoyancy generated turbulence in stably stratified flow with shear. Physics of Fluids, 18(045104), 1-11.

Iida, K., T. Mukai and D. Hwang (1996). Relationship between acoustic backscattering strength and density of zooplankton in the sound-scattering layer. ICES Journal of Marine Science, 53, 507-512.

Jaffe, J.S., M.D. Ohman and A. De Robertis (1999). Sonar estimates of daytime activity levels of Euphausia pacifica in Saanich Inlet. Canadian Journal Fisheries and Aquatic Sciences, 56, 2000-2010.

Juniper, S. K. and R. O. Brinkhurst (1986). Water-column dark CO2 fixation and bacterial-mat growth in intermittently anoxic Saanich Inlet, British Columbia. Marine Ecology Progress Series, 33, 41-50.

Kocsis, O., H. Prandke, A. Stips, A. Simon and A. Wüest (1999). Comparison of dissipation of turbulent kinetic energy determined from shear and temperature microstructure. Journal of Marine Systems, 21, 67-84.

Kunze, E., J.F. Dower, I. Beveridge, R. Dewey and K.P. Bartlett. Observations of biologically generated turbulence in a coastal inlet. Science, 313, 1767-1770.

Kunze, E., J.F. Dower, R. Dewey and E.A. D'Asaro (2007). Mixing it up with krill. Science, 318, 1239.

Lawson, G.L., P.H. Wiebe, T.K. Stanton and C.J. Ashijan (2008). Euphausiid distribution along the Western Antarctic Peninsula – Part A: Development of robust multi-frequency acoustic techniques to identify euphausiid aggregations and quantify euphausiid size, abundance, and biomass. Deep-Sea Research II, 55, 412-431.

Lavery, A.C., P.H. Wiebe, T.K. Stanton, G.L. Lawson, M.C. Benfield and N. Copley (2007). Determining dominant scatterers of sound in mixed zooplankton populations. Journal of the Acoustical Society of America, 122(6), 3304-3326.

Ledwell, J.R., A.J. Watson and C.S. Law (1993). Evidence for slow mixing accross the pycnocline from an open-ocean tracer-release experiment. Letters to Nature, 364, 701-703.

Mackas D.L., H. Sefton, C.B. Miller and A. Raich (1993). Vertical habitat partitioning by large calanoid copepods in the oceanic subarctic Pacific during spring. Progress in Oceanography, 32(14), 256-294.

Mackas, D.L. and A. Tsuda (1999). Mesozooplankton in the eastern and western subarctic Pacific: community structure, seasonal life histories, and interannual variability. Progress in Oceanography, 43, 335-363.

Mackas, D.L., M. Tsurumi, M.D. Galbraith and D.R. Yelland (2005). Zooplankton distribution and dynamics in a North Pacific eddy of coastal origin: II. Mechanisms of eddy colonization by and retention of offshore species. Deep-Sea Research II, 52, 1011-1035.

Mackie, G.O. and C.E. Mills (1983). Use of the Pisces IV Submersible for zooplankton studies in coastal waters of British Columbia. Canadian Journal of Fisheries and Aquatic Sciences 40, 763-776.

MacLennan, D.N. and E.J. Simmonds (1992). Fisheries Acoustics. Chapman and Hall, London, 325 p.

Marlowe, C.J. and C.B. Miller (1975). Patterns of vertical distribution and migration of zooplankton at Ocean Station “P”. Limnology and Oceanography, 20(5), 824-844.

Miller C.B., B.W. Frost, H.P. Batchelder, M.J. Clemons and R.E. Conway (1984). Life histories of large, grazing copepods in a Subarctic Ocean gyre: *Neocalanus plumchrus*, *Neocalanus cristatus* and *Eucalanus bungii* in the Northeast Pacific. Progress in Oceanography, 13, 201-243.

Miyashita, K., I. Aoki and T. Inagaki (1996). Swimming behaviour and target strength of isada krill (*Euphausia pacifica*). ICES Journal of Marine Science, 53, 303-308.

Moku, M., K. Kawaguchi, H. Watanabe and A. Ohno (2000). Feeding habits of three dominant myctophid fishes, *Diaphus theta*, *Stenobrachius leucopsarus* and *S. nannochir*, in the subarctic and the transitional waters of the western North Pacific. Marine Ecology Progress Series, 207, 129-140.

Moum, J.N. and I.H. Osborn (1986). Mixing in the main thermocline. Journal of Physical Oceanography, 16,1250-1259.

Muller, U.K., B.L.E. Van Del Heuvel, E.J. Stamhuis and J.J. Videler (1997). Fish foot prints: morphology and energetics of the wake behind a continuously swimming mullet (*Chelon Labrosus Risso)*. Journal of Experimental Biology, 200, 2893-2906.

Munk, W. (1966). Abyssal recipes. Deep-Sea Research, 13, 707-730.
Munk, W. and C. Wunsch (1998). Abyssal recipes II: energetics of tidal and wind mixing. Deep-Sea Research I, 45, 1977-2010.

Oakey, N.S. (1982). Determination of the rate of dissipation of turbulent energy from simultaneous temperature and velocity shear microstructure measurements. Journal of Physical Oceanography, 12(3), 256-271.

Osborn, T.R. (1980). Estimates of the local-rate of vertical diffusion from dissipation measurements. Journal of Physical Oceanography, 10(1), 83-89.

Parsons, T.R., R.I. Perry, E.D. Nutborwn, W. Hsieh and C.M. Lalli (1983). Frontal zone analysis at the mouth of Saanich Inlet, British Columbia, Canada. Marine Biology, 73, 1-5.

Parsons, T.R. and M. Takahashi (1973). Biological Oceanographic Processes. Pergamon Press.

Stanton, T.K., P.H. Wiebe, D. Chu and L. Goodman (1994). Acoustic characterization and discrimination of marine zooplankton and turbulence. ICES Journal of Marine Science, 51, 469-479.

Tabata, S. and W.E. Weichselbaumer (1992). An update of the statistics of hydrographic/CTD data taken at Ocean Station P (May 1956 – September 1990). Canadian Data Report of Hydrography and Ocean, Sciences No. 107.

Takahashi, M., D.L. Seibert and W.H. Thomas (1977). Occasional blooms of phytoplankton during summer in Saanich Inlet, B.C., Canada. Deep-Sea Research, 24(8), 775-780.

Tennekes, H. and J.L. Lumley (1972). A first course in turbulence. The MIT Press, New York, 300p.

Thorpe, S.A. (2005). The turbulent ocean. Cambridge University Press, New York, 439p.

Thurman, H.V. and A.P. Trujillo (2004). Introductory oceanography. Pearson Prentice Hall, 10th Edition, New Jersey, 608 p.

Torres, J.J. (1984). Relationship of oxygen consumption to swimming speed in *Euphausia pacifica* II. Drag, efficiency and a comparison with other swimming organisms. Marine Biology, 78, 231-237.

Torres, J.J. and Childress, J.J. (1983). Relationship of oxygen consumption to swimming speed in *Euphausia pacifica* 1. Effects of temperature and pressure. Marine Biology, 74, 79-86.

Trevorrow M.V. (2005). The use of moored inverted echo sounders for monitoring meso-zooplankton and fish near the ocean surface. Canadian Journal of Fisheries and Aquatic Sciences, 62, 1004-1018.

Trevorrow M.V., D.L. Mackas and M.C. Benfield (2005). Comparison of multifrequency acoustic and in situ measurements of zooplankton abundances in Knight inlet, British Columbia. Journal of the Acoustical Society of America, 117(6), 3574-3588.

Ueno, H., E. Oka, T. Suga, H. Onishi and D. Roemmich (2007). Formation and variation of temperature inversions in the eastern subarctic North Pacific. Geophysical Research Letters, 34(5), L05603.

Venayagamoorthy, S.K. and D.D. Stretch (2006). Lagrangian mixing in decaying stably stratified turbulence. Journal of Fluid Mechanics, 564, 197-226.

VENUS. [cited 2009 May 24]. University of Victoria – VENUS Victoria Experimental Network Under the Sea [Internet]. Available from http://www.venus.uvic.ca.

Visser, A.W. (2007). Biomixing of the oceans? Science, 316, 838-839.

Whitehead, J.A. and W. Wang (2008). A laboratory model of vertical ocean circulation driven by mixing. American Meteorological Society, 38, 1091-1106.

Whitney, F.A., W.R. Crawford and P.J. Harrison (2005). Physical processes that enhance nutrient transport and primary productivity in the coastal and open ocean of the subarctic NE Pacific. Deep-Sea Research II, 52, 681-706.

Wiese, K. and Y. Ebina (1995). Propulsion jet of *Euphausia superba*. Journal of Marine Biology Association of UK, 75(1), 43-54.

WolframMathWorld [cited 2009 July 8]. Spearman rank correlation coefficient [Internet]. Available from http://mathworld.wolfram.com/.

Yamazaki, H. and R. Lueck (1990). Why oceanic dissipation rates are not lognormal. Journal of Physical Oceanography, 19(5), 1905-1918.

Yatsu A., C. Sassa, M. Moku and T. Kinoshita (2005). Night-time vertical distribution and abundance of small epipelagic and mesopelagic fishes in the upper 100m layer of the Kuroshio-Oyashio Transition Zone in spring. Fisheries Science, 71, 1280-1286.

Yen, J. (2000). Life in transition: Balancing inertial and viscous forces by planktonic copepods. Biology Bulletin, 198, 213-224.

Yen, J., J. Brown and D.R. Webster (2003). Analysis of the flow field of the krill, *Euphausia pacifica*. Marine and Freshwater Behaviour and Physiology, 36(4), 307-319.

Zhou, M., W. Nordhausen and M. Huntley (1994). ADCP measurements of the distribution and abundance of euphausiids near the Antarctic Peninsula in winter. Deep-Sea Research I, 41(9), 1425-1445.

Zhou, M. and R.D. Dorland (2004). Aggregation and vertical migration behavior of *Euphausia superba*. Deep-Sea Research II, 51, 2119-2137.